
Atom-by-atom condensation in and electronic modification of 2D quantum box arrays

Inauguraldissertation

zur

Erlangung der Würde eines Doktors der Philosophie

vorgelegt der

Philosophisch-Naturwissenschaftlichen Fakultät

der Universität Basel

von

Sylwia Katarzyna Nowakowska

aus Bytów (Polen)

Basel, 2016

Original document stored on the publication server of the University of Basel <http://edoc.unibas.ch>



This work is licensed under agreement “Attribution Non-Commercial No Derivatives – 3.0 Switzerland”. The complete text may be viewed here:

https://creativecommons.org/licenses/by-nc-nd/3.0/ch/deed.en_US

Genehmigt von der Philosophisch-Naturwissenschaftlichen Fakultät

auf Antrag von:

Prof. Dr. Thomas Jung

Prof. Dr. Catherine E. Housecroft

Basel, 22.03.2016

Prof. Dr. Jörg Schibler

Dekan

*What would the properties of the materials be
if we could really arrange the atoms the way we want them?*

Richard Feynman

Abstract

In this thesis the influence of adsorbates on quantum states and *vice versa* is investigated. The approach taken is that regular porous networks have been produced by means of on-surface self-assembly. Each pore contains a characteristic confined state derived from substrate electrons, thus constituting a quantum box. Importantly, the boxes are electronically coupled with each other, creating quantum box arrays. Here it is shown for the first time that the quantum boxes can be used as nano-beakers offering insight into the condensation atom-by-atom (Chapter [[1]]) and that the quantum states in the boxes can be controllably modified *locally* as well as *globally* by adding adsorbates (Chapter [[2,3]]). The structural characterization of those systems with sub-atomic/sub-molecular resolution was performed by scanning tunnelling microscopy (STM), whereas the electronic properties were investigated by complementary techniques: *locally* by scanning tunneling spectroscopy (STS) and *globally* by angle-resolved photoemission spectroscopy (ARPES).

In Chapter [[1]] the condensation behaviour of xenon in quantum boxes has been investigated in depth. For these studies a quantum box array, formed by a metal-coordinated network of perylene-derived molecules self-assembled on Cu(111), was exposed to xenon. STM studies revealed, that xenon atoms adsorb in the quantum boxes and each occupancy from 1 to 12 is observed. In this way the condensation of xenon has been monitored in an atom-by-atom manner. The analysis of the condensates' structure revealed different sets of 'hierarchical filling rules' governing the condensation in low and high occupancy regimes. It was concluded that the condensation is governed by the subtle interplay of weak interactions occurring with (1) the underlying substrate (registry), (2) the border of the quantum box and (3) the electronic quantum box state. Condensation events in the low occupancy regime, *i.e.* from one to six xenon atoms per pore, occur solely at the border of the pore. In combination with xenon repositioning sequences conclusion has been drawn about the repulsive interaction between xenon and the quantum box state. The occupancy histogram spectacularly revealed the existence of more frequently observed, thus particularly stable occupancies, *i.e.* 'magic' condensates. The detailed evolution of the xenon clustering in the quantum boxes also constitutes a system to evaluate different models for first principle calculations.

In the second study (Chapter [[2]]) the influence of adsorbates on a quantum box state was investigated by dosing and controlled removal of xenon in quantum box arrays formed by a metal-coordinated network of perylene-derived molecules self-assembled on Cu(111). Thus the opposite dependence, *i.e.* how adsorbates influence electronic quantum box state, compared to the first study (Chapter [[1]]) has been studied with the same model system. The occupancy of xenon in the quantum boxes was controlled here by STM repositioning of individual xenon atoms. Remarkably decrementing the xenon occupancy discretely changes the ground state energy of the quantum box, *i.e.* shifts it towards higher binding energies, due to the reduced Pauli repulsion. In this way the electronic states embedded in the array could be configured: xenon-by-xenon. Another important feature investigated is the interaction between neighbouring quantum boxes. By analysing the electronic states in specific patterns of empty and xenon-filled pores unambiguous evidence has been provided that the electronic state in a given quantum box depends also on the electronic states of the surrounding boxes. On the basis of these pioneering investigations and results, a quantum box array can be viewed as a quantum breadboard opening up the possibility of configuring electronic quantum states by combining different adsorbates exerting distinct influence on these states.

Another important property of a quantum box array is the transmission coefficient of the confining barrier describing in this case the probability of an electron to tunnel between the neighbouring quantum boxes, as it determines the strength of the inter-box coupling. In the third study (Chapter [[3]]) it is demonstrated that the transmission coefficient of the barrier can be also modified by adsorbates. Here the investigated quantum array was formed by a porphyrin network held by C–H···F–C interactions self-assembled on Ag(111). This array exhibits the quantum box state above the Fermi level, contrary to the array formed from the metal-coordinated network of perylene-derived molecules self-assembled on Cu(111) (Chapter [[2]]). The existence of the inter-box coupling in the porphyrin array was also confirmed by combined STS/ARPES measurements. Notably, these are the first ARPES studies of a molecular array featuring its confined state above the Fermi level. The porphyrin building block exhibits two different barrier regions, *i.e.* the porphyrin macrocycle and the pentafluorophenyl substituents, which interact differently with the quantum states. To modify the transmission probability of the barrier regions two adsorbates exhibiting characteristically different electronic properties were investigated, *i.e.* xenon and C₆₀ fullerene. The STM revealed two xenon atoms adsorbed on the porphyrin macrocycle and one or two C₆₀ molecules adsorbed in the pore. Xenon interacting with the barrier by weak van der Waals

forces did not detectably affect the transmission probability, while the strong electron acceptor C_{60} reduced the transmission probability significantly. These results demonstrate that the interaction between neighbouring quantum boxes can be tuned by the appropriate selection of adsorbates.

This work established a radically new approach to engineer coupled quantum states in quantum boxes embedded in on-surface porous networks. Moreover, it is shown that the quantum boxes can be used as nano-beakers, offering real-space access to the condensation proceeding under the interplay of weak interactions in an atom-by-atom way.

List of publications / manuscripts

This thesis is based on two first-author publications and one first-author manuscript and is provided in the ‘cumulative’ format. The publications and the manuscript are listed below and are referred in the text by the double square brackets.

[[1]] Interplay of weak interactions in the atom-by-atom condensation of xenon within quantum boxes

S. Nowakowska, A. Wäckerlin, S. Kawai, T. Ivas, J. Nowakowski, S. Fatayer, C. Wäckerlin, T. Nijs, E. Meyer, J. Björk, M. Stöhr, L. H. Gade, T. A. Jung, *Nature Communications* 6, 6071 (2015).

[[2]] Configuring electronic states in an atomically precise breadboard of quantum boxes

S. Nowakowska, A. Wäckerlin, I. Piquero-Zulaica, J. Nowakowski, S. Kawai, C. Wäckerlin, M. Matena, T. Nijs, E. Meyer, S. Fatayer, O. Popova, A. Ahsan, S. F. Mousavi, T. Ivas, E. Meyer, M. Stöhr, J. E. Ortega, J. Björk, L. H. Gade, J. Lobo-Checa, T. A. Jung, *Small* 12, 3757 (2016).

[[3]] Adsorbate-induced modification of the confining barriers in a quantum box array

S. Nowakowska, F. Mazzola, M. Almperti, F. Song, T. Voigt, J. Nowakowski, A. Wäckerlin, C. Wäckerlin, J. Wiss, W. B. Schweizer, M. Broszio, C. Polley, M. Leandersson, S. Fatayer, T. Ivas, S. F. Mousavi, A. Ahsan, T. Nijs, O. Popova, J. Zhang, M. Muntwiler, C. Thilgen, M. Stöhr, F. Diederich, J. Wells, T. A. Jung, *manuscript in review*.

In addition, during my PhD studies I contributed following publications and manuscripts:

- [1] **Van der Waals interactions and the limits of isolated atom models at interfaces**
S. Kawai, A. S. Foster, T. Björkman, S. Nowakowska, J. Björk, F. F. Canova, L. H. Gade, T. A. Jung, E. Meyer, *Nature Communications* 7, 11559 (2016).
- [2] **Probing the Reactivity of Functionalized Surfaces by Porphyrin Metalation**
J. Nowakowski, S. Nowakowska, G. Srivastava, M. Baljovic, J. Girovsky, N. Ballav, T. A. Jung *Chemistry Select* 5, 891-895 (2016).
- [3] **Temperature dependence of the partially localized state in a 2D molecular nanoporous network**
I. Piquero-Zulaica, S. Nowakowska, J.E. Ortega, M. Stöhr, L. H. Gade, T. A. Jung, J. Lobo-Checa, *Applied Surface Science* (2016) doi: 10.1016/j.apsusc.2016.02.227
- [4] **Programmed assembly of 4,2':6',4''-terpyridine derivatives into porous, on-surface networks**
T. Nijs, F. J. Malzner, S. Fatayer, A. Wäckerlin, S. Nowakowska, E. C. Constable, C. E. Housecroft, T. A. Jung, *Chemical Communications* 51, 12297 (2015).
- [5] **Probing the spatial and momentum distribution of confined surface states in a metal coordination network**
J. Zhang, A. Shchyrba, S. Nowakowska, E. Meyer, T. A. Jung, M. Muntwiler, *Chemical Communications* 50, 12289 (2014).
- [6] **Synthesis of trans-A₂B₂- and trans-A₂BC-Porphyrins with Polar 4'-(Dimethylamino)-tolan-4-yl Substituents, and a Screening Protocol for Vapor-Phase Deposition on Metal Surfaces**
M. N. Alberti, S. Nowakowska, J. Nowakowski, M. D. Tzirakis, P. Fesser, W. B. Schweizer, A. Shchyrba, C. Thilgen, T. A. Jung, F. Diederich, *Chemistry – A European Journal*, 5705 (2014).

- [7] **Controlling the dimensionality of on-surface coordination polymers via endo- or exo-ligation**
A. Shchyrba, C. Wäckerlin, J. Nowakowski, S. Nowakowska, J. Björk, S. Fatayer, J. Girovsky, T. Nijs, S. Martens, A. Kleibert, M. Stöhr, N. Ballav, T. A. Jung, L. Gade, *Journal of the American Chemical Society* 136, 9355 (2014).
- [8] **Chirality Transfer in 1D Self-Assemblies: Influence of H-Bonding vs Metal Coordination between Dicyano[7]helicene Enantiomers**
A. Shchyrba, M. T. Nguyen, C. Wäckerlin, S. Martens, S. Nowakowska, T. Ivas, J. Roose, T. Nijs, S. Boz, M. Schär, M. Stöhr, C. A. Pignedoli, C. Thilgen, F. Diederich, D. Passerone, T. A. Jung, *Journal of the American Chemical Society* 135, 15270 (2013).
- [9] **Long-range ferrimagnetic order in a two-dimensional supramolecular Kondo lattice**
J. Girovsky, J. Nowakowski, Md. Ehesan Ali, M. Baljovic, H. R. Rossmann, T. Nijs, E. Aeby, S. Nowakowska, D. Siewert, G. Srivastava, C. Wäckerlin, J. Dreiser, S. Decurtins, Shi-Xia Liu, P. M. Oppeneer, T. A. Jung, N. Ballav, *manuscript submitted*.
- [10] **Supramolecular chessboard array via molecule-specific energy level alignment**
A. Wäckerlin, S. Fatayer, C. Wäckerlin, T. Nijs, S. Nowakowska, T. A. Jung, *manuscript in preparation*.

Contents

Abstract.....	4
List of publications / manuscripts.....	7
Abbreviations and molecules.....	11
Introduction.....	13
Methods.....	18
Scanning tunneling microscopy (STM).....	18
STM repositioning of single atoms/molecules.....	18
Scanning tunneling spectroscopy (STS).....	19
I(z) mapping.....	20
Angle-resolved photoemission spectroscopy (ARPES).....	20
Low-energy electron diffraction (LEED).....	20
Chapter [[1]] and Supplementary Information.....	21
Chapter [[2]] and Supplementary Information.....	32
Chapter [[3]] and Supplementary Information.....	46
Summary and outlook.....	79
Bibliography.....	82
Acknowledgements.....	86

Abbreviations and molecules

General acronyms

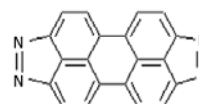
1D	one dimensional
2D	two dimensional
BE	binding energy
BEM	boundary element method
DFT	density functional theory
DOS	density of states
LDOS	local density of states
QD	quantum dot
UHV	ultra-high vacuum

Methods

ARPES	angle-resolved photoemission spectroscopy
LEED	low-energy electron diffraction
STM	scanning tunneling microscopy scanning tunneling microscope
STS	scanning tunneling spectroscopy

Molecules

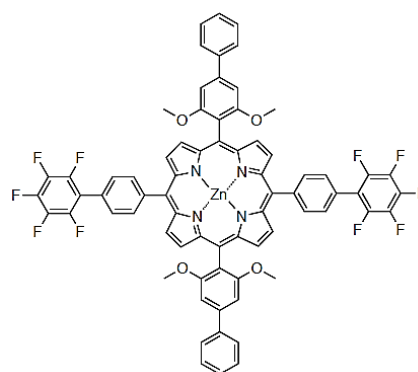
3deh-DPDI triply dehydrogenated 4,9-diaminoperylene quinone-3,10-diimine



C₆₀ Buckminsterfullerene



porphyrin **1**



Introduction

Richard Feynman in his famous lecture *There's plenty of room at the bottom* in 1959 envisioned creating new materials by "*arranging atoms the way we want*".¹ He predicted that this way of fabrication will lead to "*an enormously greater range of possible properties that substances can have*".¹ The concepts presented in Feynman's speech laid foundations of nanotechnology. Indeed, at the nanoscale, materials can exhibit new and fascinating properties as well as phenomena, which are not observed for their equivalents at the macroscale. As soon as one dimension of the material is of the same magnitude as the charge carrier wavelength, i.e. in the nanometer range, quantum confinement takes place. Thus the classical laws of physics have to give way to quantum mechanical rules.²

Nanomaterials are often classified on the basis of the number of dimensions being in the nanometer range. Among the materials having three dimensions at nanoscale, an important group constitute quantum dots². In these materials the 3D quantization of the charge carrier motion leads to discrete energy levels. The size of a quantum dot determines its optoelectronic properties: in case of a semiconductor quantum dot the band gap depends on its chemical composition, shape and size. Hence by adjusting the size of quantum dots, their optical absorption and emission characteristics can be tuned. Owing to that quantum dots are used in many applications including solar cells and light emitting devices.³ Furthermore, a quantum dot confining a single electron, thus exhibiting two spin states, can be used as a qubit for quantum technology. Embedding such quantum dots in an ordered array would allow for the realization of logical operations by changing the inter-dot exchange coupling via gate bias.^{4,5}

The vast majority of quantum dots used for applications consists of $10^2 - 10^3$ atoms.⁶ The commonly used fabrication processes, e.g. physical vapour deposition or colloidal synthesis,² result in a size distribution and thus in undesired variation of their energy levels.⁶ This is why the Feynman's concept of atom-by-atom assembly for quantum dots offers another level of control.

The first step towards its realization was the invention of a scanning tunneling microscope (STM) by G. Binnig and H. Rohrer in 1981⁷. The second step was made nine years later, when D. Eigler and E. K. Schweizer demonstrated that the STM beyond atomic resolution imaging is also capable to reposition single atoms. The scientists used 35 xenon atoms to write “IBM” on Ni(110) surface.⁸ In 1993, a quantum coral was built by precise positioning of 48 iron atoms in a circle on a Cu(111).⁹ The choice of the substrate was of crucial importance, as the noble metals (111) surfaces are characterized by the presence of the electronic Shockley state found only in the topmost atomic layers. This state decays exponentially in bulk and in vacuum but its electrons are free to move along the surface plane, thus creating a quasi 2D electron gas.^{10,11} These surface state electrons are being scattered by step edges or defects^{12–16} as well as by adsorbates like metal atoms or organic molecules^{15,17–20}. Thus, when surrounded by an on-surface structure, the electrons are confined. Therefore the structure is equivalent to a quantum dot. Later other quantum dots, in the form of nanowires^{6,21,22} and other quantum corrals^{23–25}, were built atom-by-atom with the use of STM repositioning.

An essential aspect emerging in the context of application of quantum dots in quantum devices is the modifiable inter-dot coupling. So far the coupling between on-surface quantum dots was tuned by changing the distance between them and by placement of auxiliary adatoms.⁶ Specifically, two nanowires from In atoms on InAs(111)A surface were assembled via STM repositioning sequences. The gradual increase in the spacing between those wires led to progressive decrease of the coupling strength. The coupling was also tuned by placing additional In adatoms in various configurations. However, this fabrication technique is very time consuming and not adequate for the construction of quantum dot architectures, especially not for periodic arrays of quantum dots.

Self-assembly plays a crucial role in the construction of the quantum dot architectures, as the periodic (metal-)organic porous networks are also confining the surface state electrons in their pores, hence acting as quantum dot arrays.^{26–31} In case of a regular Cu-coordinated 3deh-DPDI network grown on Cu(111), the electronic coupling between the pores was evidenced by the formation of an electronic band registered by angle-resolved photoemission spectroscopy (ARPES).²⁶ An essential question, which emerges in the context of the coupling strength between on-surface quantum dots, is how the effective mass of the surface state electrons changes upon the periodic confinement. In reports concerning the 2D modelling of the confinement in porous networks, described in detail in the following, it was assumed that

the effective mass of a confined electron is equal to the effective mass of a surface state electron. In analogy to nanoscale islands^{32–34}, a simple quantum mechanical particle-in-a-box model Eq. (1), which assumes infinitely high potential barriers, was used for the first assessment of the confinement in the pores of on-surface networks^{28,31,35}. However, the network backbones are not impenetrable for the electrons. To compensate for that a new parameter was introduced, namely an effective area.

$$E(k) = E_0 + \frac{\hbar^2}{2m^*} k^2 \quad (1)$$

where

- E_0 - the onset energy of the surface state
- m^* - the effective mass
- \hbar - the reduced Planck constant
- k - the electron wave vector

Furthermore the boundary element method (BEM) was used to reproduce the experimental STS spectra and maps reflecting spectral and lateral distribution of different eigenstates contained in the pores, respectively.^{27,28,36,37} In these calculations an effective scattering potential is ascribed to a molecule (and to an adatom). The simulation is iterated until the right scattering potential(s) is (are) found, *i.e.* an agreement with the experimental data is obtained. The scattering potentials were also calculated by the density functional theory (DFT)²⁹ and the confinement was simulated with the use of iterative finite difference algorithm by developing the wave function in Taylor series³⁸. All these models have three assumptions in common: (i) abrupt potential walls are used; (ii) the confinement phenomenon is assumed to be 2D; (iii) the effective mass of a confined electron is equal to the effective mass of a surface state electron.

Importantly, an ultimate precision of each quantum dot as well as its coupling with the surrounding dots is guaranteed by the self-assembly mechanism. Despite this advantage, the modification of the electronic levels or the inter-dot coupling requires a change of a building block constituting the barrier.^{28,37} This obstacle was overcome by combination of self-assembly and STM repositioning. Seufert *et al.*,³⁷ formed differently arranged patterns of quantum units by creating single-molecule vacancies in ordered self-assembled islands on Ag(111). It was demonstrated that the quantum units embedded in a 2D arrangement

exhibited stronger coupling than those in a 1D arrangement. However, from the point of view of applications a system exhibiting more flexibility would be desired.

Notably, on-surface 2D periodic networks, apart from their ability to confine the surface state electrons, can also trap different adsorbates.^{39–44} In the published studies the interaction between the quantum state localized in the pores and the adsorbates therein was taken into account. This interaction was identified as attractive in case of open-shell Fe atoms and π -acceptor CO molecules adsorbed in the pores of such on-surface networks^{38,45}. However, the *reverse dependence*, i.e. the influence of the adsorbates on the surface derived quantum state, has so far not been addressed.

Before the start of this thesis, it was only known that the binding energy (BE) of the Shockley surface state can be shifted by covering the surface with adsorbates, e.g. the noble gases Ar, Kr, Xe are shifting the surface state to lower BE.^{46–50} This shift is explained in the frame of the Pauli repulsion between the wave functions of the surface and the closed shell of the gases. As a result of it the charge from the exponentially decaying surface state is pushed into the substrate.⁴⁹ Notably, the noble gases are not detectably influencing the effective mass of surface state electrons.⁴⁹

The idea that it might be possible to configure the quantum states embedded in a 2D periodic array via its patterning with adsorbates laid the fundamentals for the research presented in this thesis. The goal was to achieve a flexibly modifiable *quantum breadboard*, in that different adsorbates in various arrangements can be used to modify the electronic states in quantum dots. The challenge to overcome was to find appropriate adsorbates, which have to fulfil four requirements: (i) to adsorb in the pores of the network, (ii) to have an impact on the quantum state (iii) to have an impact on the coupling between the neighbouring pores and (iv) to be manipulable by the STM tip.

In this thesis two systems were studied in detail: a Cu-coordinated 3deh-DPDI network on Cu(111) with xenon (Chapter [[2]]) and a porphyrin network on Ag(111) with xenon and C₆₀ (Chapter [[3]]). Moreover, the first system provided a fascinating possibility to reconstruct the adsorbate condensation atom-by-atom under the interplay of weak interactions with direct real-space access (Chapter [[1]]). This is of utmost importance, given the fundamental role of the adsorption and condensation processes. Owing to the nanoscale size effects such atom-by-atom studies are conceptually desired. Furthermore the *quantum box* provides interplay of weak interactions, thus being much closer to the conditions under which condensation

proceeds in a real environment than the mass spectrometry studies of condensates, in which case these are held by isotropic forces⁵¹⁻⁵⁴.

Methods

This section gives an overview of main experimental techniques used in the research included in this thesis. For structural characterization of on-surface quantum arrays scanning tunneling microscopy (STM) and low-energy electron diffraction (LEED) were used. The electronic states of these arrays were conveniently probed by the combination of scanning tunneling spectroscopy (STS) and angle-resolved photoemission spectroscopy (ARPES). STS allows for the characterization of the *local* electronic structure of quantum units embedded in the array as well as of the barrier regions, while ARPES gives access to the *coherent* part of the interactions between the quantum units of the array. The modification of the electronic structure of quantum units was performed with the use of single atom repositioning sequences. Additionally work function maps with sub-molecular resolution were obtained by means of $I(z)$ mapping.

Scanning tunneling microscopy (STM)

STM is a *local* imaging technique, in which a bias voltage is applied between a sharp tip and a sample. When the distance between these amounts to a few angstroms, the tunneling effect takes place. The resulting tunneling current depends exponentially on the sample-tip distance allowing for an unprecedented vertical resolution in the range of pm. The tip is mounted on a piezoelectric scanner, which scans the sample via line-by-line in-plane movements with sub-angstrom precision. In the constant current mode, a feedback loop is maintaining a constant value of the tunneling current by additional vertical movements of a piezoelectric scanner, which then reflect the contour of local density of states (LDOS). In the constant height mode, the feedback loop is disabled and the scanner moves the tip only vertically. The resulting tunneling current is used for achieving the LDOS contour. More detailed information can be found in Ref [55,56].

STM repositioning of single atoms/molecules

With the STM tip single atoms and molecules can be repositioned.^{8,57,58} Owing to that systems, which cannot be produced by self-assembly, can be studied.^{59,60} As mentioned in the

introduction, one of the most spectacular examples is the first demonstration of on-surface quantum confinement by arranging of 48 Fe atoms to form a corral on Cu(111) followed by the investigation of confined states via STS⁶¹. Further examples include manufacturing of quantum units in the form of atomic chains or differently arranged vacancies in self-assembled molecular domains to investigate the coupling between them.^{6,37}

There are three main modes of STM repositioning: lateral, vertical and inelastic-tunneling induced manipulation.⁶⁰ In the lateral mode the tip is brought to the vicinity of the adsorbate and then moved across the surface to an intended location. Owing to the tip-adsorbate interaction, the adsorbate follows the tip. In the vertical mode the electric field between the tip and the adsorbate causes the adsorbate to jump to the tip. After the transfer to the desired place, the polarity of bias is reversed thus putting the adsorbate back on the surface. The inelastic-tunneling manipulation is performed by injecting/withdrawing electrons from an adsorbate by the tip being above it, thus inducing excitation, which results in movement of the adsorbate.

The manipulation experiments presented in this thesis were performed in the vertical repositioning mode, as moving Xe atoms across the barriers, between the pores of a metal-organic network was required. Moreover this manipulation mode allows to decorate the STM tip with single Xe atom leading to a very well-defined tip geometry and electronic structure thus increasing significantly the STM lateral resolution. Owing to this atomic resolution was obtained on Xe condensates [[1,2]].

Scanning tunneling spectroscopy (STS)

STS is a *local* spectroscopic technique in which the tip is placed above a measured object, the bias voltage is swept and a derivative of the tunneling current, i.e. dI/dV signal, is recorded via lock-in technique. The dI/dV signal is approximately proportional to the sample density of states (DOS). In addition to its locality the advantage of this technique is its ability to probe occupied as well as unoccupied states, which is not possible in angle-resolved photoemission spectroscopy (ARPES), see below. For more details see Ref [55,56].

I(z) mapping

The work function maps presented in [[3]] were extracted from a grid spectroscopy measurement, in which at each point three I(z) curves were measured. From an exponent fit of the average curve, the work function was extracted for each point. This method was developed by Vitali *et. al.*,⁶²

Angle-resolved photoemission spectroscopy (ARPES)

In ARPES, the sample is irradiated with photons leading to the emission of electrons. The angular distribution of the kinetic energy of the electrons leaving the sample is measured and recalculated to energy vs momentum ($E(\vec{k})$) dependence, thus providing information on the band structure of solids. The ARPES signal comprises both: bulk and surface contributions. The latter makes ARPES a perfect technique for investigation of the surface states and their modifications upon confinement⁶³[[1-2]]. In contrast to STS, ARPES is a surface averaging technique thus granting access to the coherent part of the interactions between the partially localized states. On the other hand STS is a \vec{k} averaging technique. For more details see Ref. [64].

Low-energy electron diffraction (LEED)

In LEED experiments, electrons are diffracted from the sample and create a pattern on a fluorescent screen, which directly corresponds to the reciprocal lattice of the sample. Owing to the short mean free path of low-energy electrons in the order of few atomic layers, LEED is a surface-sensitive technique. Thus the information about the crystallographic orientation of the surface, its reconstruction and the adsorbate superstructure is obtained. This technique is very convenient for the determination of the unit cell of a self-assembled (metal-)organic (sub-)monolayer and its orientation with respect to the substrate unit cell. More information about LEED can be found in Ref. [11,65].

Chapter [[1]] and Supplementary Information

[[1]] **Interplay of weak interactions in the atom-by-atom condensation of xenon within quantum boxes**

S. Nowakowska, A. Wäckerlin, S. Kawai, T. Ivas, J. Nowakowski, S. Fatayer, C. Wäckerlin, T. Nijs, E. Meyer, J. Björk, M. Stöhr, L. H. Gade, T. A. Jung, *Nature Communications* 6, 6071 (2015).

Contribution of S. Nowakowska: carried out experimental investigations (STM), analysed and interpreted the data, wrote the manuscript.

Press release: <https://www.unibas.ch/en/News-Events/News/Uni-Research/Nano-Beaker-Offers-Insight-Into-the-Condensation-of-Atoms.html>

This publication is used in accordance with Creative Commons CC-BY licence.
<http://www.nature.com/ncomms/2015/150121/ncomms7071/full/ncomms7071.html>

ARTICLE

Received 25 Sep 2014 | Accepted 9 Dec 2014 | Published 21 Jan 2015

DOI: 10.1038/ncomms7071

OPEN

Interplay of weak interactions in the atom-by-atom condensation of xenon within quantum boxes

Sylwia Nowakowska¹, Aneliia Wäckerlin¹, Shigeki Kawai^{1,2}, Toni Ivas^{1,†}, Jan Nowakowski³, Shadi Fatayer^{1,4}, Christian Wäckerlin^{3,†}, Thomas Nijs¹, Ernst Meyer¹, Jonas Björk⁵, Meike Stöhr⁶, Lutz H. Gade⁷ & Thomas A. Jung³

Condensation processes are of key importance in nature and play a fundamental role in chemistry and physics. Owing to size effects at the nanoscale, it is conceptually desired to experimentally probe the dependence of condensate structure on the number of constituents one by one. Here we present an approach to study a condensation process atom-by-atom with the scanning tunnelling microscope, which provides a direct real-space access with atomic precision to the aggregates formed in atomically defined 'quantum boxes'. Our analysis reveals the subtle interplay of competing directional and nondirectional interactions in the emergence of structure and provides unprecedented input for the structural comparison with quantum mechanical models. This approach focuses on—but is not limited to—the model case of xenon condensation and goes significantly beyond the well-established statistical size analysis of clusters in atomic or molecular beams by mass spectrometry.

¹Department of Physics, University of Basel, Klingelbergstrasse 82, 4056 Basel, Switzerland. ²PRESTO, Japan Science and Technology Agency (JST), 4-1-8 Honcho, Kawaguchi, Saitama 332-0012, Japan. ³Laboratory for Micro- and Nanotechnology, Paul Scherrer Institute, 5232 Villigen PSI, Switzerland. ⁴Departamento de Física Aplicada, Instituto de Física Gleb Wataghin, Universidade Estadual de Campinas, Campinas 13083-859, Brazil. ⁵Department of Physics, Chemistry and Biology, IFM, Linköping University, Linköping 581 83, Sweden. ⁶Zernike Institute for Advanced Materials, University of Groningen, Nijenborgh 4, 9747 AG Groningen, The Netherlands. ⁷Anorganisch-Chemisches Institut, Universität Heidelberg, Im Neuenheimer Feld 270, 69120 Heidelberg, Germany. † Present addresses: Empa, Swiss Federal Laboratories for Materials Science and Technology, Überlandstrasse 129, CH-8600 Dübendorf, Switzerland (T.I.); Institute of Condensed Matter Physics (ICMP), Ecole Polytechnique Fédérale de Lausanne (EPFL), Station 3, CH-1015 Switzerland (C.W.). Correspondence and requests for materials should be addressed to S.N. (email: sylwia.nowakowska@unibas.ch) or to L.H.G. (lutz.gade@uni-hd.de) or to T.A.J. (thomas.jung@psi.ch).

Condensation is a fundamental process, and the interactions involved in the aggregation of atoms or molecules govern the structure of condensates^{1,2}. Moreover, at the nanoscale level the properties of a condensate depend on its size, structure and bonding between the atoms or molecules. Although the analysis of noble gas condensates of different sizes, interacting by isotropic van der Waals forces, has provided valuable insight into the mechanisms of particle clustering^{3–6}, the condensation in a real environment usually proceeds under the competing influence of weak forces.

In order to take an interplay of such forces into account in a model condensation process, we chose a nanopatterned vacuum/solid interface, which not only provides the competition between interparticle forces and interactions with a surface^{7–10} but may also give rise to a more complex interplay of forces^{11–13}, which, as we observe, governs the emergence of structural patterns. We demonstrate how the atom-by-atom condensation of noble gas atoms proceeds under the influence of competing interactions. This is conveniently probed within the atomically defined cavities of a supramolecular network, generated on the metal substrate. This approach is based on the ability of such on-surface networks to trap different adsorbates and thus to create host-guest systems^{14–20}.

Results

Design of the host-guest system. We employ a highly ordered Cu-coordinated, triply dehydrogenated 4,9-diaminoperylene quinone-3,10-diimine (3deh-DPDI) porous network grown on Cu(111)^{21,22} as a template. The electronic Shockley surface state of the underlying substrate is confined in the pores²³, resulting in a single quantum well state per pore with the spatial $|\Psi|^2$ maximum in its centre (Fig. 1a–c) and thus in a specific electronic environment in each pore. As a model condensate we choose Xe atoms, which provide an ideal probe of the weak interactions because of their closed-shell electronic configuration.

Repositioning sequences of single Xe atoms. Upon deposition of Xe onto the structured surface, the pores of the network were found to host different numbers of Xe atoms, as revealed in the scanning tunnelling microscopy (STM) image shown in Fig. 1d. Notably, no single Xe atom was observed to adsorb spontaneously in the centre of a pore. To investigate whether it was possible to place a single Xe atom at this position, we performed repositioning sequences as displayed in Fig. 1e–g. In each sequence the tip was first decorated with a single Xe atom and then placed above the pore centre where its deposition was performed. Despite numerous attempts to place the Xe atom in the pore centre, none was successful. Each attempt resulted in the diffusion of the Xe atom to the border of the pore (Fig. 1f) or even in its displacement to a neighbouring pore (Fig. 1g). We assign this behaviour to the Pauli repulsion⁹ between the Xe atoms and the quantum well ground state of the pore. This contrasts with the observation made for open-shell Fe atoms and the π -acceptor CO molecules adsorbed in the pores of supramolecular networks grown on Cu(111), which experienced an attractive interaction with the quantum well state^{24,25}.

Spontaneously occurring Xe condensates. The spontaneously occurring occupancies ranging from 0 to 12 Xe atoms (denoted hereafter as **occ-0**–**occ-12**) were found across the pores of the network. Figure 2 presents the various spatial arrangements of Xe atoms, with two different forms of aggregation being observed for **occ-2**, **occ-5** and **occ-7**. The histogram of pore occupancy (Fig. 2) reveals the presence of favoured occupancies, which may be related to particularly stable condensates. The most favoured

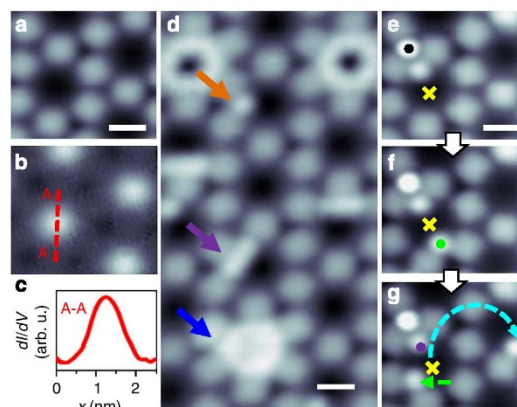


Figure 1 | Repulsive interaction between Xe and the electronic quantum well state. (a) STM image of the vacant network and (b) simultaneously acquired dI/dV map taken at the energy of the confined state: -200 meV (the bright colour reflects a local density of states maximum). (c) The cross-section taken along the red line showing the spatial distribution of the confined state. (d) STM image of Xe adsorbed in some pores after exposure to 120 L (Langmuir) of Xe at 9 K: a pore hosting a single Xe atom (orange arrow), a partially filled pore (violet arrow) and a fully filled pore (dark-blue arrow). (e–g) Subsequent STM images acquired during a sequence of Xe-repositioning experiments targeted at the addition of Xe atoms one by one to the same pore, demonstrating the repulsion between Xe and the confined state. The Xe-decorated tip was placed above the pore centre during each attempt to deposit Xe (yellow cross); (f) the first attempt of the shown sequence resulted in the migration of a Xe atom (green dot) to the pore boundary, whereas (g) the second in the diffusion of one of the Xe atoms to an unoccupied corner of the pore (green arrow) and in the jump of the other Xe atom to a neighbouring pore (blue dashed arrow). The black dot in e marks Xe adsorbed on the node of the network (Supplementary Fig. 2). All scale bars: 1 nm.

occupancies are **occ-1** and **occ-12**, whereas condensates with greater occupancies (**occ-6**–**occ-11**) were less frequently observed. We note that **occ-3** and **occ-4** occur more frequently than **occ-2**, and that there is a slight preference for **occ-8**, indicating an increased stability of multiples of a tetrameric arrangement. In contrast, the occupancy of Fe adatoms inside pores of an organic on-surface network mentioned above was found to correspond to a Poisson distribution²⁴, further accentuating the fundamental differences between (open shell) metal atom condensation and noble gas condensation in somewhat related porous confinements, both of which exhibit a quantum well state (cf. Supplementary Fig. 1).

Discussion

For an analysis of the self-assembled patterns of Xe atoms within the pores, a closer inspection of the metal-organic surface structure is essential. Each pore of the network possesses threefold symmetry because of the inequivalence of its nodes. The node labelled **A** in the schematic representation of an **occ-12** pore (Fig. 2) is centred above a hollow surface site, whereas the node **B** is centred above an on-top site of a surface atom²². Three different adsorption sites of Xe are identified: one in the inner pore (which is only occupied for **occ-7b** and larger) and two at the pore boundary either near the organic network molecule or in the vicinity of node **A**. The sites next to node **B** are never occupied in the **occ-12** condensates, and therefore the Xe

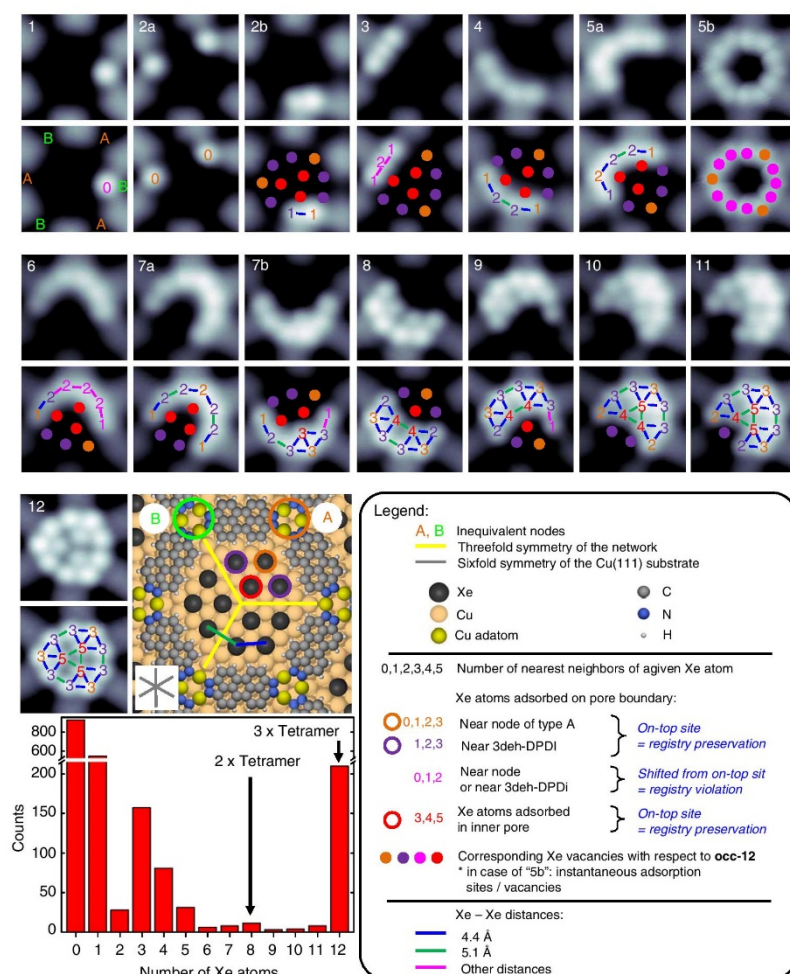


Figure 2 | Atom-by-atom self-assembly of Xe within quantum boxes influenced by the interplay of directional weak interactions. Pores with different numbers of adsorbed Xe atoms are indicated by the numbers placed in the left upper corner of each STM image (2.4 nm × 2.4 nm); letters are used to denominate condensates with the same number of Xe atoms but having different arrangements. As a guide to the eye, a colour code that defines the adsorption position and the number of nearest neighbours is used and is defined in the legend. In the bottom left corner, the histogram of the occupancy of the pores obtained from one sample exposed to 120 L of Xe at 9 K, resulting in a coverage $\Theta = 0.178$ (cf. Supplementary Note 1), is displayed (2,067 pores have been analysed).

adsorption reflects the threefold rotational symmetry of the pores as indicated by the three yellow lines in the schematic **occ-12** model in Fig. 2. In agreement with this, each **occ-12** condensate consists of three tetramers, with Xe atoms adsorbed in on-top sites of the Cu(111) atomic lattice in a $(\sqrt{3} \times \sqrt{3})R30^\circ$ overlayer structure, in accordance with previous studies of Xe on Cu(111)^{26,27}.

For the classification of the structural arrangements of the **occ-*n*** inside the pores, we initially focus on two aspects: first, whether a certain *n*-mer exhibits a subset of the adsorption sites observed for the **occ-12**, meaning that the $(\sqrt{3} \times \sqrt{3})R30^\circ$ structure, exhibited by each tetramer of **occ-12**, is preserved, and second, whether the considered **occ-*n*** can be described either as **occ-*(n-1)*** with one additional Xe atom, or as superposition of

condensate structures observed for lower occupancies. Focusing on the first aspect, we find that only condensates **occ-2b**, **occ-5a**, **occ-7a**, **occ-8**, **occ-10** and **occ-11** are always congruent with the registry of the **occ-12**. The other condensates (partially) violate the registry of the dodecamer (Figs 2 and 3, Table 1), implying that the interaction of a single Xe atom with the backbone of the organic network is sufficient to cause the Xe atom to occupy a slightly less favourable adsorption site. Moreover, the modified quantum well state may also have an impact on the favourability of the adsorption sites of Xe atoms. Furthermore, the observed registry violations retain or decrease the Xe–Xe distance, indicating an equal or increased Xe–Xe condensation energy as compared with the corresponding positions identified for **occ-12** (Figs 2 and 3).

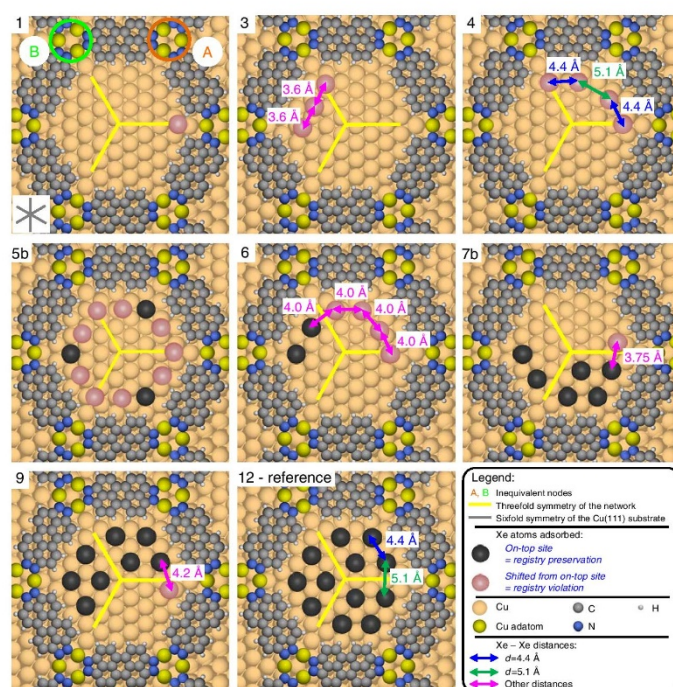


Figure 3 | Registry violation observed in Xe self-assembly within quantum boxes. Tentative models of the **occ-*n*** exhibiting registry violation (the **occ-*n*** labelling is consistent with the one presented in Fig. 2. A colour code is defined in the legend). In case of **occ-1** the single Xe atom was found to be adsorbed near both types of nodes with a slight preference for the node of type **B** (57%; Table 1). As in the proximity of this type of node no on-top site is available, the adsorption site of a Xe atom in this case is shifted to the hollow site. The same phenomenon is observed for **occ-2a**. Important to note is that the distance of ~ 3 Å between Xe and hydrogen of 3deh-DPDI is the same in both cases (adsorption near node **A** and near node **B**), implying that the proximity with the backbone can modify the Xe adsorption site. We tentatively assign this preference of Xe to adsorb in the vicinity of node **B** to be caused by the inequality of the nodes, which leads to slightly different strengths of the Xe–H interaction. In case of **occ-3**, **occ-6**, **occ-7b** and **occ-9**, a registry violation is always observed for one, three or four Xe atoms (cf. Fig. 2, Table 1).

With the second aspect brought into focus, namely the relationship between **occ-*n*** and its predecessors in the hierarchy, our analysis shows that only condensates **occ-2**, **occ-5a**, **occ-9**, **occ-11** and **occ-12** feature the same arrangement of adsorption sites as their corresponding **occ-(*n*-1)** condensates. In fact, they derive from their predecessor by having one additional adsorption site occupied. Only condensates **occ-2a**, **occ-4** and **occ-7a** can be described by a superposition of condensates observed at lower occupancies. Moreover, all observed condensates were found to be stable with the exception of **occ-5b** in which five Xe atoms are sharing 12 adsorption sites along the rim of the pore and exhibit rapid site exchange (Fig. 2; the number of Xe atoms in this condensate was identified from Xe-repositioning sequences).

In summary, the atom-by-atom condensation of Xe in the pores of the Cu-coordinated 3deh-DPDI network results in a wide range of occupancies (**occ-1**—**occ-12**), which do not follow a single set of ‘hierarchical filling rules’²⁵, but adapt their structures in the different regimes. This work demonstrates that the confinement of adsorbates in the pores of a metal–organic on-surface network provides the opportunity to study condensation under the influence of the subtle interplay of weak forces with single-atom precision. The experimental resolution providing the real-space structure of atomic condensates adsorbed on an atomically defined patterned surface provides the unique opportunity to compare experimental data and theoretical


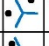



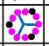
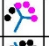
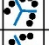
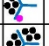
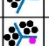



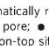
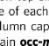
models. We note that our approach can benefit from the comparison of the condensation behaviour in differently sized pores, as owing to that, the interference of weak interactions involved can be tuned, which is expected to be stronger/weaker with decreasing/increasing pore size.

Methods

Sample preparation. The samples were prepared and investigated in an ultrahigh vacuum system with a base pressure of 5×10^{-11} mbar. The Cu(111) crystal (MaTeck GmbH) was prepared by cycles of Ar^+ sputtering at $E = 1,000$ eV performed at room temperature followed by annealing at 800 K. The DPDI molecules were deposited with the use of nine-cell commercial evaporator (Kentax, GmbH, Germany) on the Cu(111) by sublimation at ~ 240 °C. The rate was controlled before deposition by a quartz crystal microbalance. After deposition, the sample was annealed to 300 °C in order to convert DPDI into 3deh-DPDI, which creates the Cu-coordinated network²¹. Xe of purity 99.99% was dosed to the sample placed in the STM (Omicron Nanotechnology GmbH) operated at 4.2 K, with the cryoshields open and the leak valve being in line-of-sight with the sample. Supplementary Fig. 2 presents STM data acquired after exposure of the Cu-coordinated 3deh-DPDI network to 20 L of Xe performed at a pressure equal to 1.3×10^{-7} mbar for 200 s causing the increase in the sample temperature to 8 K. Xe was found to be adsorbed in the pores as well as in the nodes of the network. Figure 1d and the histogram in Fig. 2 present data after a 120-L exposure at the same pressure for 1,200 s resulting in the increase in the sample temperature to 9 K. Only Xe adsorbed in the pores was found.

Repositioning sequences of single Xe atoms. All the self-assembled condensates, except of **occ-2b**, were reproduced with the use of repositioning

Table 1 | Condensation regimes of Xe adsorbed in the pores of the Cu-coordinated 3deh-DPDI network.

Condensation regimes	occ-n	Registry preservation?	occ-(n-1) + Xe or superposition?	Xe-Xe #
Single atom(s)	1	 43% 57% ✗ (1)	n/a	0
	2a 25%	 44% 56% ✗ (1 + 2)	(1 + 1)	0
Condensation	2b 75%	 ✓	(1* + ●)	1
Chain condensation	3	 ✗ (3)	✗	2
	4	 85% 15% ✗ (4)	85% ✓ (2b + 2b)	3
	5a 37%	 ✓	(4* + ●)	4
Mobile ring	5b 63%	 ✗ (9)	✗	?
Chain condensation	6	 ✗ (4)	(2b + ● + ● + ● + ●)	5
	7a 25%	 ✓	(5a + 2b)	6
2D condensation in tetrameric units and subunits	7b 75%	 ✗ (1)	(2b + ● + ● + ●)	8
	8	 ✓	(● + ● + ● + ●)	12
	9	 ✗ (1)	(● + ● + ● + ●)	13
	10	 ✓	(● + ● + ● + ●)	16
	11	 ✓	(● + ● + ● + ●)	18
12	 ✓	(● + ● + ● + ●)	21	

The column 'occ-n' schematically represents each condensate; the blue lines indicate the threefold symmetry of the pore: ● marks a Xe atom adsorbed in an on-top site; ● marks a Xe atom not adsorbed in an on-top site; in case two different structures occur for the same occupancy, the occurrence of each is stated in percent. The signs ✓ and ✗ indicate, if the condition stated in the column caption is fulfilled. The column 'Registry preservation?' lists whether Xe atoms of certain 'occ-n' preserve the $(\sqrt{3} \times \sqrt{3})R30^\circ$ structure exhibited by each tetramer of 'occ-12'. If only a part of the observed 'occ-n' of concern preserves the registry, their occurrence in percent is given; red numbers in brackets indicate the number of Xe atoms, which are not adsorbed in on-top sites. The column 'occ-(n-1) + Xe or superposition?' relates the structure of each condensate to its predecessors in the hierarchy by taking into consideration the registry of the underlying Cu(111); *marks an 'occ-(n-1)' without registry violation (for example, 'occ-2b' can be described as the sum of one Xe adsorbed near node A, that is, 'occ-1' without registry violation, and one Xe atom adsorbed in on-top site). ● indicates Xe atoms arranged in a trimer; ● indicates Xe atoms arranged in a tetramer. The column 'Xe-Xe #' lists the number of interactions between two Xe atoms independently of the interatomic distances.

sequences, by taking away Xe atoms from the 12-fold occupied pore as these are represented in Fig. 2. The difficulty in reproducing 'occ-2b' can be connected with increased stability of 'occ-3', as revealed by the histogram of pore occupancy (Fig. 2). To perform Xe manipulations in a reproducible manner, a home-written Labview software compatible with the Nanonis SPM control system (Specs GmbH) was used. To pick up a single Xe atom, in the first step the sample bias was set to -2 mV and the tip was moved towards the atom until a not-continuous change in the resistance of the tunnelling junction occurred. Then the tip was retracted. To place a Xe atom in a desired place, the sample bias was set to 800 mV and the procedure was repeated.

STM measurements and data analysis. STM measurements were performed in the constant current mode with Pt-Ir tips (90% Pt, 10% Ir), prepared by mechanical cutting followed by sputtering and controlled indentation in the bare Cu(111). The STM images shown in Fig. 1a,b were acquired with such prepared metallic tip, whereas the others with additionally Xe-decorated tips, which allowed achieving atomic resolution on Xe condensates (Supplementary Fig. 3). The STM image with the simultaneously acquired dI/dV map, shown in Fig. 1a,b, was measured with -200 mV/200 pA and with a lock-in frequency of 512 Hz and a zero-to-peak value of 8 mV. To avoid modification of the condensates via interaction with the tip, the sample bias was selected within a range of -10 to -80 mV, whereas the tunnelling current was set within the range 5–50 pA. The exact tunnelling parameters of STM images presented in the main text are as follows: -10 mV/10 pA (Fig. 2, 'occ-3', 'occ-5b', 'occ-9', 'occ-10'), -10 mV/20 pA (Fig. 2, 'occ-11'), -10 mV/50 pA (Fig. 2, 'occ-1', 'occ-8', 'occ-12'), -20 mV/5 pA (Fig. 2, 'occ-7b'), -20 mV/10 pA (Fig. 2, 'occ-2a'), -50 mV/5 pA (Fig. 2, 'occ-6'),

-50 mV/10 pA (Figs 1d and 2, 'occ-2b', 'occ-4', 'occ-7a'), -80 mV/5 pA (Fig. 2, 'occ-5a'), -200 mV/80 pA (Fig. 1e) and -500 mV/50 pA (Fig. 1f,g). The STM data were processed with the WSxM software²⁸. For better comparability of the data, the colour histograms have been adjusted. Low-pass filtering was used for noise reduction.

References

- Lennard-Jones, J. E. On the forces between atoms and ions. *Proc. R. Soc. A* **109**, 584–597 (1925).
- Jansen, J. & Dawson, L. M. On intermolecular forces and the crystal structures of the rare gases. *J. Chem. Phys.* **23**, 482–486 (2004).
- Dehmer, P. M. & Dehmer, J. L. Photoelectron spectrum of Xe₂ and potential energy curves for Xe²⁺. *J. Chem. Phys.* **68**, 3462–3470 (1978).
- Poliakoff, E. D., Dehmer, P. M., Dehmer, J. L. & Stockbauer, R. The photoelectron spectrum of Xe₃ by the photoelectron-photoion coincidence technique. *J. Chem. Phys.* **75**, 1568–1569 (1981).
- Echt, O., Sattler, K. & Recknagel, E. Magic numbers for sphere packings: experimental verification in free xenon clusters. *Phys. Rev. Lett.* **47**, 1121–1124 (1981).
- Tschaplyguine, M., Öhrwall, G. & Björneholm, O. in *Handbook of Nanophysics: Clusters and Fullerenes 2* (CRC Press, 2011).
- Sullivan, D. E. Van der Waals model of adsorption. *Phys. Rev. B* **20**, 3991–4000 (1979).
- Park, J.-Y. *et al.* Adsorption and growth of Xe adlayers on the Cu(111) surface. *Phys. Rev. B* **60**, 16934–16940 (1999).
- Forster, F., Hüfner, S. & Reinert, F. Rare gases on noble-metal surfaces: an angle-resolved photoemission study with high energy resolution. *J. Phys. Chem. B* **108**, 14692–14698 (2004).
- Chang, C.-S., Chiu, Y.-P., Su, W.-B. & Tsong, T.-T. in *Handbook of Nanophysics: Clusters and Fullerenes 2* (CRC Press, 2011).
- Joshi, S. *et al.* Control of molecular organization and energy level alignment by an electronically nanopatterned boron nitride template. *ACS Nano* **8**, 430–442 (2014).
- Widmer, R., Passerone, D., Mattle, T., Sachdev, H. & Gröning, O. Probing the selectivity of a nanostructured surface by xenon adsorption. *Nanoscale* **2**, 502–508 (2010).
- Dil, H. *et al.* Surface trapping of atoms and molecules with dipole rings. *Science* **319**, 1824–1826 (2008).
- Theobald, J. A., Oxtoby, N. S., Phillips, M. A., Champness, N. R. & Beton, P. H. Controlling molecular deposition and layer structure with supramolecular surface assemblies. *Nature* **424**, 1029–1031 (2003).
- Stepanov, S. *et al.* Steering molecular organization and host-guest interactions using two-dimensional nanoporous coordination systems. *Nat. Mater.* **3**, 229–233 (2004).
- Barth, J. V., Costantini, G. & Kern, K. Engineering atomic and molecular nanostructures at surfaces. *Nature* **437**, 671–679 (2005).
- Stöhr, M., Wahl, M., Spillmann, H., Gade, L. H. & Jung, T. A. Lateral manipulation for the positioning of molecular guests within the confinements of a highly stable self-assembled organic surface network. *Small* **3**, 1336–1340 (2007).
- Wahl, M., Stöhr, M., Spillmann, H., Jung, T. A. & Gade, L. H. Rotation-libration in a hierarchic supramolecular rotor-stator system: Arrhenius activation and retardation by local interaction. *Chem. Commun.* **7**, 1349–1350 (2007).
- Bartels, L. Tailoring molecular layers at metal surfaces. *Nat. Chem.* **2**, 87–95 (2010).
- Cheng, Z. *et al.* Power of confinement: adsorbate dynamics on nanometer-scale exposed facets. *Nano. Lett.* **10**, 3700–3703 (2010).
- Shchyrba, A. *et al.* Controlling the dimensionality of on-surface coordination polymers via endo- or exo-ligation. *J. Am. Chem. Soc.* **136**, 9355–9363 (2014).
- Matena, M. *et al.* On-surface synthesis of a two-dimensional porous coordination network: unraveling adsorbate interactions. *Phys. Rev. B* **90**, 125408 (2014).
- Lobo-Checa, J. *et al.* Band formation from coupled quantum dots formed by a nanoporous network on a copper surface. *Science* **325**, 300–303 (2009).
- Pivetta, M., Pacchioni, G. E., Schlickum, U., Barth, J. V. & Brune, H. Formation of Fe cluster superlattice in a metal-organic quantum-box network. *Phys. Rev. Lett.* **110**, 086102 (2013).
- Cheng, Z. *et al.* Adsorbates in a box: titration of substrate electronic states. *Phys. Rev. Lett.* **105**, 066104 (2010).
- Chesters, M. A., Hussain, M. & Pritchard, J. Xenon monolayer structures on copper and silver. *Surf. Sci.* **35**, 161–171 (1973).
- Seyller, T., Caragiu, M., Diehl, R. D., Kaukasoina, P. & Lindroos, M. Observation of top-site adsorption for Xe on Cu(111). *Chem. Phys. Lett.* **291**, 567–572 (1998).
- Horcas, I. *et al.* WSxM: A software for scanning probe microscopy and a tool for nanotechnology. *Rev. Sci. Instrum.* **78**, 013705 (2007).

Acknowledgements

We would like to acknowledge the financial support from the National Centre of Competence in Research 'Nanoscience' (NCCR-Nano), Swiss Nanoscience Institute (SNI), Swiss National Science Foundation (grants no. 200020-149713, 206021-121461), the São Paulo Research Foundation (grant no. 2013/04855-0), Netherlands Organisation for Scientific Research NWO (Chemical Sciences, VIDI-grant no. 700.10.424), the European Research Council (ERC-2012-StG 307760-SURFPRO), University of Basel, University of Heidelberg, Linköping University, University of Groningen, Paul Scherrer Institute and the Japan Science and Technology Agency (JST) 'Precursory Research for Embryonic Science and Technology (PRESTO)' for a project of 'Molecular technology and creation of new function'. We sincerely thank Marco Martina, Rémy Pawlak and Alexander Bubendorf for the support during measurements, as well as Gerhard Meyer, Silvia Schintke, Jorge Lobo-Checa, Manfred Matena and Miloš Baljović for helpful discussions.

Author contributions

S.N., A.W., S.K., T.I., J.N., S.F., C.W. and T.N. conducted the STM measurements and analysed the data under the supervision of T.A.J., L.H.G., M.S. and E.M.; J.B. and T.I. provided theoretical models; S.N., T.A.J. and L.H.G. wrote the manuscript.

Additional information

Supplementary Information accompanies this paper at <http://www.nature.com/naturecommunications>

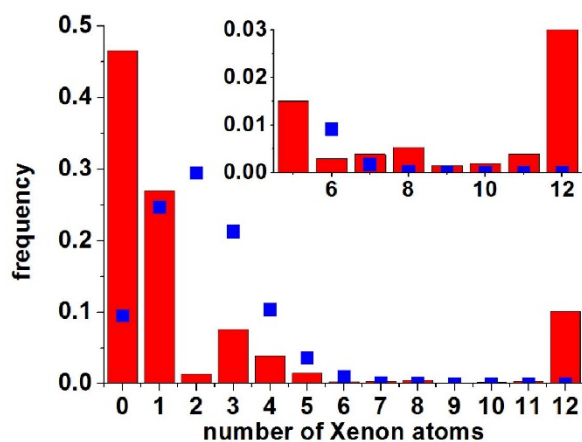
Competing financial interests: The authors declare no competing financial interests.

Reprints and permission information is available online at <http://npg.nature.com/reprintsandpermissions/>

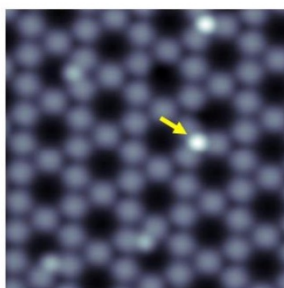
How to cite this article: Nowakowska, S. *et al.* Interplay of weak interactions in the atom-by-atom condensation of xenon within quantum boxes. *Nat. Commun.* 6:6071 doi: 10.1038/ncomms7071 (2015).



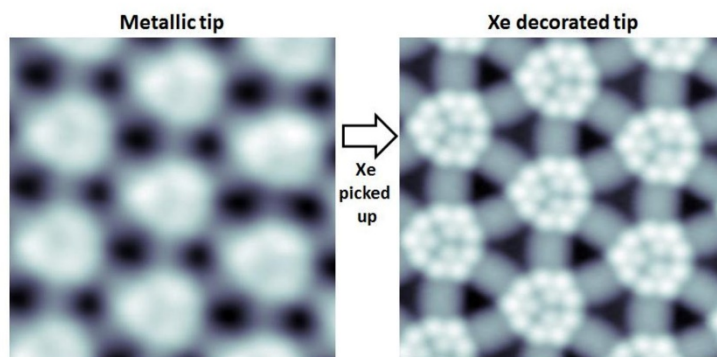
This work is licensed under a Creative Commons Attribution 4.0 International License. The images or other third party material in this article are included in the article's Creative Commons license, unless indicated otherwise in the credit line; if the material is not included under the Creative Commons license, users will need to obtain permission from the license holder to reproduce the material. To view a copy of this license, visit <http://creativecommons.org/licenses/by/4.0/>



Supplementary Figure 1 | The comparison of the frequency histogram of the occupancy of the pores obtained from the sample exposed to 120 L of Xe at 9 K, resulting in a coverage of $\Theta=0.178$ (red bars), with the binomial distribution for this coverage value (blue squares). Clearly, $occ-n$ do not follow a statistical distribution.



Supplementary Figure 2 | Adsorption of Xe on the nodes and in the pores of the Cu-coordinated 3deh-DPDI network; STM image of the network after exposure to 20 L of Xe during which the sample temperature did not exceed 8 K. In addition to Xe adsorbed in the pores, single Xe atoms were found to adsorb on the nodes of the network as indicated by the yellow arrow (10 nm x 10 nm; tunneling parameters: -1 V/10 pA; metallic tip). On the contrary, after Xe exposure at higher sample temperature (9 K) Xe was only found to be adsorbed in the pores, which points at a temperature dependent site selectivity of Xe adsorption.



Supplementary Figure 3 | Comparison of the STM contrast of Xe condensates acquired with a metallic and a Xe decorated tip (6 nm x 6 nm; tunneling parameters: 10 mV/50 pA). By warming up the sample (Cu-coordinated 3deh-DPDI on Cu(111) + 120 L of Xe) to 45 K followed by cooling to 5 K for STM measurements all pores could be filled with 12 Xe atoms due to the diffusion of Xe from the islands grown around the network domains. This is in line with the study of Park et al., [Ref.1] who reported that above 25 K the diffusion of Xe on Cu(111) occurs. Moreover, Xe atoms have been employed for a functionalization of STM tips for high resolution imaging.²

Supplementary Note 1

The coverage (Θ) of Xe in the pores of the Cu-coordinated 3-deh DPDI network was calculated in a following way:

$$\Theta = \frac{N}{a \cdot n}$$

N – total number of Xe atoms adsorbed in the pores;

a – number of adsorption sites per one pore;

n – total number of pores;

The binomial distribution, determined according to Ref. [3], for the $\Theta=0.178$ (sample exposed to 120 L of Xe at 9 K) is displayed in Fig. 2 together with the experimentally obtained frequency histogram. Clearly, the **occ- n** do not follow a binomial distribution, which means that Xe atoms are able to diffuse from pore to pore before being cooled down to 4.2 K for the STM measurements.

Supplementary References

1 Park, J.-Y. *et al.* Adsorption and growth of Xe adlayers on the Cu(111) surface. *Phys. Rev. B* **60**, 16934–16940 (1999).

2 Kichin, G., Weiss, C., Wagner, C., Tautz, F. S. & Temirov, R. Single Molecule and Single Atom Sensors for Atomic Resolution Imaging of Chemically Complex Surfaces. *J. Am. Chem. Soc.* **133**, 16847–16851 (2011).

3 Pivetta, M., Pacchioni, G. E., Schlickum, U., Barth, J. V. & Brune, H. Formation of Fe Cluster Superlattice in a Metal-Organic Quantum-Box Network. *Phys. Rev. Lett.* **110**, 086102 (2013).

Chapter [[2]] and Supplementary Information

[[2]] **Configuring electronic states in an atomically precise breadboard of quantum boxes**

S. Nowakowska, A. Wäckerlin, I. Piquero-Zulaica, J. Nowakowski, S. Kawai, C. Wäckerlin, M. Matena, T. Nijs, E. Meyer, S. Fatayer, O. Popova, A. Ahsan, S. F. Mousavi, T. Ivas, E. Meyer, M. Stöhr, J. E. Ortega, J. Björk, L. H. Gade, J. Lobo-Checa, T. A. Jung, *Small* 12, 3757 (2016).

Contribution of S. Nowakowska: carried out experimental investigations (STM/STS, ARPES), analysed and interpreted the data (STM/STS), wrote the manuscript.

Press release: <https://www.unibas.ch/en/News-Events/News/Uni-Research/Controlling-Quantum-States-Atom-by-Atom.html>

Copyright Wiley-VCH Verlag GmbH & Co. KGaA. Reproduced with permission.

Configuring Electronic States in an Atomically Precise Array of Quantum Boxes

Sylwia Nowakowska,* Aneliia W ckerlin, Ignacio Piquero-Zulaica, Jan Nowakowski, Shigeki Kawai, Christian W ckerlin, Manfred Matena, Thomas Nijs, Shadi Fatayer, Olha Popova, Aisha Ahsan, S. Fatemeh Mousavi, Toni Ivas, Ernst Meyer, Meike St hr, J. Enrique Ortega, Jonas Bj rk, Lutz H. Gade,* Jorge Lobo-Checa,* and Thomas A. Jung*

The development of quantum architectures, aimed to be employed, e.g., in sensors and information technologies, relies upon the detailed understanding of the cooperative interaction of the unit systems involved. Toward this end, exploratory device architectures may be based on well-defined interacting units of limited complexity assembled in highly ordered arrays. Implementations of this concept include optical lattices generated by laser beam interference and microfabricated ion trap chips.^[1,2] Whereas the former approach benefits from the strict periodicity of the interference pattern, the addressability of the unit components

remains a challenge.^[3] In contrast, in the latter case the traps can be controlled individually but the reliability of their fabrication is limited by the accuracy of the top-down micro/nanofabrication techniques employed.

On-surface quantum units exhibit discrete electronic states originating from the confinement of electrons in structures of different sizes and shapes.^[4–13] Using scanning tunneling microscopy (STM) repositioning, well-defined quantum systems have been created.^[7,8,14–16] More recently, these have been manufactured in the form of chains of atoms or vacancies in a self-assembled island to assess how

S. Nowakowska, Dr. A. W ckerlin, Dr. S. Kawai, Dr. M. Matena, T. Nijs, S. Fatayer, O. Popova, A. Ahsan, S. F. Mousavi, Dr. T. Ivas, Prof. E. Meyer

Department of Physics
University of Basel
Klingelbergstrasse 82, 4056 Basel, Switzerland
E-mail: sylwia.k.nowakowska@gmail.com

I. Piquero-Zulaica, Prof. J. E. Ortega
Centro de Física de Materiales (CSIC/UPV-EHU)—Materials
Physics Center

Manuel Lardizabal 5, 20018 San Sebastián, Spain

J. Nowakowski, Dr. C. W ckerlin, Prof. T. A. Jung

Laboratory for Micro- and Nanotechnology

Paul Scherrer Institute

5232 Villigen, PSI, Switzerland

E-mail: thomas.jung@psi.ch

Dr. S. Kawai

PRESTO

Japan Science and Technology Agency (JST)

4-1-8 Honcho, Kawaguchi, Saitama 332-0012, Japan

Dr. M. Matena, Prof. J. E. Ortega

Donostia International Physics Center (DIPC)

Manuel Lardizabal 4, 20018 San Sebastián, Spain

S. Fatayer

Departamento de Física Aplicada

Instituto de Física Gleb Wataghin

Universidade Estadual de Campinas

Campinas 13083-859, Brazil

DOI: 10.1002/sml.201600915

Prof. M. St hr
Zernike Institute for Advanced Materials
University of Groningen
Nijenborgh 4, 9747 AG, Groningen
The Netherlands

Prof. J. E. Ortega
Departamento Física Aplicada I
Universidad del País Vasco
20018 San Sebastián, Spain

Dr. J. Bj rk
Department of Physics, Chemistry and Biology
IFM

Linköping University
Linköping 581 83, Sweden

Prof. L. H. Gade
Anorganisch-Chemisches Institut
Universität Heidelberg
Im Neuenheimer Feld 270, 69120 Heidelberg, Germany
E-mail: lutz.gade@uni-heidelberg.de

Dr. J. Lobo-Checa
Instituto de Ciencia de Materiales de Aragón (ICMA)
CSIC-Universidad de Zaragoza
E-50009 Zaragoza, Spain
E-mail: jorge.loboc@csic.es

Dr. J. Lobo-Checa
Departamento de Física de la Materia Condensada
Universidad de Zaragoza
E-50009 Zaragoza, Spain



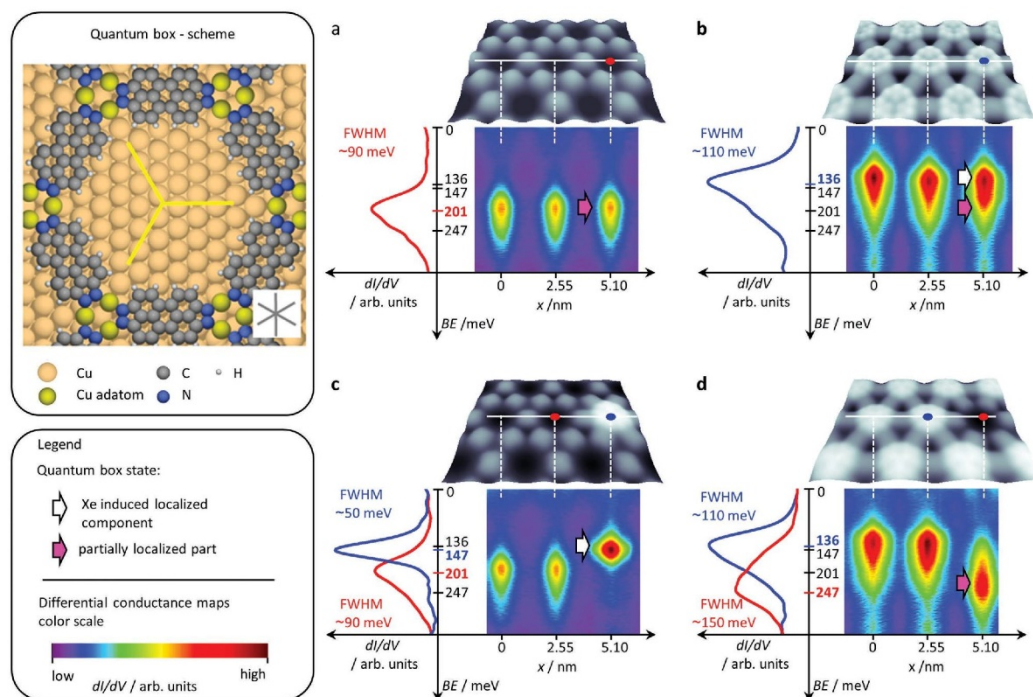


Figure 1. Xe patterning of quantum boxes. Upper inset: Schematic representation of a pore of the Cu-coordinated 3deh-DPDI network constituting a quantum box. The quantum box states contained in the pores of the on-surface network are modified by Xe atoms deposition and their subsequent removal by STM repositioning sequences. The dI/dV spectra reflect the spectral distribution of the quantum box state for each configuration. Right-hand side: Four different network configurations for investigating cooperative interactions between the quantum box states: a) empty network, b) filled network with 12 Xe atoms adsorbed in each box, c) filled quantum box with 12 Xe atoms surrounded by empty boxes, and d) empty quantum box surrounded by filled quantum boxes with 12 Xe atoms adsorbed in each box. In each case, a series of dI/dV spectra was acquired along the white line (indicated in the STM images) crossing three quantum boxes. The spectra are visualized as spatially resolved dI/dV traces. The dI/dV spectra taken at the red and blue colored dots superimposed on the STM images are plotted on the left-hand side of the dI/dV traces (size of STM images $7.8 \text{ nm} \times 4.3 \text{ nm}$).

their interaction depends on the unit size and arrangement.^[17,18] Our approach goes beyond this concept in that we can configure the electronic states contained in quantum boxes (QBs) within extended 2D arrays by directed perturbation. The self-assembly approach allows for the manufacturing of identical QBs which are coupled in an inherently precise way,^[4] and are addressable by targeted filling with an adsorbate which specifically perturbs, and thus modifies, the quantum box state (QBS). In particular, by changing the adsorbate occupancy via STM repositioning the energy levels of the QBSs and their coupling are modulated.

The array of coupled QBs employed in this work is based on a highly stable Cu-coordinated triply dehydrogenated 4,9-diaminoperylene quinone-3,10-diimine (3deh-DPDI) network generated on Cu(111) (Figure 1),^[19–21] the pores of which partially confine the Shockley surface state of the underlying substrate.^[4] In this system each pore contains a partially localized electronic ground state, while the $n = 2$ state is practically lying at the Fermi level (see Section 1 of the Supporting Information).^[4] The low intensity of the latter state and the absence of higher order bound states

simplify the analysis of the targeted perturbation of the ground state by adsorbates and by its interaction with surrounding QBs. To modify the QBS in these pores we chose Xe atoms, for their well-defined interaction with the surface state electrons of Cu(111), which is dominated by Pauli repulsion,^[22,23] and for its preferential adsorption in the pores of the Cu-coordinated 3deh-DPDI network with the maximal occupancy of 12 atoms,^[24] which offers the opportunity to discretely modify the electronic state in each QB by STM repositioning.

In our studies we characterize the 2D array of QBs by scanning tunneling microscopy/spectroscopy (STM/STS) providing site specific, “local” information on the effect of Xe adsorption on the QBS and by complementary angle-resolved photoemission spectroscopy (ARPES) giving access to the coherent, “ensemble,” part of the interaction between the partially localized states.

In the following we characterize two extreme network states: the vacant network and the fully filled network with 12 Xe atoms adsorbed in each QB to study the corresponding QBSs. The corresponding STM/STS and ARPES

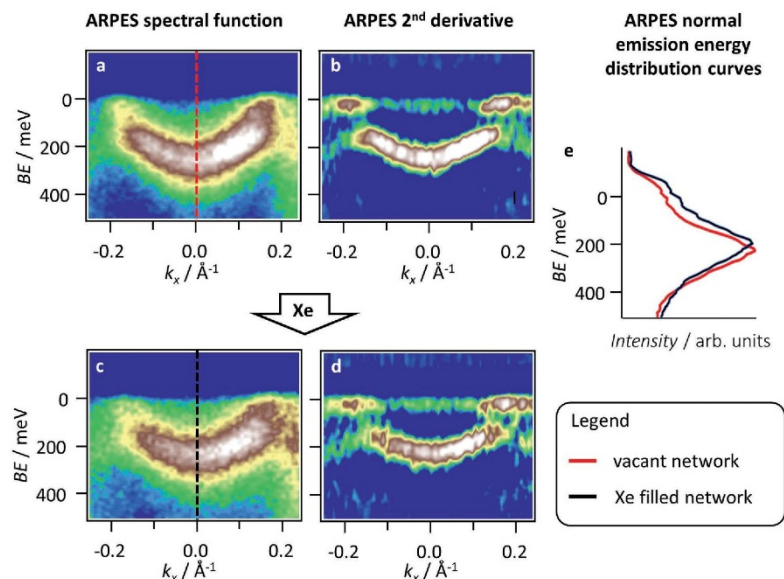


Figure 2. Influence of Xe adsorption on the coherent (ensemble) interaction between the partially localized parts of the quantum state hosted by the pores of the network. a) ARPES experimental spectral function acquired for the empty network and b) its second derivative measured along the $\bar{\Gamma}\bar{M}$ high symmetry direction. c) ARPES experimental spectral function after Xe adsorption in the pores and d) its second derivative. e) Normal emission energy distribution curves ($k_x = 0$) from (a) and (c). The spectra acquired between these two cases are shown in Supporting Information Figure S1 (cf. Section 2 of the Supporting Information).

data are presented in Figure 1a,b and Figure 2, respectively. The emergence of an electronic band registered by ARPES in both cases (Figure 2) provides evidence for the partial localization and thus for the coupling between the QBSs.^[4] The spatially resolved dI/dV trace in Figure 1a illustrates the spectral and spatial distribution of the partially localized state within the vacant network, whose maximum is observed at 201 ± 6 meV binding energy (BE). Upon adsorption of 12 Xe atoms in each pore of the network, an additional, dominating, Xe induced localized component at lower BE appeared, whose maximum is observed at 136 ± 7 meV (Figure 1b, white arrow). This Xe related component is superimposed on the signal coming from partial localization of the QBS. The shift toward lower BE of the latter component upon Xe adsorption, as measured by

Table 1. Band structure parameters extracted from ARPES measurements.

Sample	BE _{max} at $\bar{\Gamma}^a$ [meV]	m^*/m_0^b	Bandwidth [meV]
Cu(111)	434 ± 2^d	0.43 ± 0.01^d	–
Xe/Cu(111)	291 ± 2^d	0.44 ± 0.02^d	–
Network ^c /Cu(111)	270 ± 10	0.57 ± 0.02	90 ± 10
Xe/network ^c /Cu(111)	240 ± 10	0.66 ± 0.02	70 ± 10

^aThe values refer to the binding energy at normal emission (band bottom); ^bThe effective mass and the bandwidth of the $n = 1$ state along $\bar{\Gamma}\bar{M}$; the details of extracting the effective mass from the ARPES spectral functions before and after filling of the pores with Xe can be found in Figure 3; ^c“Network” here denotes the Cu-coordinated 3deh-DPDI network formed on Cu(111); ^dValues from ref. [23].

ARPES, amounts to ≈ 30 meV (Table 1). We interpret this energy shift as the result of Pauli repulsion between the electronic states of Xe and the QBS, similar to the previously reported shift of the Shockley surface state of bare Cu(111) toward lower BE caused by the adsorption of Xe (Table 1).^[23] Notably, our results demonstrate that there is an apparent increase of the electron effective mass upon the filling of the network pores with Xe (Table 1 and Figure 3). This is in contrast with the case of the free-electron-like Cu(111) Shockley state, where no significant change of the effective mass is observed with an adsorbed Xe layer (cf. Table 1).^[23] In the present case, we speculate that the extra increase of the effective mass in the network upon Xe pore filling is related to a weaker inter-pore coupling, i.e. to a change in the 2D network potential. A detailed theoretical study is under way to address this issue.

To investigate whether the filling of the surrounding QBs influenced the electronic state in a chosen unit, we generated different configurations by repositioning single Xe atoms with the STM tip.^[25–27] Two model arrangements were studied in detail: a filled QB surrounded by empty ones (Figure 1c) and an empty QB surrounded by filled ones (Figure 1d).

In the first model case (Figure 1c), the spatially resolved dI/dV trace of the QBS for the filled pore is significantly different from the one observed for the individual pore in the Xe filled network (cf. Figure 1b): the Xe induced component at lower BE dominates (Figure 1c, white arrow), whereas the signal at higher BE originating from the electronic band created by the surrounding empty network is strongly attenuated: a sharp QBS peak with a full width at half maximum

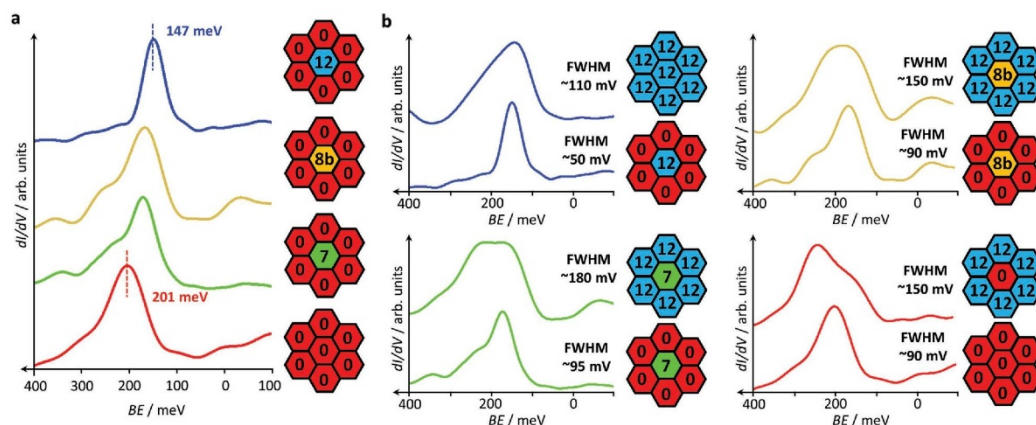


Figure 5. Influence of the number of Xe atoms adsorbed in a central QB and the influence of the filling level of the surrounding ones on the quantum box state. a) The influence of the number of Xe contained in a central QB with the surrounding QBs empty. With decreasing occupancy a gradual shift of the electronic state is observed to higher BEs (like in the case of surrounding QBs filled, cf. Figure 4). b) Comparison of the dI/dV spectra acquired in the QB featuring the same Xe occupancy surrounded by all empty and all filled QBs. Upon filling of the surrounding pores with Xe the spectral distribution of the quantum box state significantly changes.

pore in 12 steps configures a self-assembled array of quantum boxes: the Pauli repulsion imposed by Xe atom(s) modifies the quantum box states and, notably, adds an additional confining dimension to the coupled quantum boxes. Therefore our work demonstrates that the simplified picture of the emergence of the confined states from the 2D electron gas needs to be extended to include potential confinement effects in the out-of-plane dimension and underpins the well-established fact that the observed physical effects at interfaces are not by nature strictly 2D. Moreover, we would like to point out that there are similarities between our discussion of the coupling in artificial QB systems and the interatomic interactions in molecular physics. Our approach opens up the possibility to use a combination of various adsorbates in order to create more complex experimentally addressable patterns of quantum states, well beyond the scope of this Communication.

Experimental Section

Sample Preparation for STM/STS Measurements: The Cu-coordinated 3deh-DPDI network on Cu(111) was prepared according to the procedure described in ref. [20]. Xe of purity 99.99% was dosed onto the sample placed in the STM (Omicron Nanotechnology GmbH with Nanonis SPM control system) operated at 4.2 K, with the cryoshields open and the leak valve being in line-of-sight with the sample. The sample was exposed to 120 L (Langmuir) of Xe (1.3×10^{-7} mbar for 1200 s) resulting in the increase of the sample temperature to 9 K. The STM measurements performed after cooling the sample back to 4.2 K revealed different numbers of Xe atoms adsorbed in the pores as well as at the domain boundaries and step edges. Filling of all pores with 12 Xe atoms was performed by subsequent annealing to 45 K followed by cooling to 4.2 K for the STM measurements.

Repositioning of Single Xe Atoms: All the condensates discussed in the manuscript were obtained by controllable removing of Xe atoms from the pores of the network by means of STM repositioning. Noticeably, new configurations that are not occurring spontaneously upon Xe exposure can be created in this way (i.e., occ-4, occ-6b, and occ-8b; cf. Figure 3 and ref. [24]).

STM/STS Measurement Details and Data Analysis: In the STM the bias voltage is applied to the tip. The bias voltages given in the manuscript and the Supporting Information refer to a grounded tip.

STM measurements were performed in constant current mode with Pt-Ir tips (90% Pt, 10% Ir), prepared by mechanical cutting followed by sputtering and controlled indentation in the bare Cu(111) substrate. All STM images were acquired with a Xe functionalized tip, which allows for obtaining atomic resolution on Xe condensates.^[24]

To avoid modification of the condensates via interaction with the tip, the sample bias was selected within a range of -10 mV to -80 mV, whereas the tunneling current was set within the range of 5–50 pA. The exact tunneling parameters for the STM images presented in the main text are displayed in Table S1 (Supporting Information).

The STM data were processed with the WSxM software.^[29] For better comparability of the data the color histograms of the STM images were adjusted. Low-pass filtering was used for noise reduction.

All dI/dV spectra were recorded with open-feedback loop and with Xe functionalized tip. Control spectra were acquired with a metallic tip and no difference was observed in accordance with ref. [30].

The dI/dV data presented in Figure 1 were extracted from the grid spectroscopy measurements, in which area of $7.8 \text{ nm} \times 4.3 \text{ nm}$ was mapped by acquisition of dI/dV spectra above each point with the resolution of 50 points \times 30 points for the empty network and 60 points \times 30 points for the other three cases. The initial tip

conditions amounted to 400 mV/70 pA (lock-in frequency: 513 Hz; zero-to-peak amplitude: 8 mV). As described in detail in ref. [31] the value of the initial voltage was chosen such that no quantum box state or network backbone related contribution was present. Owing to that normalization could be performed by setting the same dI/dV value at the setpoint energy for all dI/dV spectra. In this way artifacts originating from local work function variations are minimized.

The dI/dV spectra presented in Figures 4 and 5 were acquired with the initial tip conditions amounting to -800 mV/50 pA (lock-in frequency: 513 Hz; zero-to-peak amplitude: 5 mV).

ARPES Setup: The ARPES measurements were performed on a lab-based experimental setup equipped with a display type hemispherical analyzer (Phoibos150) with an energy/angle resolution of 40 meV/0.1° and a monochromatized Helium I ($h\nu = 21.2$ eV) source.

Sample Preparation and ARPES Acquisition Details: To avoid contributions from the Shockley surface state of bare Cu(111) to the ARPES signal, it was crucial to achieve a homogeneous Cu-coordinated 3deh-DPDI network completely covering the surface. Therefore, DPDI was sublimed onto Cu(111) held at room temperature in wedge geometry (coverage gradient) in the proximity of the optimal coverage and then annealed until a sharp and intense signal emerging from partial localization of the quantum box state, as in ref. [4], was visible in the ARPES channel plate detector. The annealing step is crucial for conversion of the DPDI molecules into 3deh-DPDI molecules, which create the Cu-coordinated network.^[20,21] The Xe dosing experiment was started immediately after the sample temperature dropped below 60 K, but was higher than 25 K to keep the adsorbate mobility.^[32] Xe core level (9–5 eV BE) and surface state (close to Fermi energy) regions at normal emission were acquired alternatively as a function of time while keeping Xe pressure in the chamber constant (5×10^{-10} mbar). The evolution of the $5p_{3/2}$ and $5p_{1/2}$ core levels and the partially localized part of the quantum box state as function of the Xe exposure time is shown in Supporting Information Figure S1 (total exposure time amounted to ≈ 30 min).

Supporting Information

Supporting Information is available from the Wiley Online Library or from the author.

Acknowledgements

The authors would like to acknowledge financial support from the Swiss Nanoscience Institute (SNI), Swiss National Science Foundation (Grants Nos. 200020-149713 and 206021-121461), the Spanish Ministry of Economy (Grant No. MAT2013-46593-C6-4-P), the Basque Government (Grant No. IT621-13), the São Paulo Research Foundation (Grant No. 2013/04855-0), Swiss Government Excellence Scholarship Program, Netherlands Organization for Scientific Research NWO (Chemical Sciences, VIDI-Grant No. 700.10.424), the European Research Council (ERC-2012-StG

307760-SURFPRO), University of Basel, University of Heidelberg, Linköping University, University of Groningen, Paul Scherrer Institute, and the Japan Science and Technology Agency (JST) "Preliminary Research for Embryonic Science and Technology (PRESTO)" for a project of "Molecular technology and creation of new function." The authors sincerely thank Marco Martina and Rémy Pawlak for support during the measurements.

- [1] I. Bloch, *Nat. Phys.* **2005**, *1*, 23.
- [2] T. D. Ladd, F. Jelezko, R. Laflamme, Y. Nakamura, C. Monroe, J. L. O'Brien, *Nature* **2010**, *464*, 45.
- [3] I. Buluta, F. Nori, *Science* **2009**, *326*, 108.
- [4] J. Lobo-Checa, M. Matena, K. Müller, J. H. Dil, F. Meier, L. H. Gade, T. A. Jung, M. Stöhr, *Science* **2009**, *325*, 300.
- [5] F. Klappenberger, D. Kühne, W. Krenner, I. Silanes, A. Arnau, F. J. García de Abajo, S. Klyatskaya, M. Ruben, J. V. Barth, *Nano Lett.* **2009**, *9*, 3509.
- [6] F. Klappenberger, D. Kühne, W. Krenner, I. Silanes, A. Arnau, F. J. García de Abajo, S. Klyatskaya, M. Ruben, J. V. Barth, *Phys. Rev. Lett.* **2011**, *106*, 026802.
- [7] M. F. Crommie, C. P. Lutz, D. M. Eigler, *Science* **1993**, *262*, 218.
- [8] E. J. Heller, M. F. Crommie, C. P. Lutz, D. M. Eigler, *Nature* **1994**, *369*, 464.
- [9] P. Avouris, I.-W. Lyo, *Science* **1994**, *264*, 942.
- [10] N. Nilius, T. M. Wallis, W. Ho, *Science* **2002**, *297*, 1853.
- [11] Y. Pennec, W. Auwärter, A. Schiffrin, A. Weber-Bargioni, A. Riemann, J. V. Barth, *Nat. Nanotechnol.* **2007**, *2*, 99.
- [12] S. Wang, W. Wang, L. Z. Tan, X. G. Li, Z. Shi, G. Kuang, P. N. Liu, S. G. Louie, N. Lin, *Phys. Rev. B* **2013**, *88*, 245430.
- [13] A. Shchyrba, S. C. Martens, C. Wäckerlin, M. Matena, T. Ivas, H. Wadepohl, M. Stöhr, T. A. Jung, L. H. Gade, *Chem. Commun.* **2014**, *50*, 7628.
- [14] J. Repp, G. Meyer, S. Paavilainen, F. E. Olsson, M. Persson, *Science* **2006**, *312*, 1196.
- [15] F. Mohn, J. Repp, L. Gross, G. Meyer, M. Dyer, M. Persson, *Phys. Rev. Lett.* **2010**, *105*, 266102.
- [16] C. Krull, R. Robles, A. Mugarza, P. Gambardella, *Nat. Mater.* **2013**, *12*, 337.
- [17] K. Seufert, W. Auwärter, F. J. García de Abajo, D. Eciija, S. Vijayaraghavan, S. Joshi, J. V. Barth, *Nano Lett.* **2013**, *13*, 6130.
- [18] S. Fölsch, J. Martínez-Blanco, J. Yang, K. Kanisawa, S. C. Erwin, *Nat. Nanotechnol.* **2014**, *9*, 505.
- [19] M. Stöhr, M. Wahl, C. H. Galka, T. Riehm, T. A. Jung, L. H. Gade, *Angew. Chem., Int. Ed.* **2005**, *44*, 7394.
- [20] A. Shchyrba, C. Wäckerlin, J. Nowakowski, S. Nowakowska, J. Björk, S. Fatayer, J. Girovsky, T. Nijs, S. C. Martens, A. Kleibert, M. Stöhr, N. Ballav, T. A. Jung, L. H. Gade, *J. Am. Chem. Soc.* **2014**, *136*, 9355.
- [21] M. Matena, J. Björk, M. Wahl, T.-L. Lee, J. Zegenhagen, L. H. Gade, T. A. Jung, M. Persson, M. Stöhr, *Phys. Rev. B* **2014**, *90*, 125408.
- [22] J.-Y. Park, U. Ham, S.-J. Kahng, Y. Kuk, K. Miyake, K. Hata, H. Shigekawa, *Phys. Rev. B* **2000**, *62*, R16341.
- [23] F. Forster, S. Hübner, F. Reinert, *J. Phys. Chem. B* **2004**, *108*, 14692.
- [24] S. Nowakowska, A. Wäckerlin, S. Kawai, T. Ivas, J. Nowakowski, S. Fatayer, C. Wäckerlin, T. Nijs, E. Meyer, J. Björk, M. Stöhr, L. H. Gade, T. A. Jung, *Nat. Commun.* **2015**, *6*, 6071.
- [25] D. M. Eigler, C. P. Lutz, W. E. Rudge, *Nature* **1991**, *352*, 600.
- [26] A. Yazdani, D. M. Eigler, N. D. Lang, *Science* **1996**, *272*, 1921.
- [27] G. Kichin, C. Weiss, C. Wagner, F. S. Tautz, R. Temirov, *J. Am. Chem. Soc.* **2011**, *133*, 16847.
- [28] E. Merzbacher, *Quantum Mechanics*, Wiley, New York **1970**.

- [29] I. Horcas, R. Fernández, J. M. Gómez-Rodríguez, J. Colchero, J. Gómez-Herrero, A. M. Baro, *Rev. Sci. Instrum.* **2007**, *78*, 013705.
- [30] H. C. Manoharan, C. P. Lutz, D. M. Eigler, *Nature* **2000**, *403*, 512.
- [31] W. Krenner, D. Kühne, F. Klappenberger, J. V. Barth, *Sci. Rep.* **2013**, *3*, 1454.
- [32] J.-Y. Park, S.-J. Kahng, U. Ham, Y. Kuk, K. Miyake, K. Hata, H. Shigekawa, *Phys. Rev. B* **1999**, *60*, 16934.

Received: March 17, 2016

Revised: April 25, 2016

Published online:



Supporting Information

for *Small.*, DOI: 10.1002/smll.201600915

Configuring Electronic States in an Atomically Precise Array of Quantum Boxes

*Sylvia Nowakowska, * Aneliia Wäckerlin, Ignacio Piquero-Zulaica, Jan Nowakowski, Shigeki Kawai, Christian Wäckerlin, Manfred Matena, Thomas Nijs, Shadi Fatayer, Olha Popova, Aisha Ahsan, S. Fatemeh Mousavi, Toni Ivas, Ernst Meyer, Meike Stöhr, J. Enrique Ortega, Jonas Björk, Lutz H. Gade, * Jorge Lobo-Checa, * and Thomas A. Jung**

Supporting Information

Configuring Electronic States in an Atomically Precise Array of Quantum Boxes

Sylwia Nowakowska, Aneliia Wäckerlin, Ignacio Piquero-Zulaica, Jan Nowakowski, Shigeki Kawai, Christian Wäckerlin, Manfred Matena, Thomas Nijs, Shadi Fatayer, Olha Popova, Aisha Ahsan, S. Fatameh Mousavi, Toni Ivas, Ernst Meyer, Meike Stöhr, J. Enrique Ortega, Jonas Björk, Lutz H. Gade,* Jorge Lobo-Checa,* Thomas A. Jung**

1. Second level of the quantum box state

The onset of the second level of the quantum box state ($n=2$) is practically at the Fermi energy.^[1] Because of this, the data fit for this second level is not reliable. We roughly estimate the gap energy between ground state and first excited state to be ~120 meV. The gap seems to be unaffected upon Xe adsorption. We note that calculations would be necessary to quantify the gap size.

2. ARPES lineshape evolution with Xe adsorption

Due to its closed-shell electron configuration, Xe can be used to probe the energy landscape of on-surface architectures.^[2] As evidenced by the STM data Xe preferentially adsorbs in the pores of the Cu-coordinated 3deh-DPDI network, when the sample temperature exceeds 8 K,^[3] which is the case for our ARPES measurements. Therefore we assign the observed shift of the $5p_{3/2}$ and $5p_{1/2}$ Xe core levels upon progressive Xe exposure (**Figure S1**) to the adsorption of Xe on the network backbone once all pores have been completely filled. This reflects a difference in the work function between the pores and the network backbone. A similar observation was done in the case of the boron nitride nanomesh, in which the trapping potential was localized in the holes of the nanomesh.^[2]

3. Energy difference between QBS peak of a filled pore in the filled network and a filled pore surrounded by empty pores

The filled pore in the filled network has a QBS peak at energy of 136 ± 7 meV (statistics from 136 pores), whereas the filled pore surrounded by empty ones 147 ± 3 meV (statistics from 6 pores: a larger statistics is very difficult to obtain as it requires to create the pattern in a long series of repositioning, but also it is not so much needed due to the sharpness of the peak).

4. Comment on the change in binding energy (*BE*) of quantum box state with previous work

In a previous publication^[1] the *BE* of the quantum box state measured by ARPES was reported to be (230 ± 30) meV, which is 40 meV lower than in the present work. This is related to the fact that the used ARPES experimental setups were different: in previous work,^[1] a channeltron type hemispherical analyzer and no tilt correction of the manipulator was used, whereas the ARPES measurements for the present work were done using a 2D display analyzer with the channelplate acceptance angle perpendicular to the polar rotation. Our new equipment is insensitive to sample mounting misalignments, which allows us to determine the bottom of the band coming from partially localized part of the quantum box state with a higher degree of precision than previously.

5. Comment on the difference between the quantum box state energies observed by ARPES and STS

In ARPES data the energy positions of the corresponding quantum box states are found to be farther from the Fermi energy than in STS data (Fig. 1a vs. Fig. 2a). These differences are likely related to the technical aspects of each technique. In particular ARPES averages over

the whole illuminated region, losing its local character, and probes the coherent part of the electron wavefunction, whereas STS is a local technique also sensitive to the non-coherent part.^[4] This gives rise to the fundamental divergence between these two techniques: ARPES is *k*-selective, whereas STS integrates over *k*-space. As a result, ARPES can quantify the minimum energy value of the quantum box state, whereas in STS a large fraction of the projected density of states (convoluted with tip local density of states) contributes to the observed dI/dV lineshape.^[5] In this way, the STS energy maximum shifts towards the bandwidth centre (towards the E_F) as compared to the ARPES result.

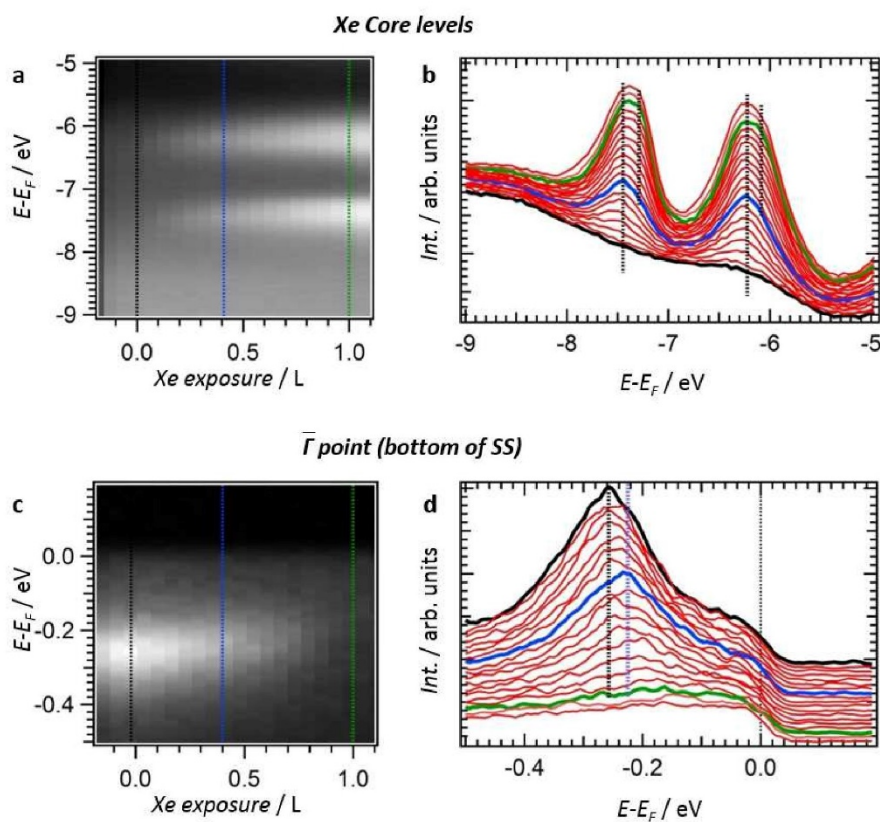


Figure S1. The changes in electronic structure of the Cu-coordinated 3deh-DPDI network on Cu(111) upon Xe exposure monitored with ARPES (a-b) The $5p_{3/2}$ and $5p_{1/2}$ Xe core levels (c-d) and the surface state region alternatively recorded during Xe exposure expressed in Langmuirs (L). In **a** the photoemission intensity is represented as a grayscale plot, whereas in **b** selected energy distribution curves are shown as a waterfall. Initially, a single component (doublet at 7.46/6.23 eV), which we attribute to the adsorption within the network pores, increases in intensity up to ~ 0.4 L (blue line in **a**; blue spectra in **b**). From that moment, a less bound component (doublet at 7.29/6.08 eV) develops, which we attribute to adsorption at the network backbone, until completion of the full layer (green line in **a**; green spectra in **b**). Both doublet energies are indicated as vertical dotted lines. The evolution of the quantum box state at $\bar{\Gamma}$ is shown as a grayscale plot in **c** and as selected energy distribution curves in **d**. We observe a strong attenuation of the state and a decrease of its BE upon increase of Xe exposure. The ~ 30 meV shift of the partially localized part of the quantum box state is determined from the black and blue spectra which were acquired at the same Xe exposure as the black and blue spectra in **a-b**.

Table S1. Tunneling parameters of STM images presented in the main text.

STM image	Voltage [mV]	Current [pA]
Fig. 1a	-200	700
Fig. 1b	-10	50
Fig. 1c	-145	100
Fig. 1d	-145	100
Fig. 3 occ-0	-10	10
Fig. 3 occ-1	-10	10
Fig. 3 occ-4	-50	10
Fig. 3 occ-5a	-80	5
Fig. 3 occ-5b	-10	10
Fig. 3 occ-6a	-50	5
Fig. 3 occ-6b	-30	10
Fig. 3 occ-7	-20	5
Fig. 3 occ-8a	-10	10
Fig. 3 occ-8b	-10	10
Fig. 3 occ-10	-10	10
Fig. 3 occ-12	-10	50

Supporting References:

- [1] J. Lobo-Checa, M. Matena, K. Müller, J. H. Dil, F. Meier, L. H. Gade, T. A. Jung, M. Stöhr, *Science* **2009**, *325*, 300.
- [2] H. Dil, J. Lobo-Checa, R. Laskowski, P. Blaha, S. Berner, J. Osterwalder, T. Greber, *Science* **2008**, *319*, 1824.
- [3] S. Nowakowska, A. Wäckerlin, S. Kawai, T. Ivas, J. Nowakowski, S. Fatayer, C. Wäckerlin, T. Nijs, E. Meyer, J. Björk, M. Stöhr, L. H. Gade, T. A. Jung, *Nat. Commun.* **2015**, *6*, 6071.
- [4] J. E. Ortega, J. Lobo-Checa, G. Peschel, S. Schirone, Z. M. Abd El-Fattah, M. Matena, F. Schiller, P. Borghetti, P. Gambardella, A. Mugarza, *Phys. Rev. B* **2013**, *87*, 115425.
- [5] C. J. Chen, *Introduction to Scanning Tunneling Microscopy*, Oxford University Press, **2007**.

Chapter [[3]] and Supplementary Information

[[3]] Adsorbate-induced modification of the confining barriers in a quantum box array

S. Nowakowska, F. Mazzola, M. Almperti, F. Song, T. Voigt, J. Nowakowski, A. Wäckerlin, C. Wäckerlin, J. Wiss, W. B. Schweizer, M. Broszio, C. Polley, M. Leandersson, S. Fatayer, T. Ivas, S. F. Mousavi, A. Ahsan, T. Nijs, O. Popova, J. Zhang, M. Muntwiler, C. Thilgen, M. Stöhr, F. Diederich, J. Wells, T. A. Jung, *manuscript in review*.

Adsorbate-induced modification of the confining barriers in a quantum box array

In memoriam Max Broszio

Sylwia Nowakowska^{1*}, Federico Mazzola², Mariza N. Alberti³, Fei Song^{4,5}, Tobias Voigt³, Jan Nowakowski⁶, Aneliia Wäckerlin¹, Christian Wäckerlin⁶, Jérôme Wiss¹, W. Bernd Schweizer³, Max Broszio³, Craig Polley⁷, Mats Leandersson⁷, Shadi Fatayer^{1,8}, Toni Ivas¹, S. Fatameh Mousavi¹, Aisha Ahsan¹, Thomas Nijs¹, Olha Popova¹, Jun Zhang⁹, Matthias Muntwiler⁹, Carlo Thilgen³, Meike Stöhr⁴, François Diederich^{3*}, Justin Wells^{2*}, Thomas A. Jung^{6*}

¹ Department of Physics, University of Basel, Klingelbergstrasse 82, 4056 Basel, Switzerland.

² Department of Physics, Norwegian University of Science and Technology (NTNU), 7491 Trondheim, Norway.

³ Laboratory of Organic Chemistry, ETH Zurich, Vladimir-Prelog-Weg 3, 8093 Zurich, Switzerland.

⁴ Zernike Institute for Advanced Materials, University of Groningen, Nijenborgh 4, 9747 AG Groningen, The Netherlands.

⁵ Shanghai Institute of Applied Physics, Chinese Academy of Sciences, 201204, P. R. China.

⁶ Laboratory for Micro- and Nanotechnology, Paul Scherrer Institute, 5232 Villigen PSI, Switzerland.

⁷ MAX IV Laboratory, Lund University, P.O. Box 118, 22100 Lund, Sweden.

⁸ Departamento de Física Aplicada, Instituto de Física Gleb Wataghin, Universidade Estadual de Campinas, Campinas 13083-859, Brazil.

⁹ Laboratory for Synchrotron Radiation – Condensed Matter, Paul Scherrer Institute, 5232 Villigen PSI, Switzerland.

* e-mail: S.N. sylwia.nowakowska@unibas.ch, F.D. diederich@org.chem.ethz.ch, J. Wells justin.wells@ntnu.no, T.A.J. thomas.jung@psi.ch.

Quantum devices depend on addressable elements, which can be modified separately and in their mutual interaction. Self-assembly at surfaces, *e.g.* formation of a porous (metal-) organic network, provides an ideal way to manufacture arrays of identical quantum boxes, arising in this case from the confinement of the electronic (Shockley) surface state within the pores. We show that the electronic quantum box state as well as the inter-box coupling can be modified to a varying extent by a selective choice of adsorbates, here C₆₀, interacting with the barrier. In view of the wealth of differently acting adsorbates, this work opens up a new dimension for engineering quantum states in on-surface network architectures.

Configurable quantum states are indispensable for the development of optoelectronic devices, including quantum-dot photovoltaics and light emitting devices¹⁻³. Being able to govern the coupling between addressable quantum states, *e.g.* arranged in an array, provides the next level of control, which is needed for the further advancement of quantum technologies⁴. Towards higher level integration of quantum circuitry, *i.e.* for performing operations between different quantum states, the reliable manufacturing of identical quantum units at large numbers and the reproducible control of their interaction is of utmost importance.

Individual adsorbates on metallic surfaces exhibiting a Shockley surface state are known to scatter this electronic state.⁵⁻⁷ Thus, with the help of artificially fabricated on-surface structures, the surface state can be confined and thereby, quantum units can be generated.⁸⁻²² A practical way to fabricate arrays consisting of hundreds of quantum units is provided by on-surface self-assembly, ultimately assuring high precision concerning the individual quantum unit, the periodicity of the array and the coupling with the surrounding units.⁸ Importantly, the coupling strength depends on the properties of the confining barrier, specifically on its interaction with the surface. For example, this dependence has been demonstrated by the comparison of the confinement strength in quantum systems featuring the same arrangement but being constructed from slightly different building blocks (*i.e.* metal free vs metalated porphyrin).¹¹ Here, we use the self-assembly of porphyrin derivatives on a Ag(111) surface to fabricate a 2D periodic array of coupled quantum units, and we demonstrate that the transmission probability of the confining barrier, hence the inter-unit coupling, can be modified by deposition of adsorbates. As a result, a perfect playground is

obtained to test various fundamental concepts related to quantum confinement and its use in quantum devices.

Periodic 2D arrays of quantum units are best probed by two complementary techniques: *spatially-resolved* and *momentum-averaging* scanning tunneling spectroscopy (STS) as well as *spatially-averaging* and *momentum-resolved* angle-resolved photoemission spectroscopy (ARPES). STS accesses the local electronic structure of the quantum units and the barriers between them, whereas ARPES reveals how the overlap of the electronic wavefunctions of such units, *i.e.* coupling, gives rise to a well-defined band dispersing in energy and momentum. The dispersion of bottom or top of a band can be approximated with a certain effective mass, thus giving information about the carrier velocity. These properties are of fundamental interest for carrier mobility and ultimately for quantum devices as well as their architectures. Worthy of note is that ARPES has been successfully used to probe quantum confinement in different materials^{23,24} and can even give an accurate description of many-body interactions^{23,25}.

Results

The design of the building block. To fabricate a 2D periodic array of quantum units, we designed a porphyrin building block **1** to self-assemble into a porous network via C–H···F–C interactions, which have been reported for 3D crystals^{26–30} as well as 2D assemblies on surfaces^{31–35}. Specifically, 2',3',4',5',6'-pentafluorobiphenyl-4-yl and 3,5-dimethoxybiphenyl-4-yl substituents have been employed (Fig. 1a, for the synthesis see the Supplementary Synthesis file) on the basis of earlier reports regarding 2D interactions between arenes and fluoroarenes^{31–35} and the experience that functionalized porphyrins with two different, oppositely positioned binding groups are ideal building blocks for porous networks on crystal surfaces having 111 orientation, as reported for e.g. cyanophenyl³⁶, alkoxyphenyl³⁷ and pyridine-derived³⁸ substituents.

Structure of the porous porphyrin network. Zn(II) porphyrin **1** self-assembles in an extended hexagonal porous network on Ag(111) and is characterized by the presence of two mirror-image domains creating a $(14 \times 14)R \pm 10^\circ$ overlayer structure as evidenced by scanning tunneling microscopy (STM) and low energy electron diffraction (LEED) (Fig. 1). High resolution STM images reveal that each domain is homochiral, *i.e.* it exclusively

consists of a single one out of two conformational enantiomers, labelled as either “L” or “R”, which occur upon adsorption of Zn(II) porphyrin **1** on the Ag(111) substrate and which are characterized by opposite torsion angles around the bond connecting the porphyrin macrocycle and the 3,5-dimethoxybiphenyl-4-yl substituents (Supplementary Fig. S1). As intended, the network is held together primarily by C–H···F–C interactions (Fig. 2 and Supplementary Fig. S1), although other interactions may also play a role. Noteworthy is the absence of any phenyl-pentafluorophenyl stacking interactions, which are observed in the 3D crystal structure of **1** (cf. Section 3.2 in Synthesis file) and typically in crystals of molecules with aryl and perfluoroaryl sub-units^{39–43}. The on-surface 2D network is mainly comprised of regular pores enclosed by six Zn(II) porphyrin molecules **1** (Fig. 2, Supplementary Fig. S1), denoted hereafter as *small*. Between supra-molecular islands, a domain boundary in the form of a linear array of larger pores enclosed by eight molecules (Fig. 2) is observed (cf. Supplementary Fig. S2). The latter pores are hereafter referred to as *big*.

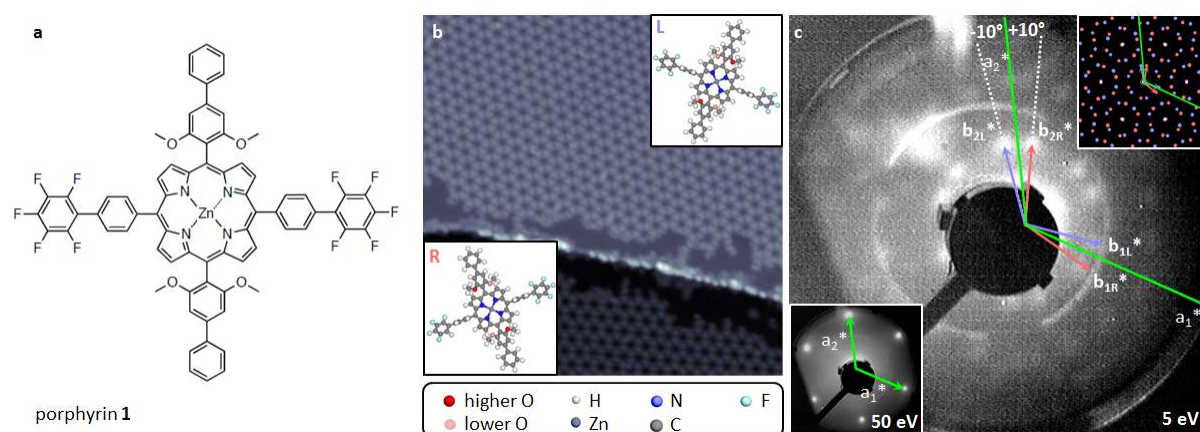


Figure 1 | Quantum box array formed by deposition of Zn(II) porphyrin **1 on Ag(111).** (a) Molecular structure of Zn(II) porphyrin **1**. (b) STM image (100 nm × 100 nm) of two terraces covered by enantiomeric domains of a porous network of **1**. Each domain consists of a single conformational enantiomer: “L” on the upper terrace and “R” on the lower terrace; for high resolution STM images see Supplementary Fig. S1. (c) LEED data of the porous network of **1** on Ag(111) taken at room temperature. The pattern of the porous network of **1** was recorded at a beam energy of 5 eV, that of the Ag(111) substrate at 50 eV (lower inset). The reciprocal unit cell vectors b_{1L}^* (b_{1R}^*) and b_{2L}^* (b_{2R}^*) of “L” (“R”) domains are indicated by violet (coral) arrows. The reciprocal unit cell vectors of the Ag(111) substrate are indicated by green arrows (lines). The sets of spots for the “L” or “R” domains draw an angle of $\pm 10^\circ$ with the principle Ag(111) directions. The simulated LEED pattern is shown in the upper inset (cf. Supplementary Fig. S3).

Quantum confinement in the pores of the network. On Ag(111) the Shockley surface state disperses across the Fermi level with its energy maximum just below the Fermi level, *i.e.* at

the binding energy (BE) of 65 meV.⁴⁴ In the presence of the porous network, the surface state is shifted above the Fermi level, due to the confinement of the surface state electrons by the pores of the network, as evidenced by the characteristic peaks in our dI/dV spectra (Fig. 2). Thus, each pore constitutes a quantum box (QB) embedded in a quantum array. The *small* pore features a quantum box state (QBS) peak at BE of -40 meV (Fig. 2a, red spectrum), whereas the *big* pore exhibits two peaks: one at -5 meV (Fig. 2b, violet spectrum), dominating in the centre of the pore and the second one at -80 meV (Fig. 2c, violet spectrum), located at the rim of the pore (the exact spatial distribution of those QBSs is shown in Supplementary Fig. S4).

Electronic inter-pore coupling. To modify the transmission probability of the molecular barrier, first the properties of the unmodified barrier have to be understood. For this purpose, spatially resolved dI/dV measurements were performed across the network backbone (Fig. 2). Specifically, the barrier regions of three different pore arrangements were investigated, *i.e.* between two *small* pores, between two *big* pores, and between a *small* and a *big* pore. The barrier between two *small* pores is characterized by the presence of a QBS peak, which is shifted towards higher BE by either ~ 5 meV at the position of the porphyrin macrocycle or by ~ 15 meV at the position of the pentafluorophenyl substituents (Fig. 2a, Supplementary Fig. S5). At the barrier between two *big* pores, the shift amounts to ~ 5 meV at the position of both the porphyrin macrocycle and the pentafluorophenyl substituents (Fig. 2b, Supplementary Fig. S5).

Importantly, first-principle density functional theory calculations of a Zn(II) porphyrin **1** molecule adsorbed on Ag(111) revealed that there is a HOMO-LUMO gap centered around the Fermi level (Supplementary Fig. S6). Thus, the features close to the Fermi level detected in the dI/dV spectra taken at the barriers are QBSs-related. The penetration into the barrier, and hence also the electronic interaction of the neighbouring pores, is critically dependent on the interaction of the components of the barrier with the confined surface state. In our example, both the porphyrin macrocycle and the pentafluorophenyl substituents affect the confined surface state and thus, both influence the lateral coupling between neighbouring quantum states.

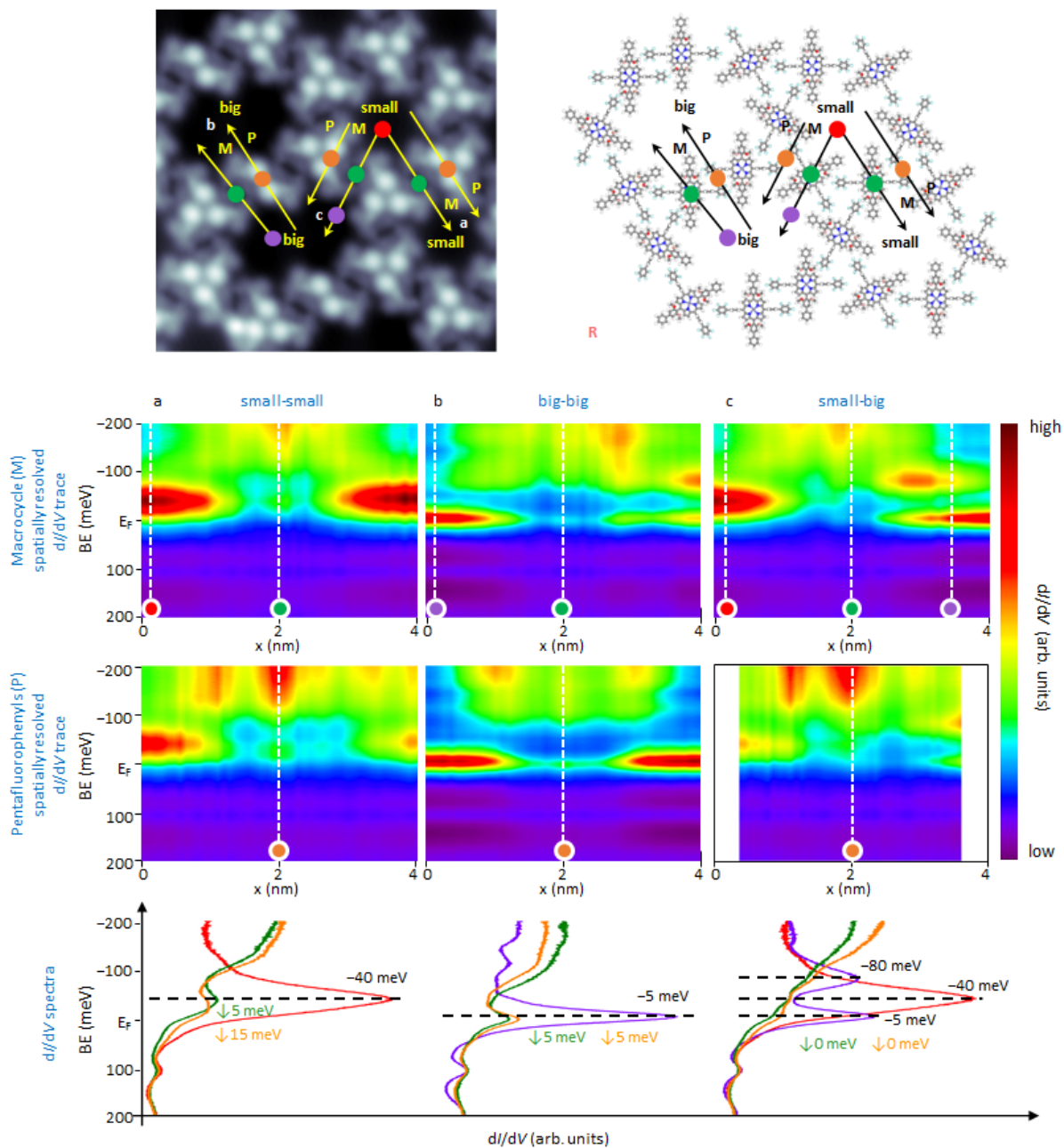


Figure 2 | dI/dV characterization of the barrier regions between the quantum boxes. (1st row) STM image (11 nm \times 11 nm) and corresponding molecular model showing the arrangement of the individual molecules. The barriers between three different arrangements of the quantum boxes were investigated, namely between: (a) two *small* boxes, (b) two *big* boxes and (c) a *small* and a *big* box. For each barrier region dI/dV data were taken along a line through (2nd row) a porphyrin macrocycle and (3rd row) the pentafluorophenyl substituents as indicated by the yellow and black arrows superimposed on the STM image and the molecular model, respectively (the arrows illustrate the starting and the final points of each dI/dV line). (4th row) Selected dI/dV spectra taken at the positions marked by colored dots in the STM image, the molecular model and in the spatially resolved dI/dV spectra. The green and orange numbers indicate the value of the QBS peak shift towards higher BE at the position of the porphyrin macrocycle and the pentafluorophenyl substituents, respectively. The close-up dI/dV spectra of the QBS peak regions are shown in Supplementary Fig. S5. Please note that the

asymmetry between the starting and ending point of the dI/dV line acquired across the porphyrin macrocycle in (b) is caused by the fact that the former was acquired closer to the pore centre, which is dominated by the state at -5 meV, whereas the latter closer to the rim of the pore dominated by the state at -80 meV (cf. Supplementary Fig. S4).

It is worth mentioning that the QBS shifts in the barriers of electronically coupled quantum systems towards higher BE are in accordance with the observations reported by Seufert *et al.*¹¹ for two coupled quantum wells. The authors demonstrated that in such a system the bonding component Ψ_n of the quantum state dominates in the barrier region over the antibonding component Ψ_n^* . Therefore the former mainly contributes to the dI/dV signal measured above the barrier, causing the overall shift of the quantum state towards higher BE.

At the barrier connecting a *small* pore with a *big* pore, the quantum states of these pores are both detected with a very low intensity (Fig. 2c, Supplementary Fig. S5). That means that they both penetrate the barrier without an energy shift. This demonstrates the lack of electronic coupling between these pores due to the energy level misalignment.

The partial confinement of the Shockley surface state in the pores of the Zn(II) porphyrin **1** network on the Ag(111) surface is directly demonstrated by ARPES. In Fig. 3a ARPES data collected for a sample partially covered with the network domains is shown. The electronic structure of this system is characterized by two states: the Ag(111) Shockley state, which crosses the Fermi level and reaches its maximum dispersion at BE ~ 65 meV, and a state dispersing above the Fermi level, which we attribute to the partially confined state, resulting from the coupling between the electronic states of the QBs embedded in the array⁸ (for better visualization, the ARPES spectrum was integrated over a small k -range around the band centre, Fig. 3b). The *small* pores are in vast majority on the sample, as the *big* pores are observed only at the domain boundaries (cf. Supplementary Fig. S2), meaning that mainly the QBS of the former will contribute to the spatially-averaged ARPES signal. The QBS, however, is detected slightly further away from the Fermi level as by STS (cf. Fig. 2a and Fig. 3). This difference is presumably because of the temperature dependence of the energy of the QBS: the higher the temperature the more the confined state shifts towards lower BE⁴⁵, likewise the Shockley surface state⁴⁶ (note that the STS data were acquired at 4.2 K, whereas the ARPES data at room temperature). Additionally an uncertainty in Fermi level determination of ± 10 meV needs to be taken into account. By fitting the bottom of both

ARPES spectra of Fig. 3a with parabolas, we extract the effective mass, resulting in $m^* = 0.40 \pm 0.08 m_e$ for the Ag(111) Shockley surface state in agreement with the literature⁴⁴, and $m^* = 0.38 \pm 0.11 m_e$ for the QBS. The fact that the effective mass of these two states is the same, within the experimental error, suggests that the formation of the network does not impose any strong modification on the potential felt by surface state electrons. A similar observation was made by Pennec *et al.*,¹⁵ who derived the effective mass for 1D confinement on Ag(111) by Fourier transform of the STS data and also obtained the same value as for the bare surface.

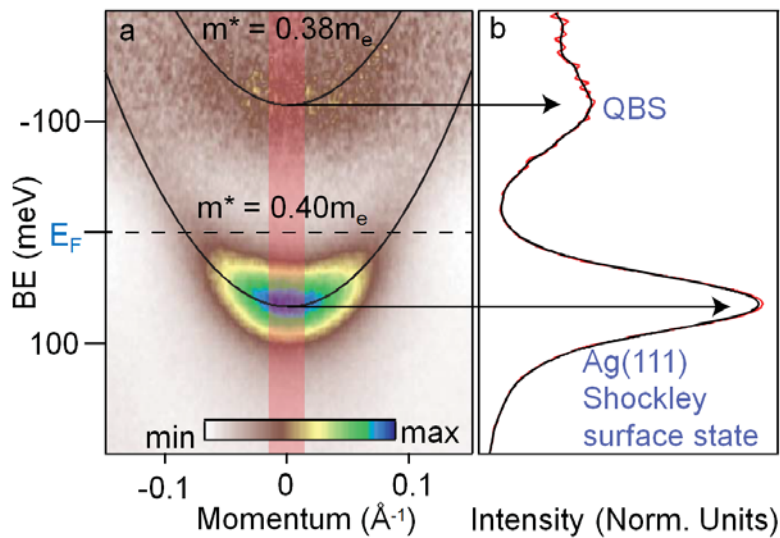


Figure 3 | Synchrotron-based ARPES measurements of a 2D periodic array of quantum units formed by a Zn(II) porphyrin 1 porous network on Ag(111). (a) ARPES spectrum for a Ag(111) surface partially covered with the Zn(II) porphyrin 1 network: two electronic states are revealed, the Shockley surface state dispersing across the Fermi level and the quantum box state dispersing above the Fermi level. The bottom of both states is fitted by two parabolic dispersions (black lines) and an effective mass is extracted. (b) Intensity profile for the spectra in (a) (red curve) obtained by integrating the spectra over the momentum ranges illustrated by the red area in (a). The black line and arrows are guides for the eyes. The ARPES measurements were carried out at room temperature and at a photon energy of 21 eV. The data were normalized with a Fermi function with a constant offset added to increase the visibility of the state above the Fermi level (see the Materials and methods section for details about the ARPES data analysis).

It is important to note that ARPES, in principle, gives only information about the occupied electronic band structure of a system, hampering the understanding of its unoccupied part. The reason is that the electron availability, indispensable for this technique, is dictated by the Fermi-Dirac distribution, according to which, at 0 K, the Fermi level is the highest energy

level with non-zero possibility of finding an electron. However, at room temperature, at which the presented ARPES data were acquired, the Fermi-Dirac distribution broadens, thus allowing the access to states slightly above the Fermi level.

Modification of the electronic inter-pore coupling by adsorbates. Next we investigated the possibility of a modification of the barriers via their interaction with adsorbates. For that purpose we chose two adsorbates exhibiting characteristically different electronic properties: a closed-shell noble gas Xe and a strong electron acceptor, fullerene C₆₀.

STM images acquired after Xe exposure revealed that two Xe atoms can adsorb on top of one porphyrin macrocycle (Fig. 4a). Besides, single Xe atom adsorbs: i) on the porphyrin macrocycle, ii) between three pentafluorophenyl substituents and iii) between methoxy, pentafluorophenyl and phenyl groups (Supplementary Fig. S7). Significantly increased Xe exposure resulted in the decoration of the network backbone and adsorption at the rim of the pores. No Xe was found to be adsorbed at the centre of the pores (Supplementary Fig. S8) pointing at the repulsive interaction between Xe and the QBS (having its maximum at the centre of the pore), similar to the case of Xe adsorbed in the pores of the Cu-coordinated 3deh-DPDI network on Cu(111)⁴⁷. As revealed by dI/dV measurements (Fig. 4a), the two Xe atoms adsorbed on the porphyrin macrocycle have almost no influence on the transmission probability of the barrier (cf. red and green spectra in Fig. 2a), which is in line with the expected weak van der Waals interaction between the Xe atoms and the molecule **1**.

In contrast, a single C₆₀ molecule adsorbed in the pore between two Zn(II) porphyrin molecules **1** (Fig. 4b) reduces the barrier transmission probability (cf. spatially resolved dI/dV traces in Fig. 4b and in Fig. 2a 2nd row). Our work function map (Supplementary Fig. S10) indicates that there is an interaction between Zn(II) porphyrin **1** and C₆₀ detected as a modification of the work function of the nearest pyrrole unit of the porphyrin macrocycle and the methoxy group. We attribute this interaction to be responsible for the change of the interaction of the barrier with the confined state, which results in the modification of the transmission probability of the barrier. An even larger reduction of the transmission probability is caused by two C₆₀ molecules adsorbed in the pore close to the phenyl groups of three Zn(II) porphyrin molecules **1** (Fig. 4c, spatially resolved dI/dV trace and orange dI/dV spectrum). The presence of C₆₀ molecule(s) in a pore additionally shifts the QBS to lower BE: to ~ -55 meV in case of a single C₆₀ and to ~ -65 meV in case of two C₆₀ molecules. Importantly, the reduction of the coupling between the pores is not caused by energy level

misalignment, as there is still an overlap between the quantum states of an empty pore and a pore filled with one C_{60} or two C_{60} molecules. Furthermore C_{60} molecules do not locally destroy the QBS on the rim of the pore and thus the inter-pore coupling, as evidenced by the presence of the modified QBS in the blue dI/dV spectrum in Fig. 4b and the magenta dI/dV spectrum in Supplementary Figure S11. Thus, our results demonstrate that the adsorption of C_{60} causes both: the modification of the barrier transmission probability and changes in the quantum box state.

In summary, we created an on-surface 2D array of coupled quantum boxes by careful design of the molecular building block. Upon adsorption of Zn(II) porphyrin **1** on Ag(111), an extended porous molecular network is formed. The pores confine the Ag(111) surface state and, in particular, the surface state-derived quantum box state is shifted above the Fermi level. The quantum boxes are electronically coupled, as evidenced by our STS/ARPES measurements. Notably, also ARPES is used to access states above the Fermi level, thereby offering a powerful and complementary approach to further investigate the electronic properties of the self-assembled structures. The porphyrin derivative constituting the quantum barrier exhibits two different regions, *i.e.* the macrocycles and the pentafluorophenyl substituents, which interact differently with the quantum states. Notably, adsorbates, *i.e.* Xe and C_{60} , show a distinct influence on the transmission probability of the barrier: while Xe does not detectably affect it, C_{60} reduces it significantly. These results suggest that a wide range of quantum arrays formed from functional molecular building blocks can be fabricated, and, in combination with different adsorbates, provide a rich playground for the modification of the quantum box properties. Thus, the quantum states embedded in on-surface structures can be engineered for exploring new physical phenomena, which could be implemented into future quantum devices.

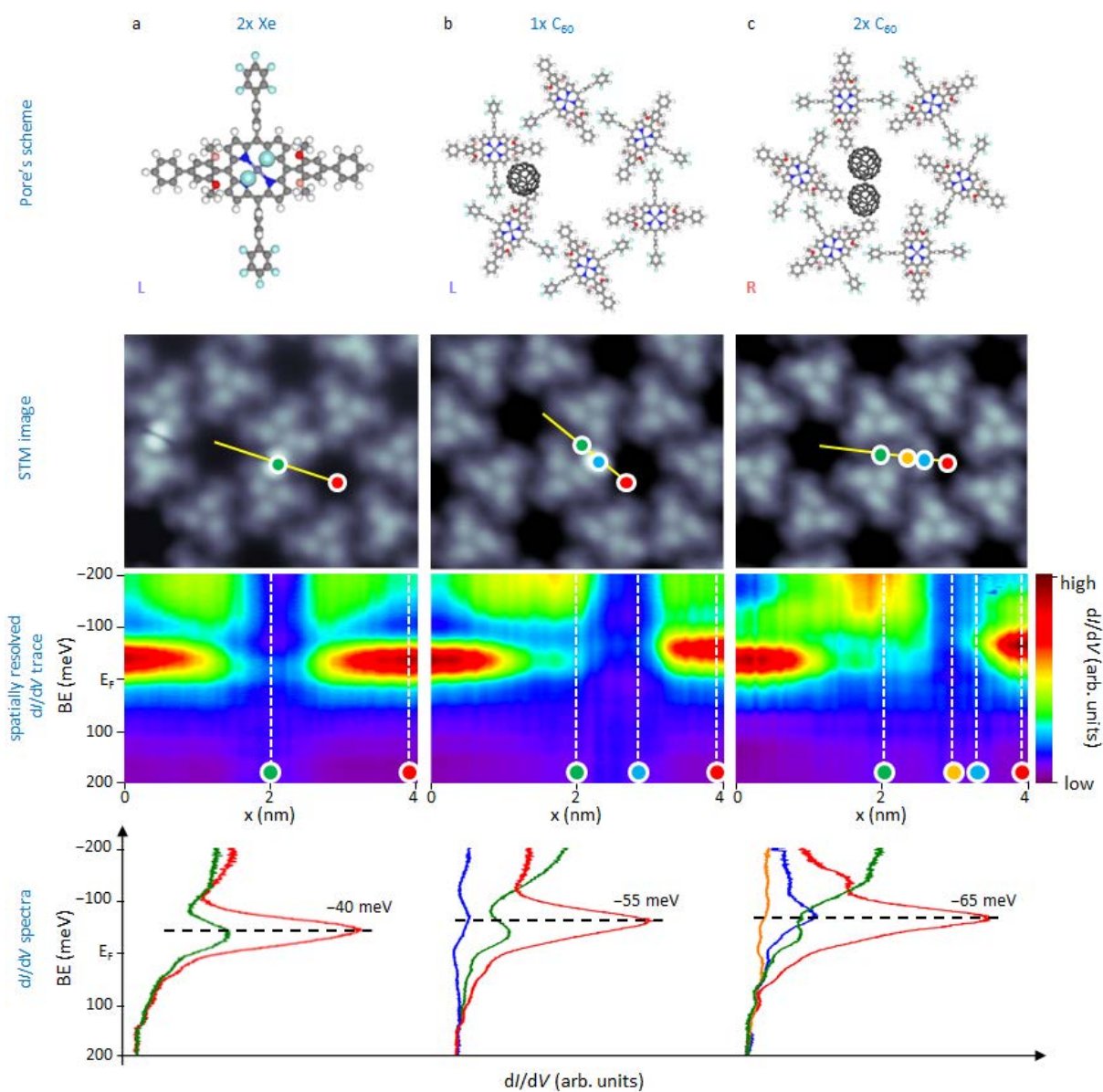


Figure 4 | Modification of barrier regions between the quantum boxes by adsorbates. (a) A barrier with two Xe atoms; (b) a barrier with a single C_{60} molecule; (c) a barrier with two C_{60} molecules. (1st row) Molecular models. (2nd row) Corresponding STM images (10 nm x 8 nm). (3rd row) Spatially resolved dI/dV traces acquired along the yellow lines superimposed on the STM images. (4th row) Selected dI/dV spectra taken at the positions indicated by the colored dots in the STM images and in the dI/dV traces. The molecular models overlaid on the STM pictures are presented in Supplementary Fig. S7b and Fig. S9.

Materials and methods

Synthesis of porphyrin 1. The synthesis of Zn(II) porphyrin **1** is described in detail in the Supplementary Synthesis file.

Sample preparation for STM/STS measurements. The Ag(111) substrate was prepared by cycles of Ar⁺ sputtering at $E = 1000$ eV followed by annealing at 800 K. The Zn(II) porphyrin molecules **1** were deposited with the use of a 9-cell evaporator (Kentax GmbH, Germany) on the Ag(111) substrate held at room temperature (RT). The glass crucible with the Zn(II) porphyrin **1** inside was heated up to the sublimation temperature (~ 320 °C). The rate was controlled prior to sublimation with a quartz crystal microbalance (QCMB). In order to obtain a porous network, the molecular rate was lower than $0.4 \text{ \AA}/\text{min}$. Otherwise, the formation of a close-packed assembly took place. The C₆₀ molecules (sublimation temperature ~ 350 °C) were deposited onto the sample with the porous network held at RT. Xe of purity 99.99% was dosed onto the sample placed in the STM operating at 4.2 K (Omicron Nanotechnology GmbH with Nanonis SPM control system) with the cryoshields open and the leak valve being in line-of-sight with the sample. The STM/STS measurements were performed after cooling the sample back to 4.2 K. In the main text and Supplementary Figures S1,2,4,7 the STM/STS data for a sample after 10 Langmuir (1.3×10^{-7} mbar for 100 s) of Xe exposure are shown. Supplementary Figure S8 presents the STM data taken after 100 Langmuir of Xe exposure, in which case the dosing time was increased 10 times by maintaining the same pressure as in the previous case. Both exposures resulted in an increase of the sample temperature to 8 K due to opening the cryoshield.

STM/STS measurements and their analysis. For the STM measurements, the bias voltage is applied to the tip. The bias voltages in the manuscript and the Supplementary Information refer to a grounded tip, such that the voltage axis in the dI/dV data can be related to the binding energy (BE) of the ARPES data.

STM measurements were performed in constant current mode with Pt-Ir tips (90% Pt, 10% Ir), prepared by mechanical cutting followed by sputtering and controlled indentation in the bare Ag(111) substrate. The majority STM images was acquired with a single Xe atom functionalized tip (cf. Supplementary Tab. S1), which increases the spatial resolution. The exact tunneling parameters for the STM images presented in the main text and Supplementary Information are displayed in Supplementary Tab. S1. The STM data were processed with the WSxM software⁴⁸. For better comparability of the data, the color histograms of the STM images were adjusted. Low-pass filtering was used for noise reduction.

All dI/dV spectra were recorded with open-feedback loop and with Xe-functionalized tips. Control spectra were acquired with a metallic tip, and no difference was observed in accordance with Ref. 49. The lock-in parameters were 513 Hz (frequency) and 8 mV (zero-to-peak amplitude).

The dI/dV data presented in Fig. 2, Fig. 4 and Supplementary Fig. S4 were acquired along the line indicated in the corresponding STM images and are displayed in form of spatially resolved dI/dV traces. The amount of measurement points for the traces was adjusted in dependence on the measured barrier (from 40 to 80 points per line). The initial tip conditions when taking dI/dV spectra amounted to -200 mV/150 pA, with the exception of the dI/dV data shown Fig. 4a, in which case -200 mV/50 pA was used. The reason for more delicate initial tip conditions when investigating Xe atoms adsorbed on a Zn(II) porphyrin **1** macrocycle is the relatively weak

interaction strength, which led to desorption when harsher dI/dV parameters were applied. The dI/dV maps presented in Supplementary Figure S4 were extracted from a grid spectroscopy measurement, in which an area of $6\text{ nm} \times 5\text{ nm}$ was mapped with a resolution of $30\text{ points} \times 25\text{ points}$. At each point, a dI/dV spectrum was measured (initial tip conditions $-200\text{ mV}/150\text{ pA}$). As described in detail in Ref. 50, the value of the initial voltage was chosen such, that no quantum box state or network backbone-related contribution was present. Owing to this, a normalization could be performed by setting the same dI/dV value at the setpoint energy for all dI/dV spectra. In this way, artefacts originating from local work function variations are minimized.

I(z) measurements and their analysis. The work function maps presented in Supplementary Figure S10 were obtained with the use of methods developed by Vitali *et al.*⁵¹ The maps were extracted from a grid spectroscopy measurement, in which at each point $I(z)$ curves were measured. From an exponential fit of the average of three $I(z)$ curves, the work function was extracted for each point.

LEED measurements and their analysis. The LEED measurements were performed with the use of a V. G. Electrovac LTD 474 unit. The LEED data were taken at energies between 5 eV and 60 eV . For simulating the experimentally obtained patterns the software LEEDpat 2.1 (K. Hermann, M. A. van Hove, LEED pattern simulator LEEDpat Version 2.1, 2006) was used (cf. Fig. 1c, Supplementary Figure S3).

ARPES measurements and their analysis. ARPES data were acquired at the beamline I3 of the synchrotron radiation source of MAX-III (Lund, Sweden). The $\text{Ag}(111)$ crystal was prepared by consecutive cycles of Ar^+ sputtering and annealing, similarly to the preparation used for the STM/STS measurements. The $\text{Zn}(\text{II})$ porphyrin molecules **1** were deposited with the use of a home-made evaporator. The rate prior to deposition was checked by QCMB.

It is worth mentioning that collecting ARPES data from organic materials is a challenging task⁸, as organic molecules can be destroyed by the incident UV light (beam-damage). A way to overcome this problem is to use a defocused light source and low photon energies for the experiment. Therefore beamline undulator was detuned in order to reduce the intensity of the photon beam, hence avoiding any radiation damage to the sample. The slits were set such that a light spot of 0.5 mm on the sample was obtained. Such a large light spot minimizes flux (and hence beam-damage), but causes a reduction in the angular resolution (and hence momentum resolution) of the ARPES measurement, estimated to be 0.04 1/\AA for the measurements presented in Fig. 3 of the main text. A photon energy of 21 eV was sufficient to keep the molecules intact over the whole acquisition time amounting to $\sim 1\text{ h}$. Moreover, no signs of degradation in the ARPES data were observed, even after several hours of experimental time, demonstrating the full viability of this approach for studying the particular system presented here.

The ARPES measurements were carried out at normal emission and at RT. The choice of the temperature is extremely important, since it induces a broadening of the Fermi-Dirac distribution, resulting in a promotion of thermal electrons from states below to states above the Fermi level. This allows the detection of electronic states even at energies above the Fermi level. However, the spectral intensity of such states is so weak that it is barely detectable by eye. In order to enhance the intensity of these states with respect to the intensities below the Fermi

level, we normalized the data by a Fermi function at RT. In addition, since the Fermi function goes exponentially to zero for low BE values, in order to avoid numerical issues in dividing the spectral intensity by 'zero', we added a small constant to the Fermi function (*i.e.* 0.03). Whilst the normalization allows an exceptionally good enhancement of the spectral features above the Fermi level, it artificially moves the centre of mass of the spectral intensity towards the Fermi level, resulting in an apparent small energy shift of the band minimum. Supplementary Fig. S12 displays the raw data, the raw data with amplified intensity and the normalized data. In Supplementary Fig. S13 raw and normalized ARPES data of bare Ag(111) is shown. In the such treated data, there is no additional state, which demonstrates the validity of the used normalization procedure.

Computational methods First-principle density functional theory calculations were performed using the Vienna ab-initio simulation code (VASP) with the generalized gradient approximation (PBE-GGA) and the projector augmented wave (PAW) method.

For the Ag($4d^{10}5s^1$), C($2s^22p^2$), F($2s^22p^5$), O($2s^22p^4$), Zn($3d^{10}4s^2$), H($1s^1$), and N ($2s^22p^3$) atoms states were treated as valence states with a plane-wave cutoff at 400 eV. We modelled the four layer FCC slab of Ag (111) with size of 26 Å and a vacuum layer of about 15 Å. A single Zn(II) porphyrin **1** molecule was placed on the Ag (111) substrate and was characterized by opposite torsion angles around the bond interconnecting the porphyrin macrocycle and the 3,5-dimethoxybiphenyl-4-yl substituents. The supercell was kept constant in order to keep the vacuum layer from collapsing. Additionally, selective dynamics was chosen, fixing the lowermost atoms in the Ag slab so that a much thicker layer is emulated. All calculations are done until the structures were fully relaxed and forces converged below 0.02 eV/Å.

References:

1. Kagan, C. R. & Murray, C. B. Charge transport in strongly coupled quantum dot solids. *Nat. Nanotechnol.* **10**, 1013–1026 (2015).
2. Shirasaki, Y., Supran, G. J., Bawendi, M. G. & Bulović, V. Emergence of colloidal quantum-dot light-emitting technologies. *Nat. Photonics* **7**, 13–23 (2012).
3. Stranks, S. D. & Snaith, H. J. Metal-halide perovskites for photovoltaic and light-emitting devices. *Nat. Nanotechnol.* **10**, 391–402 (2015).
4. Ladd, T. D. *et al.* Quantum computers. *Nature* **464**, 45–53 (2010).
5. Gross, L. *et al.* Scattering of Surface State Electrons at Large Organic Molecules. *Phys. Rev. Lett.* **93**, (2004).
6. Silly, F. *et al.* Creation of an Atomic Superlattice by Immersing Metallic Adatoms in a Two-Dimensional Electron Sea. *Phys. Rev. Lett.* **92**, 016101 (2004).
7. Han, P. & Weiss, P. S. Electronic substrate-mediated interactions. *Surf. Sci. Rep.* **67**, 19–81 (2012).
8. Lobo-Checa, J. *et al.* Band Formation from Coupled Quantum Dots Formed by a Nanoporous Network on a Copper Surface. *Science* **325**, 300–303 (2009).
9. Klappenberger, F. *et al.* Dichotomous Array of Chiral Quantum Corrals by a Self-Assembled Nanoporous Kagomé Network. *Nano Lett.* **9**, 3509–3514 (2009).

10. Klappenberger, F. *et al.* Tunable Quantum Dot Arrays Formed from Self-Assembled Metal-Organic Networks. *Phys. Rev. Lett.* **106**, 026802 (2011).
11. Seufert, K. *et al.* Controlled Interaction of Surface Quantum-Well Electronic States. *Nano Lett.* **13**, 6130–6135 (2013).
12. Li, J., Schneider, W.-D., Berndt, R. & Crampin, S. Electron Confinement to Nanoscale Ag Islands on Ag(111): A Quantitative Study. *Phys. Rev. Lett.* **80**, 3332–3335 (1998).
13. Crommie, M. F., Lutz, C. P. & Eigler, D. M. Confinement of electrons to quantum corrals on a metal surface. *Science* **262**, 218–220 (1993).
14. Nilius, N., Wallis, T. M. & Ho, W. Development of One-Dimensional Band Structure in Artificial Gold Chains. *Science* **297**, 1853–1856 (2002).
15. Pennec, Y. *et al.* Supramolecular gratings for tuneable confinement of electrons on metal surfaces. *Nat. Nanotechnol.* **2**, 99–103 (2007).
16. Shchyryba, A. *et al.* Covalent assembly of a two-dimensional molecular ‘sponge’ on a Cu(111) surface: confined electronic surface states in open and closed pores. *Chem. Commun.* **50**, 7628–7631 (2014).
17. Zhang, J. *et al.* Probing the spatial and momentum distribution of confined surface states in a metal coordination network. *Chem. Commun.* **50**, 12289–12292 (2014).
18. Schouteden, K. *et al.* Alkoxylated dehydrobenzo[12]annulene on Au(111): From single molecules to quantum dot molecular networks. *Chem. Commun.* **51**, 10917–10920 (2015).
19. Wang, S. *et al.* Tuning two-dimensional band structure of Cu(111) surface-state electrons that interplay with artificial supramolecular architectures. *Phys. Rev. B* **88**, 245430 (2013).
20. Cheng, Z. *et al.* Adsorbates in a Box: Titration of Substrate Electronic States. *Phys. Rev. Lett.* **105**, 066104 (2010).
21. Pivetta, M., Pacchioni, G. E., Schlickum, U., Barth, J. V. & Brune, H. Formation of Fe Cluster Superlattice in a Metal-Organic Quantum-Box Network. *Phys. Rev. Lett.* **110**, 086102 (2013).
22. Müller, K., Enache, M. & Stöhr, M. Confinement properties of 2D porous molecular networks on metal surfaces. *J. Phys. Condens. Matter* **28**, 153003 (2016).
23. Mazzola, F., Polley, C. M., Miwa, J. A., Simmons, M. Y. & Wells, J. W. Disentangling phonon and impurity interactions in δ -doped Si(001). *Appl. Phys. Lett.* **104**, 173108 (2014).
24. Ortega, J. E. *et al.* Scattering of surface electrons by isolated steps versus periodic step arrays. *Phys. Rev. B* **87**, 115425 (2013).
25. Mazzola, F. *et al.* Kinks in the σ Band of Graphene Induced by Electron-Phonon Coupling. *Phys. Rev. Lett.* **111**, (2013).
26. Howard, J. A. K., Hoy, V. J., O’Hagan, D. & Smith, G. T. How good is fluorine as a hydrogen bond acceptor? *Tetrahedron* **52**, 12613–12622 (1996).
27. Schneider, H.-J. Hydrogen bonds with fluorine. Studies in solution, in gas phase and by computations, conflicting conclusions from crystallographic analyses. *Chem. Sci.* **3**, 1381 (2012).
28. Dunitz, J. D. & Taylor, R. Organic Fluorine Hardly Ever Accepts Hydrogen Bonds. *Chem. - Eur. J.* **3**, 89–98 (1997).
29. Meanwell, N. A., Eastman, K. J. & Gillis, E. P. in *Fluorine in Heterocyclic Chemistry Volume 1* (ed. Nenajdenko, V.) **Chapter 6.1**, 1–54 (Springer International Publishing, 2014).

30. Shimoni, L. & Glusker, J. P. in *Science of Crystal Structures* (eds. Hargittai, I. & Hargittai, B.) 187–203 (Springer International Publishing, 2015).
31. Hipps, K. W., Scudiero, L., Barlow, D. E. & Cooke, M. P. A Self-Organized 2-Dimensional Bifunctional Structure Formed by Supramolecular Design. *J Am Chem Soc* **124**, 2126–2127 (2002).
32. Mu, Z., Shu, L., Fuchs, H., Mayor, M. & Chi, L. Two Dimensional Chiral Networks Emerging from the Aryl–F···H Hydrogen-Bond-Driven Self-Assembly of Partially Fluorinated Rigid Molecular Structures. *J Am Chem Soc* **130**, 10840–10841 (2008).
33. Calzolari, A., Jin, W., Reutt-Robey, J. E. & Buongiorno Nardelli, M. Substrate-Mediated Intermolecular Hybridization in Binary Phthalocyanine Superstructures. *J. Phys. Chem. C* **114**, 1041–1045 (2010).
34. Wäckerlin, C. *et al.* Two-Dimensional Supramolecular Electron Spin Arrays. *Adv. Mater.* **25**, 2404–2408 (2013).
35. Kawai, S. *et al.* Obtaining Detailed Structural Information about Supramolecular Systems on Surfaces by Combining High-Resolution Force Microscopy with *ab Initio* Calculations. *ACS Nano* **7**, 9098–9105 (2013).
36. Wintjes, N. *et al.* A Supramolecular Multiposition Rotary Device. *Angew. Chem. Int. Ed.* **46**, 4089–4092 (2007).
37. Wintjes, N. *et al.* Supramolecular Synthons on Surfaces: Controlling Dimensionality and Periodicity of Tetraarylporphyrin Assemblies by the Interplay of Cyano and Alkoxy Substituents. *Chem. - Eur. J.* **14**, 5794–5802 (2008).
38. Ćija, D. *et al.* Hierarchic Self-Assembly of Nanoporous Chiral Networks with Conformationally Flexible Porphyrins. *ACS Nano* **4**, 4936–4942 (2010).
39. Pace, C. J. & Gao, J. Exploring and Exploiting Polar– π Interactions with Fluorinated Aromatic Amino Acids. *Acc. Chem. Res.* **46**, 907–915 (2013).
40. Reichenbacher, K., Süß, H. I. & Hulliger, J. Fluorine in crystal engineering—‘the little atom that could’. *Chem Soc Rev* **34**, 22–30 (2005).
41. Schwarzer, A. & Weber, E. Penta- and Decafluorinated Dibenzalacetones: Synthesis, Crystal Structure, and CocrySTALLIZATION Experiments. *Cryst. Growth Des.* **14**, 2335–2342 (2014).
42. Ponzini, F., Zagha, R., Hardcastle, K. & Siegel, J. S. Phenyl/Pentafluorophenyl Interactions and the Generation of Ordered Mixed Crystals: sym-Triphenethynylbenzene and sym-Tris(perfluorophenethynyl)benzene. *Angew. Chem. Int. Ed.* **39**, 2323–2325 (2000).
43. Coates, G. W., Dunn, A. R., Henling, L. M., Dougherty, D. A. & Grubbs, R. H. Phenyl–Perfluorophenyl Stacking Interactions: A New Strategy for Supermolecule Construction. *Angew. Chem. Int. Ed. Engl.* **36**, 248–251 (1997).
44. Reinert, F., Nicolay, G., Schmidt, S., Ehm, D. & Hüfner, S. Direct measurements of the L-gap surface states on the (111) face of noble metals by photoelectron spectroscopy. *Phys. Rev. B* **63**, 115415 (2001).
45. Piquero-Zulaica, I. *et al.* Temperature dependence of the partially localized state in a 2D molecular nanoporous network. *Appl. Surf. Sci.* (2016). doi:10.1016/j.apsusc.2016.02.227
46. Paniago, R., Matzdorf, R., Meister, G. & Goldmann, A. Temperature dependence of Shockley-type surface energy bands on Cu(111), Ag(111) and Au(111). *Surf. Sci.* **336**, 113–122 (1995).
47. Nowakowska, S. *et al.* Interplay of weak interactions in the atom-by-atom condensation of xenon within quantum boxes. *Nat. Commun.* **6**, 6071 (2015).

48. Horcas, I. *et al.* WSXM: A software for scanning probe microscopy and a tool for nanotechnology. *Rev. Sci. Instrum.* **78**, 013705 (2007).
49. Manoharan, H. C., Lutz, C. P. & Eigler, D. M. Quantum mirages formed by coherent projection of electronic structure. *Nature* **403**, 512–515 (2000).
50. Krenner, W., Kühne, D., Klappenberger, F. & Barth, J. V. Assessment of Scanning Tunneling Spectroscopy Modes Inspecting Electron Confinement in Surface-Confined Supramolecular Networks. *Sci. Rep.* **3**, (2013).
51. Vitali, L. *et al.* Portrait of the potential barrier at metal-organic nanocontacts. *Nat. Mater.* **9**, 320–323 (2010).

Acknowledgements

We would like to acknowledge the financial support from the National Centre of Competence in Research “Nanoscience” (NCCR-Nano, project “Nanoscale Science”), Swiss Nanoscience Institute (SNI) (Project No. P1204 and P1203), Swiss National Science Foundation (grants No. 200020-149713, 206021-121461, 206021-113149, 206021-144991), Marie-Curie Research Training Network PRAIRIES (grant No. MRTN-CT-2006-035810), Norwegian University of Science and Technology, MAX-lab, the São Paulo Research Foundation (grant No. 2013/04855-0), Swiss Government Excellence Scholarship Program (grant No. 2013.0942), Netherlands Organization for Scientific Research NWO (Chemical Sciences, VIDI-grant No. 700.10.424) the European Research Council (ERC-2012-StG 307760-SURFPRO), the Hundred Talents project of the Chinese Academy of Sciences, Knut and Alice Wallenberg Foundation and the Swedish Research Council, Commission for Technology and Innovation (CTI) Contract No. 16464.1 PFNM-NM, University of Basel, ETH Zürich, University of Groningen, Swiss Light Source, Wolfermann Naegeli Foundation and Paul Scherrer Institute. The research of M.N.A. is implemented within the framework of the Action «Supporting Postdoctoral Researchers» of the Operational Program "Education and Lifelong Learning" (Action's Beneficiary: General Secretariat for Research and Technology), and is co-financed by the European Social Fund (ESF) and the Greek State. We sincerely thank Marco Martina for technical support.

Author contributions

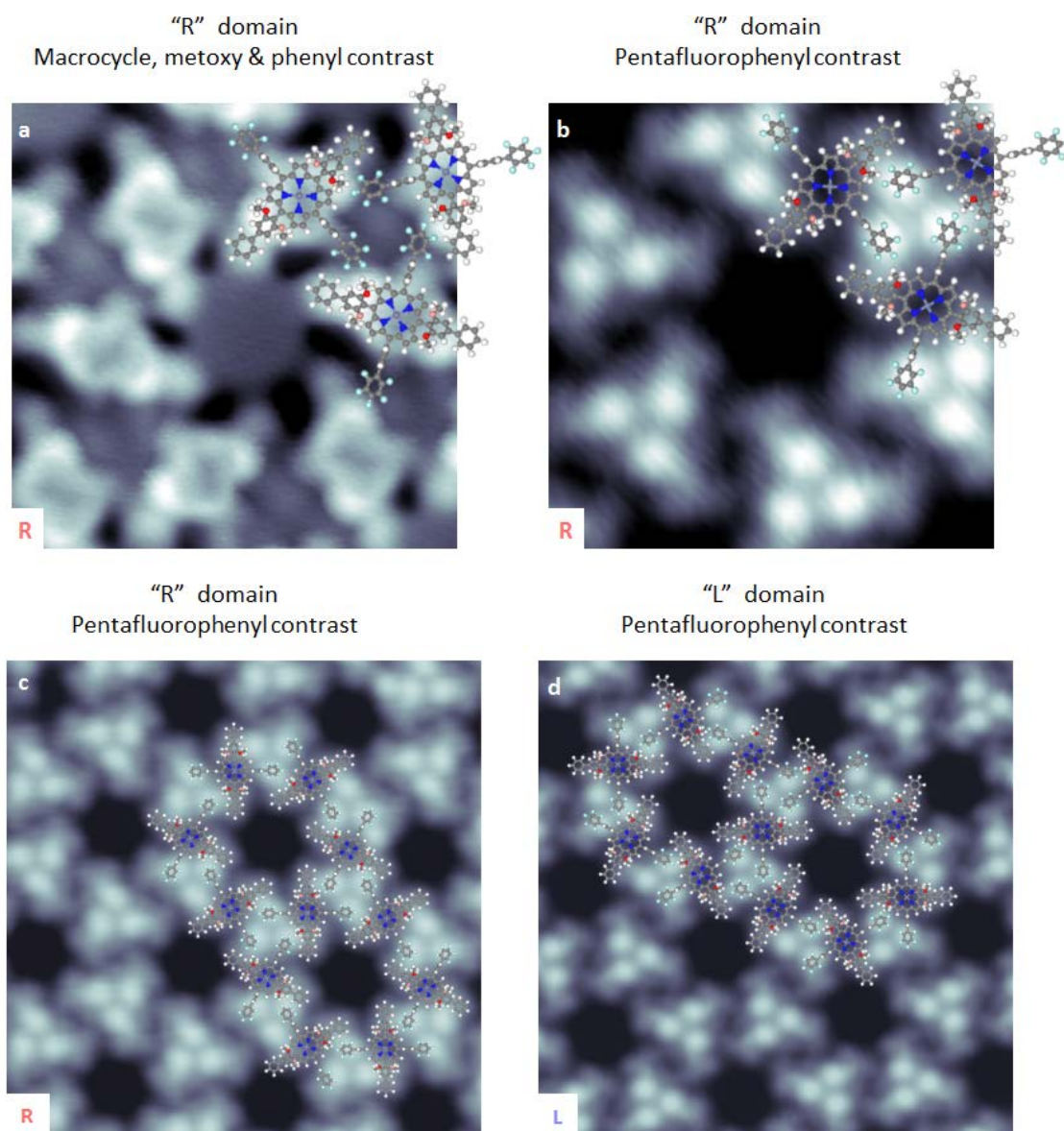
The molecular material was provided by M.N.A., T.V., M.B., C.T. and F.D. The X-ray crystal structure analysis was performed by W.B.S. The STM/STS, I(z) and LEED measurements and their analysis was conducted by S.N., J.N., A.W., C.W., J.Wiss., S.F., T.I., S.F.M., A.A., T.N., O.P., M.S. and discussed with T.A.J., J. Wells, F.M., J.Z. and M.M. The ARPES measurements were performed by J.Wells, F.M., F.S., C.P., M.L. and S.N. and analysed by F.M. and J. Wells. The DFT calculations were performed by T.I. The manuscript was written by S.N., T.A.J., M.N.A., F.M. and J. Wells.

Additional information

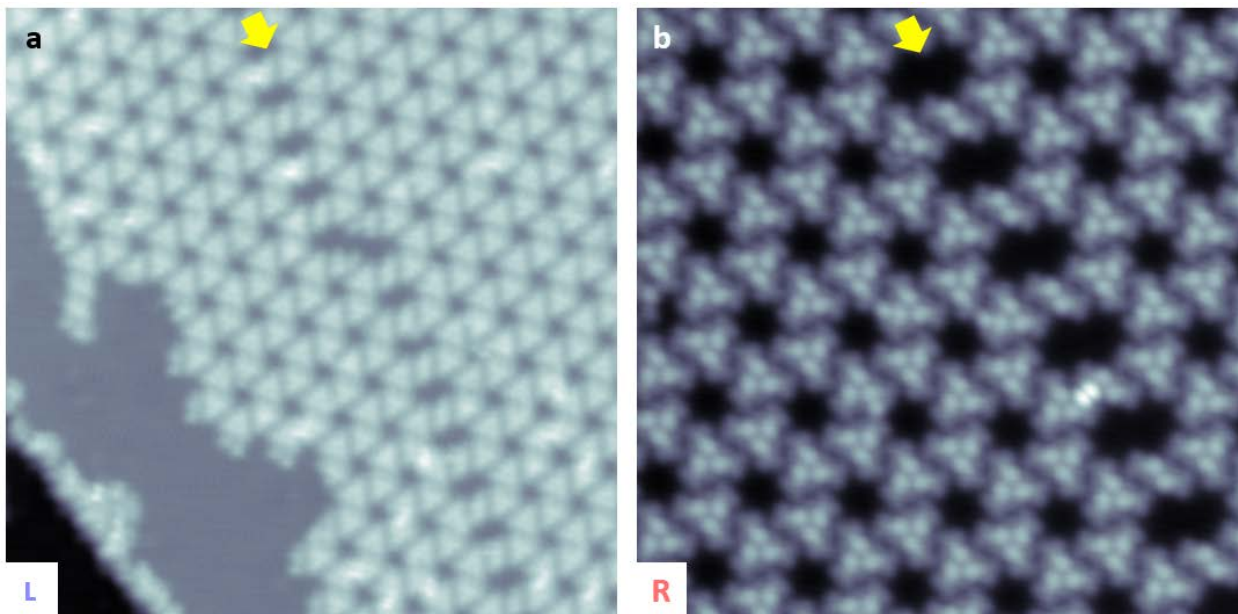
Supplementary information is available in the online version of the paper. Correspondence and request for materials should be addressed to S.N., F.D., J. Wells and T.A.J.

Competing financial interest

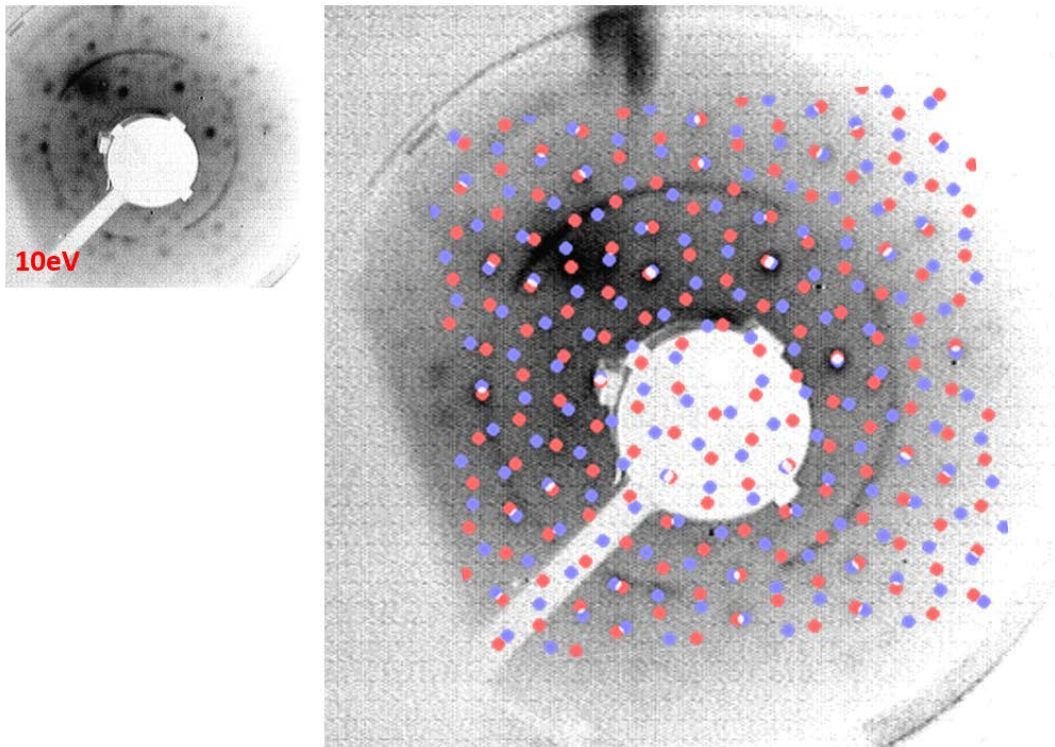
The authors declare no competing financial interest.



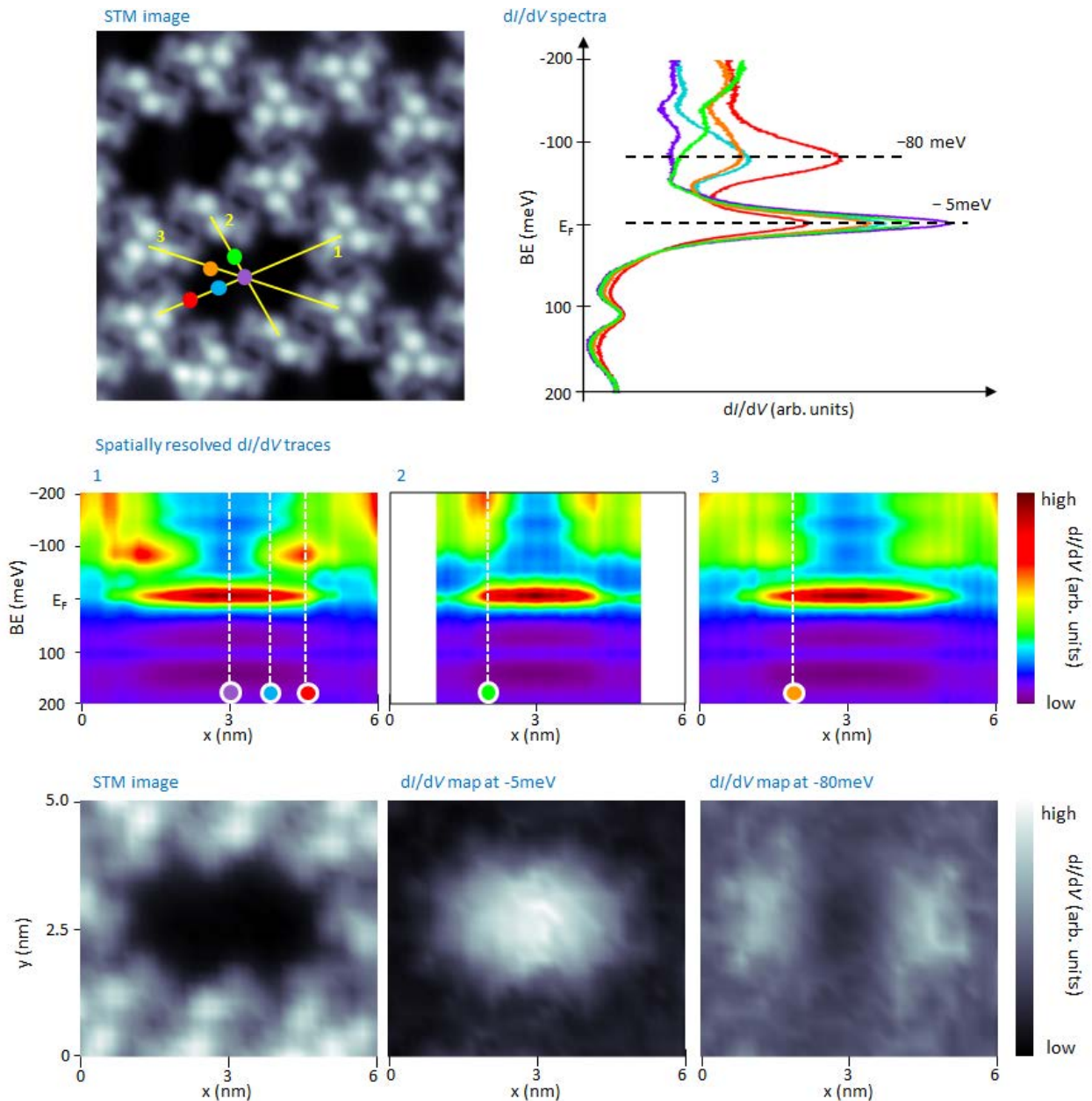
Supplementary Figure S1 | Comparison of two different STM contrasts allowing for unambiguous determination of the adsorption sites of Zn(II) porphyrin 1 in enantiomorphous “R” and “L” domains. STM image of (a) an “R” domain, in which macrocycle, methoxy and phenyl groups are emphasized, allowing for a clear assignment of the adsorption sites of the raised methoxy groups; (b-c) an “R” domain revealing the adsorption sites of the pentafluorophenyl groups; (d) an “L” domain revealing the adsorption sites of the pentafluorophenyl groups. Size of STM images: (a-b) 6 nm × 6 nm (c-d) 12.5 nm × 12 nm. STM image (a) was acquired with the tip exhibiting unknown functionalization, whereas (b-d) were acquired with the tip functionalized with a single Xe atom.



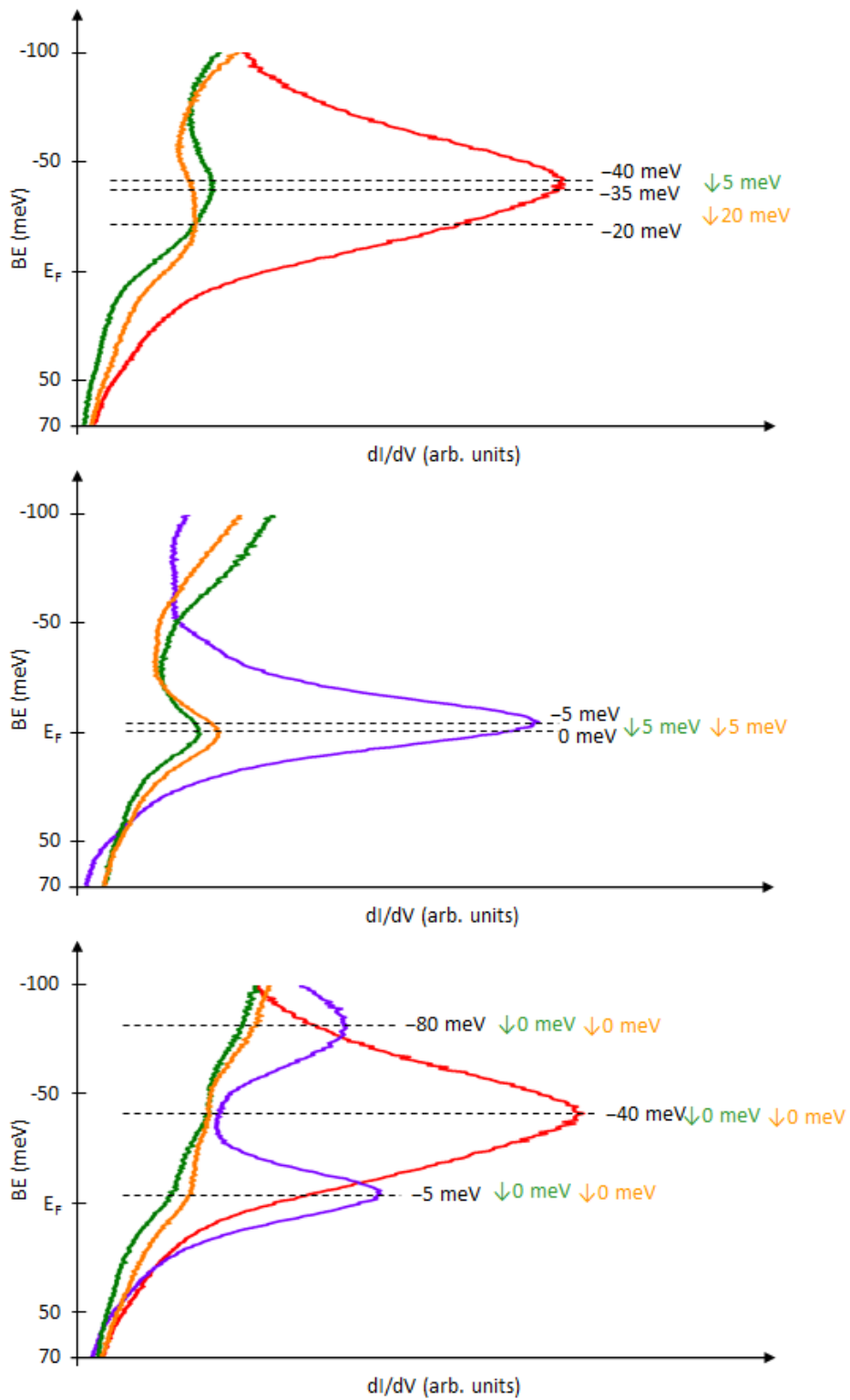
Supplementary Figure S2 | Domain boundaries, indicated by yellow arrows, in the form of linear arrays of *big* pores observed between supra-molecular islands consisting of *small* pores. The size of STM images (a) 50 nm x 50 nm and (b) 25 nm x 25 nm.



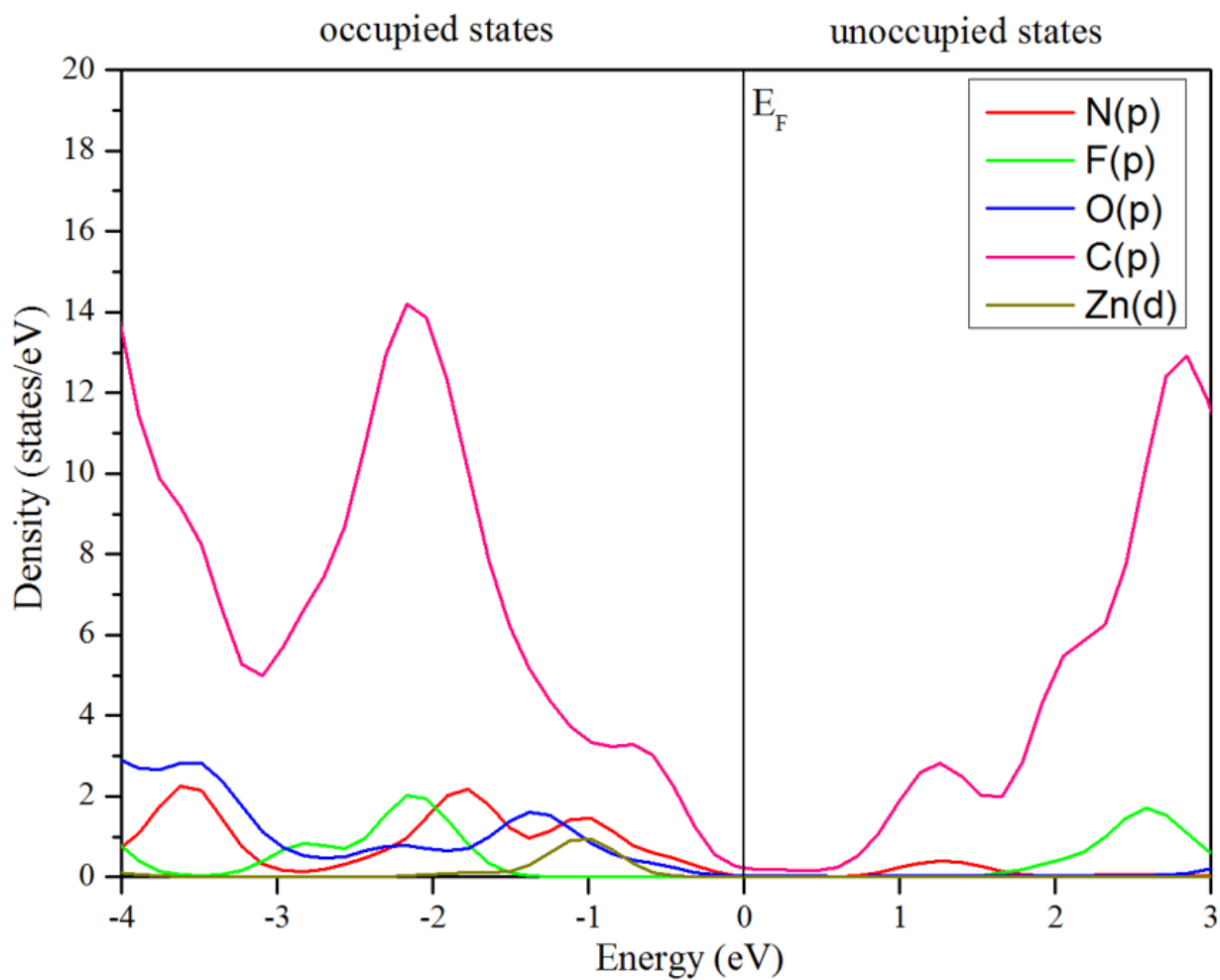
Supplementary Figure S3 | Comparison of the experimental LEED pattern taken at $E=10$ eV with the simulated pattern. In the simulated pattern the violet (coral) spots correspond to the “L” (“R”) domains.



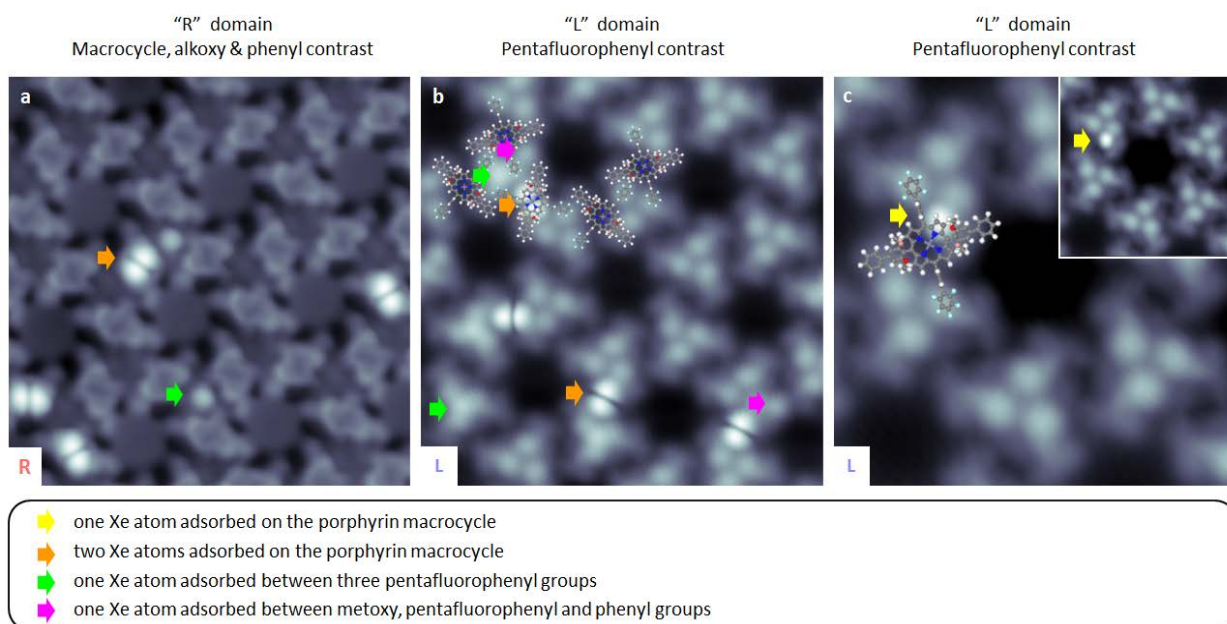
Supplementary Figure S4 | dI/dV characterization of a *big* pore. (1st row - left hand side) STM image of the measured area containing the *big* pore (11 nm \times 11 nm). (2nd row) Spatially resolved dI/dV traces acquired along the yellow lines superimposed on the upper STM image. (1st row - right hand side) Selected dI/dV spectra taken at the positions of the colored dots indicated in the upper STM image and in the dI/dV traces. Two peaks characteristic for the QBSs are present at -5 meV and -80 meV. (3rd row) STM image of the *big* pore and corresponding dI/dV maps (6 nm \times 5 nm) at the energies of the QBSs to access their spatial distribution: the state at -5 meV is dominating in the centre of the pore, whereas the state at -80 meV is dominating at the rim of the pore. These data were extracted from the grid spectroscopy measurement (details in Materials and Methods section).



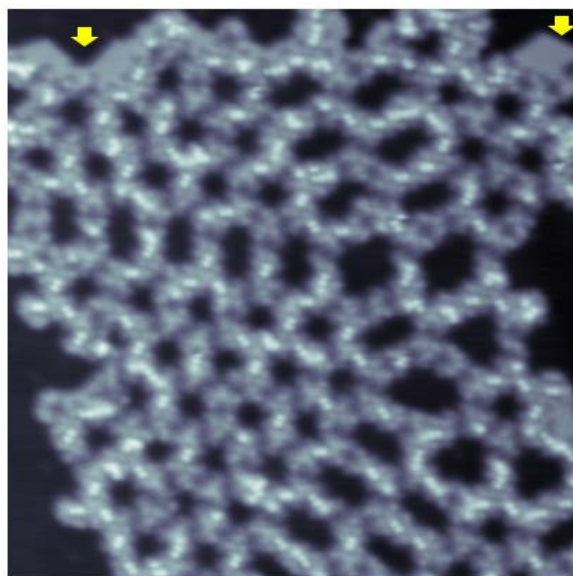
Supplementary Figure S5 | Close-ups of the QBS peaks of the dI/dV spectra shown in Figure 2 of the main text.



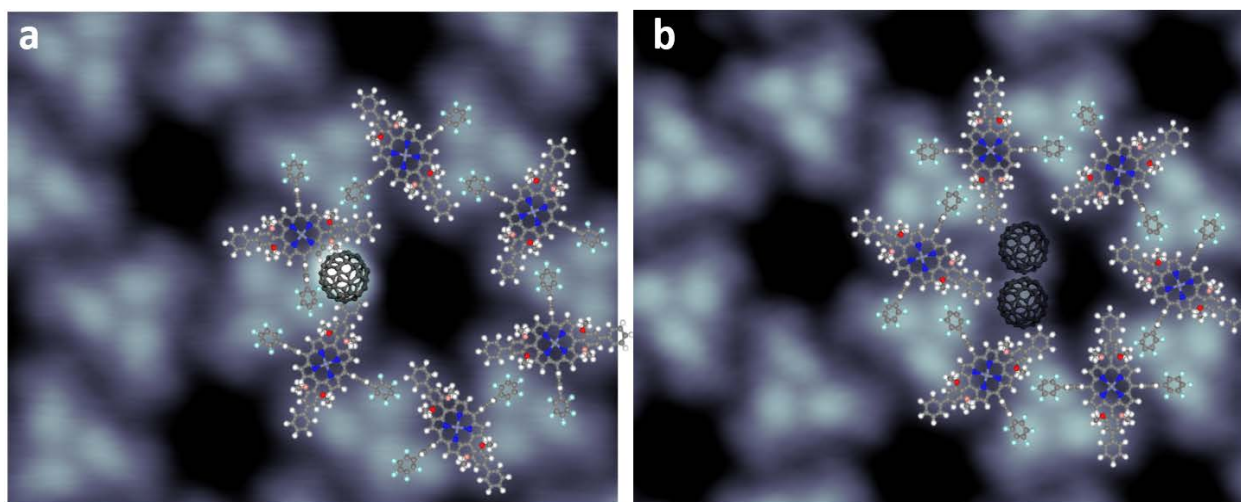
Supplementary Figure S6 | First-principle density functional theory calculations for a Zn(II) porphyrin 1 adsorbed on Ag(111) surface. The projected density of states for different atoms is plotted. There is a HOMO-LUMO gap centered around the Fermi level.



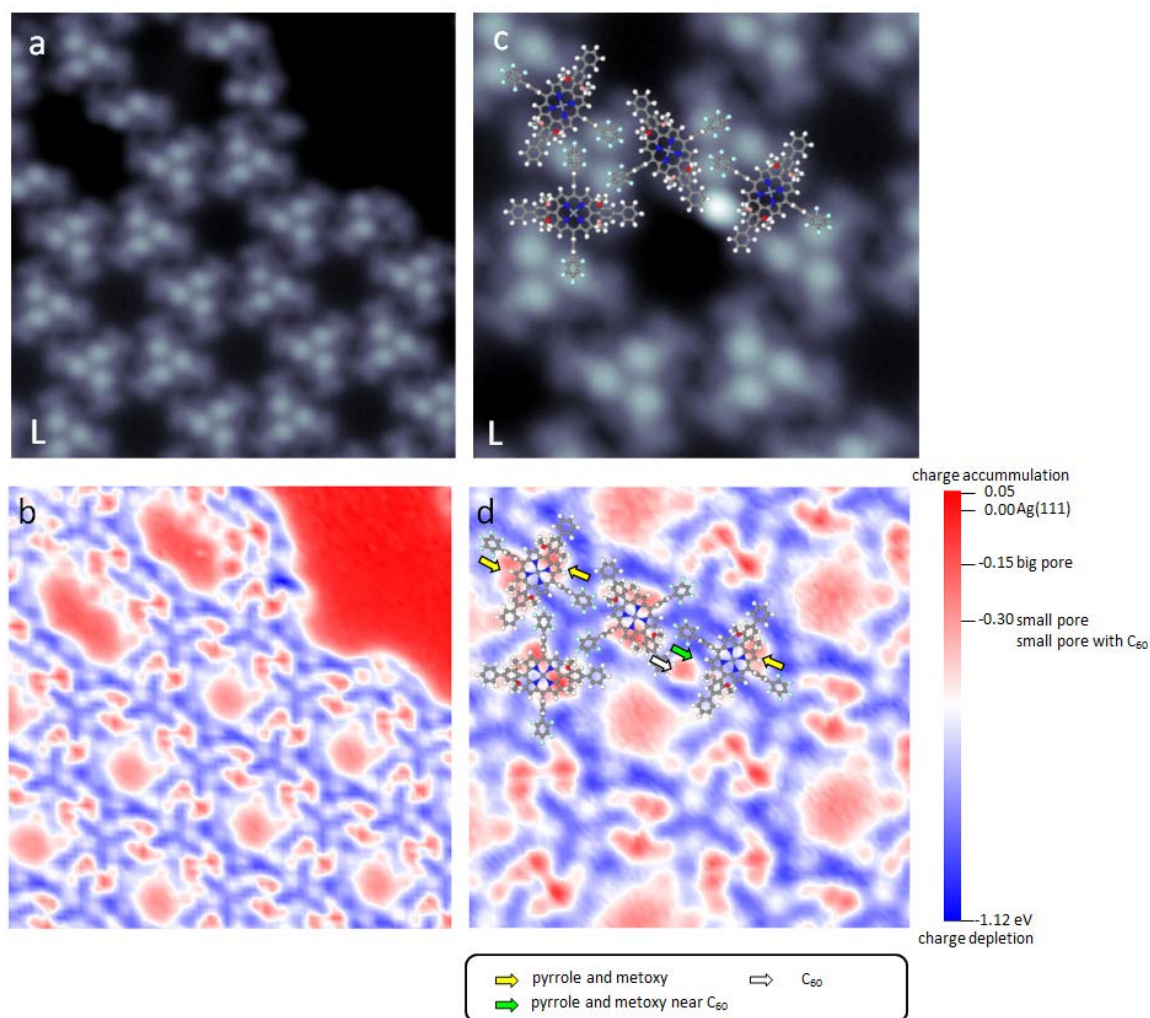
Supplementary Figure S7 | Adsorption sites of Xe on the porous network created from Zn(II) porphyrin 1 on Ag(111). Four different adsorption sites are observed, as specified in the legend (size of the STM images: (a - b) 12 nm × 12 nm, (c) 7 nm × 7nm).



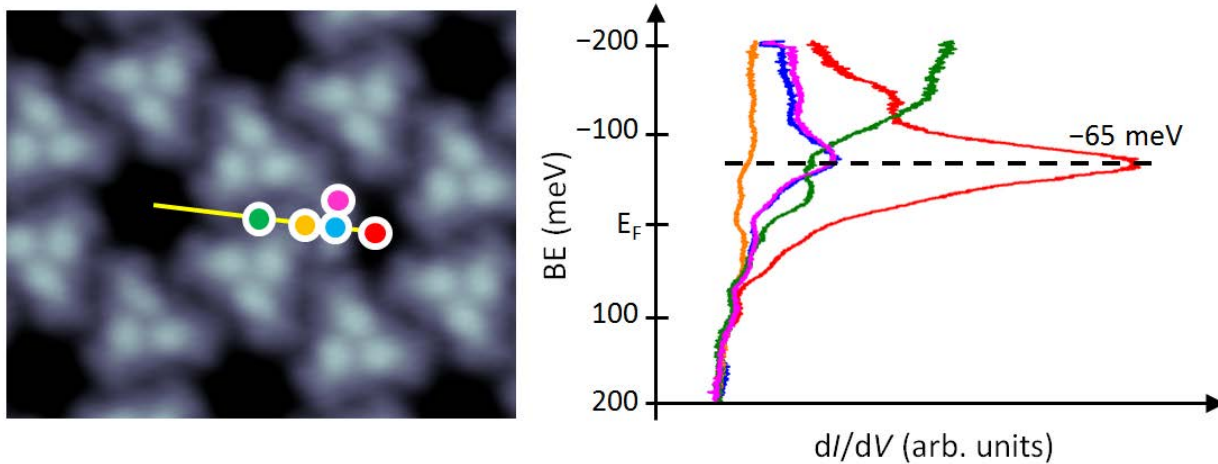
Supplementary Figure S8 | STM image of the porous network of Zn(II) porphyrin 1 on Ag(111) after 100 Langmuir of Xe exposure. No adsorption of Xe in the center of the pores is observed. Small Xe islands are observed near the network domains (yellow arrows) (size of the STM image: 40 nm × 40 nm).



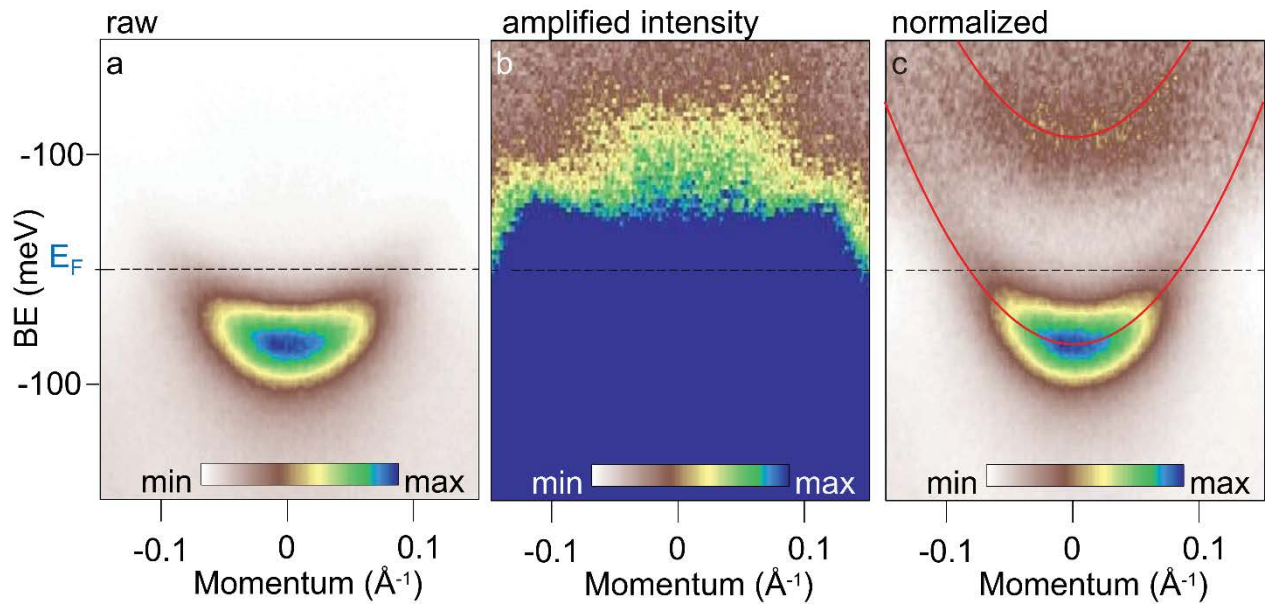
Supplementary Figure S9 | Adsorption sites of C_{60} on the porous network created from Zn(II) porphyrin 1 on Ag(111). Molecular models of the Zn(II) porphyrin 1 and C_{60} overlaid on STM images of pores containing (a) a single C_{60} molecule and (b) two C_{60} molecules. The STM images are the same as in Figure 4b,c of the main text (size: 10 nm x 8 nm)



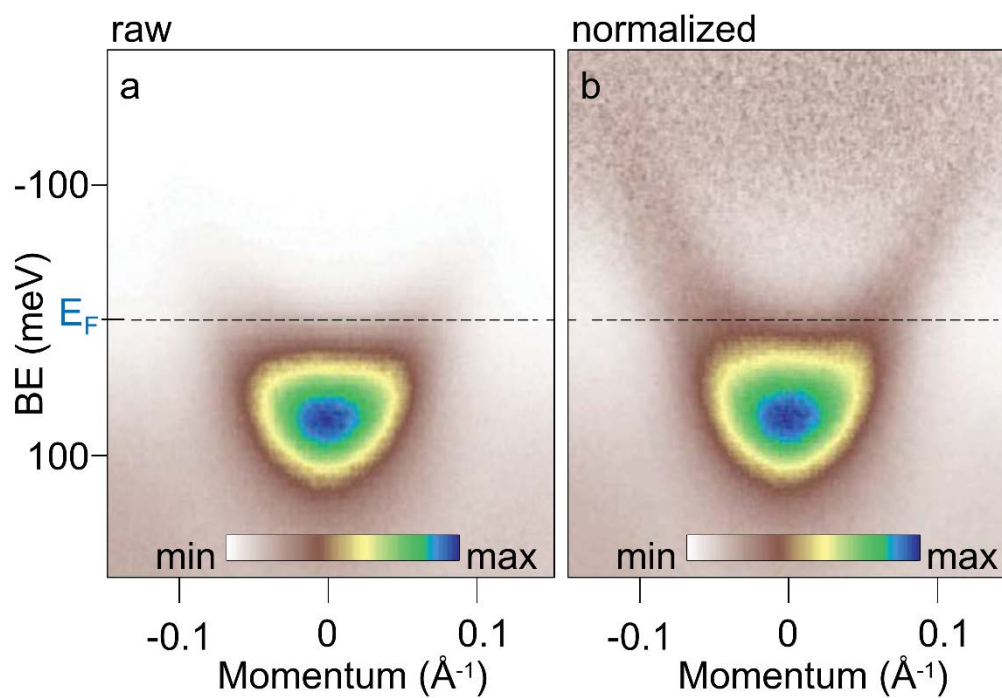
Supplementary Figure S10 | Electronic landscape modification upon deposition of C₆₀ (a) STM image taken at the network boundary and (b) the corresponding work function map to set the reference work function value $\Phi = 0$ on Ag(111). (c) STM image of a pore with a single C₆₀ molecule adsorbed and (d) the corresponding work function map. The pyrrole of the macrocycle and the lower methoxy group close to the adsorbed C₆₀ is more electropositive (green arrow) than the corresponding groups of a Zn(II) porphyrin **1** surrounding an empty pore (yellow arrows). This difference indicates an interaction between the porphyrin and C₆₀, which we assign to cause the local change in the corresponding barrier transmission probability (Fig. 4b of the main text). Both work function maps are plotted using the same color scale. Size of the STM images and the corresponding work function maps: (a-b) 14 nm x 14 nm, (c-d) 8 nm x 8nm.



Supplementary Figure S11 | STM image of a quantum box filled with two C₆₀ molecules and corresponding dI/dV spectra, taken at the positions indicated by the colored dots in the STM image, as in Figure 4c of the main text. Here, the dI/dV spectrum (magenta) acquired above the C₆₀ molecule is additionally shown. The fact, that the modified QBS is detected above the C₆₀ molecule shows that the pore area is not simply reduced by the presence of this adsorbate.



Supplementary Figure S12 | ARPES data of a 2D periodic array of quantum units formed by a Zn(II) porphyrin 1 porous network on Ag(111). (a) Raw data, (b) data with amplified intensity and (c) normalized data as in Fig. 3 of the main text (procedure described in Materials and Methods section). In both **b** and **c**, the intensity above the Fermi level, where the quantum box state is, is clearly visible.



Supplementary Figure S13 | ARPES data of bare Ag(111) surface. a) Raw and b) normalized data with the use of the same procedure as was applied to the ARPES data presented in Fig. 3 of the main text. Importantly, in the treated data of clean Ag(111) surface, there is no additional state dispersing above the Fermi level, which demonstrates that the state dispersing above the Fermi level (Fig. 3) is coming from the porous network.

Supplementary Table S1 | Tunneling parameters of STM images presented in the main text and the SI.

	Voltage [mV]	Current [pA]	Tip functionalization
Fig. 1a	-1000	1	metallic
Fig. 2	45	150	Xe
Fig. 4a	45	40	Xe
Fig. 4b	-800	10	Xe
Fig. 4c	-800	10	Xe
Fig. S1a	-1000	10	unknown
Fig. S1b	45	5	Xe
Fig. S1c	-1000	5	Xe
Fig. S1d	45	150	Xe
Fig. S2a	-1000	10	metallic
Fig. S2b	-1000	5	Xe
Fig. S4 (upper STM image)	45	150	Xe
Fig. S4 (lower STM image)	-200	150	Xe
Fig. S7a	45	5	unknown
Fig. S7b	45	40	Xe
Fig. S7c	45	80	Xe
Fig. S8	-1000	10	Xe
Fig. S9a	-800	10	Xe
Fig. S9b	-800	10	Xe
Fig. S10a	45	150	Xe
Fig. S10b	45	150	Xe
Fig. S11	-800	10	Xe

Summary and outlook

In this thesis a novel approach of an atom-by-atom investigation of the condensation as well as an achievement of quantum arrays allowing for flexible configuration of their electronic states by adsorbates are presented. The realization of these concepts utilized the capability of the scanning tunneling microscope (STM) tip to reposition single adsorbates as well as the ability of self-assembled on-surface porous networks to trap different adsorbates and to confine the surface state electrons. Therefore each pore functions as a quantum box and a network can be viewed as a quantum array.

The first system comprised of xenon and a Cu-coordinated 3deh-DPDI network grown on Cu(111). Each pore of the network can host each number of xenon atoms ranging from 1 to 12. Our studies show that the condensation of xenon in each of these pores is governed by the interplay of weak interactions originating from (i) the registry of the underlying substrate, (ii) the border of the confinement and (iii) an electronic quantum box state localized therein. As a result the aggregates do not follow simple ‘hierarchical filling rules’, but exhibit a complex self-assembly behavior governed by different competing principles [[1]]. This system was also extensively characterized to assess its potential for being used as a *quantum breadboard*. Indeed, this system fulfills all four requirements listed in the introduction: (i) xenon adsorbs in the pores of the network; (ii) xenon modifies the quantum states; (iii) by an appropriate arrangement of the empty/xenon-filled quantum boxes the electronic coupling can be maintained or significantly reduced; (iv) xenon can be easily repositioned by the STM tip. [[2]]

With the second presented system it is demonstrated that also the barrier walls of a quantum array formed by a porphyrin porous network on Ag(111) can be locally modified by C₆₀ adsorption. This system fulfills the first three requirements for forming a quantum breadboard: (i) C₆₀ adsorbs in the pores of the network; (ii) C₆₀ influences the quantum states; (iii) C₆₀ significantly reduces of the transmission probability of the barrier, thus the electronic coupling between the pores. The 4th requirement, *i.e.* the STM repositioning of the adsorbate,

is not met, as the strong interaction between the C₆₀ and the porphyrin molecule and/or the Ag(111) surface does not allow for its manipulation. [[3]]

For both quantum box arrays investigated in this thesis, [[2,3]] the scalability of the governing physics has been evidenced by angle-resolved photoemission spectroscopy (ARPES) demonstrating the long range order, reproducibility of manufacturing and the possibility to determine macroscopic cooperative properties by the self-assembled nanoscale architectures. Moreover the effective mass of the partially confined electrons in the pores of a network was measured experimentally by ARPES and it was shown that in case of the Cu-coordinated 3deh-DPDI network on Cu(111) it is higher than the effective mass of electrons of the Shockley surface state, in contrast to what was assumed in the previous reports concerning the modeling of on-surface confinement in the porous networks (cf. Introduction). Further increase of the effective mass was registered after the adsorption of xenon in the pores. Interestingly, no such change was observed for the Shockley surface state of Cu(111) upon adsorption of a monolayer of xenon. In case of the porphyrin network on Ag(111) the effective mass of an electron was equal to the effective mass of the electron of the Shockley surface state. Notably, these were the first ARPES measurements of a quantum array featuring its quantum state above the Fermi level.

Some of the beauty of the systems investigated in this PhD thesis derives from the direct experimentation with a quantum box. While first experiments with confined electronic states in quantum boxes of different architectures have been demonstrated more than 20 years ago, this thesis shows the first example of a non-conventional adsorption case in such quantum boxes and with the use of adsorbates reveals the electronic inter-box interaction. In view of the unprecedented character of the quantum arrays presented in this thesis and manifold options for their systematic modification there remain many open questions and ideas for further experiments which are briefly described in the following.

Atom-by-atom (molecule-by-molecule) condensation studies can be performed for different atoms (molecules) as well as in differently sized pores. The former allows for modification of the inter-atomic / intermolecular interactions and the latter would allow for tuning the interplay of the weak interactions, which are expected to have smaller/bigger influence in bigger/smaller pores. Furthermore the observation of the particularly stable, *i.e.* the ‘magic’, condensates motivates temperature dependent studies: due to their higher stability the ‘magic’

condensates are expected to start to librate / diffuse at higher temperature than other ‘non-magic’ clusters. Varying the temperature offers also a fascinating possibility to study phase transitions on the atomic level. Moreover the complexity of the obtained results asks for theoretical investigations which may capture the complex xenon condensation in the quantum boxes. This approach is able to provide benchmark results for first principle calculations to be assessed and improved towards the more accurate prediction of the properties of nanostructures.

The *quantum arrays* studies also opened many important questions. Our STS/ARPES data in conjunction with follow-up experimental studies and the *ab-initio* calculations shall provide an insight into the fascinating phenomenon of on-surface confinement. It would be desirable to resolve and to understand the substructure of the dI/dV peaks for different arrangements of the empty/adsorbate-filled pores and to find the reason of the effective mass change upon xenon deposition in the pores of the Cu-coordinated 3deh-DPDI network. The studies of a porphyrin porous network with C₆₀ motivate *ab-initio* calculations to find the exact mechanism of the reduction of the barrier transmission. The presented quantum arrays also suggest further and deeper investigations with similar ‘quantum lego’ systems, *i.e.* combinations of self-assembled on-surface architectures with suited adsorbates. In this way an unprecedented toolbox for quantum states engineering will be achieved, as a quantum array can be configured with basically unlimited number of combinations owing to the universality of the here presented approach.

Bibliography

1. Feynman, R. P. There's plenty of room at the bottom [data storage]. *J. Microelectromechanical Syst.* **1**, 60–66 (1992).
2. *Nanoscale science and technology*. (John Wiley, 2005).
3. Wang, Z. M. *Quantum dot devices*. (Springer, 2012).
4. Ladd, T. D. *et al.* Quantum computers. *Nature* **464**, 45–53 (2010).
5. Kloeffel, C. & Loss, D. Prospects for Spin-Based Quantum Computing in Quantum Dots. *Annu. Rev. Condens. Matter Phys.* **4**, 51–81 (2013).
6. Fölsch, S., Martínez-Blanco, J., Yang, J., Kanisawa, K. & Erwin, S. C. Quantum dots with single-atom precision. *Nat. Nanotechnol.* **9**, 505–508 (2014).
7. Binnig, G., Rohrer, H., Gerber, C. & Weibel, E. Surface studies by scanning tunneling microscopy. *Phys. Rev. Lett.* **49**, 57–61 (1982).
8. Eigler, D. M. & Schweizer, E. K. Positioning single atoms with a scanning tunnelling microscope. *Nature* **344**, 524–526 (1990).
9. Crommie, M. F., Lutz, C. P. & Eigler, D. M. Confinement of electrons to quantum corrals on a metal surface. *Science* **262**, 218–220 (1993).
10. Shockley, W. On the surface states associated with a periodic potential. *Phys. Rev.* **56**, 317 (1939).
11. Oura, K. *Surface science: an introduction*. (Springer, 2003).
12. Hasegawa, Y. & Avouris, P. Direct observation of standing wave formation at surface steps using scanning tunneling spectroscopy. *Phys. Rev. Lett.* **71**, 1071–1074 (1993).
13. Crommie, M. F., Lutz, C. P. & Eigler, D. M. Imaging standing waves in a two-dimensional electron gas. *Nature* **363**, 524–527 (1993).
14. Bürgi, L., Knorr, N., Brune, H., Schneider, M. A. & Kern, K. Two-dimensional electron gas at noble-metal surfaces. *Appl. Phys. A* **75**, 141–145 (2002).
15. Han, P. & Weiss, P. S. Electronic substrate-mediated interactions. *Surf. Sci. Rep.* **67**, 19–81 (2012).
16. Ortega, J. E. *et al.* Scattering of surface electrons by isolated steps versus periodic step arrays. *Phys. Rev. B* **87**, 115425 (2013).
17. Silly, F. *et al.* Creation of an Atomic Superlattice by Immersing Metallic Adatoms in a Two-Dimensional Electron Sea. *Phys. Rev. Lett.* **92**, 016101 (2004).
18. Gross, L. *et al.* Scattering of Surface State Electrons at Large Organic Molecules. *Phys. Rev. Lett.* **93**, (2004).
19. Kulawik, M. *et al.* Interaction of CO molecules with surface state electrons on Ag(1 1 1). *Surf. Sci.* **590**, L253–L258 (2005).
20. Forster, F., Bendounan, A., Ziroff, J. & Reinert, F. Importance of surface states on the adsorption properties of noble metal surfaces. *Phys. Rev. B* **78**, 161408 (2008).

21. Nilius, N., Wallis, T. M. & Ho, W. Development of One-Dimensional Band Structure in Artificial Gold Chains. *Science* **297**, 1853–1856 (2002).
22. Crain, J. N. & Pierce, D. T. End States in One-Dimensional Atom Chains. *Science* **307**, 703–706 (2005).
23. Heller, E. J., Crommie, M. F., Lutz, C. P. & Eigler, D. M. Scattering and absorption of surface electron waves in quantum corrals. *Nature* **369**, 464–466 (1994).
24. Manoharan, H. C., Lutz, C. P. & Eigler, D. M. Quantum mirages formed by coherent projection of electronic structure. *Nature* **403**, 512–515 (2000).
25. Fiete, G. A. & Heller, E. J. Colloquium: Theory of quantum corrals and quantum mirages. *Rev. Mod. Phys.* **75**, 933–948 (2003).
26. Lobo-Checa, J. *et al.* Band Formation from Coupled Quantum Dots Formed by a Nanoporous Network on a Copper Surface. *Science* **325**, 300–303 (2009).
27. Klappenberger, F. *et al.* Dichotomous Array of Chiral Quantum Corrals by a Self-Assembled Nanoporous Kagomé Network. *Nano Lett.* **9**, 3509–3514 (2009).
28. Klappenberger, F. *et al.* Tunable Quantum Dot Arrays Formed from Self-Assembled Metal-Organic Networks. *Phys. Rev. Lett.* **106**, 026802 (2011).
29. Wang, S. *et al.* Tuning two-dimensional band structure of Cu(111) surface-state electrons that interplay with artificial supramolecular architectures. *Phys. Rev. B* **88**, 245430 (2013).
30. Iancu, V., Braun, K.-F., Schouteden, K. & Van Haesendonck, C. Probing the Electronic Properties of Trimesic Acid Nanoporous Networks on Au(111). *Langmuir* **29**, 11593–11599 (2013).
31. Schouteden, K. *et al.* Alkoxyated dehydrobenzo[12]annulene on Au(111): From single molecules to quantum dot molecular networks. *Chem. Commun.* (2015). doi:10.1039/C5CC03255E
32. Pennec, Y. *et al.* Supramolecular gratings for tuneable confinement of electrons on metal surfaces. *Nat. Nanotechnol.* **2**, 99–103 (2007).
33. Li, J., Schneider, W.-D., Berndt, R. & Crampin, S. Electron Confinement to Nanoscale Ag Islands on Ag(111): A Quantitative Study. *Phys. Rev. Lett.* **80**, 3332–3335 (1998).
34. Li, J., Schneider, W.-D., Crampin, S. & Berndt, R. Tunnelling spectroscopy of surface state scattering and confinement. *Surf. Sci.* **422**, 95–106 (1999).
35. Schouteden, K. & Van Haesendonck, C. Lateral Quantization of Two-Dimensional Electron States by Embedded Ag Nanocrystals. *Phys. Rev. Lett.* **108**, 076806 (2012).
36. Shchyrba, A. *et al.* Covalent assembly of a two-dimensional molecular ‘sponge’ on a Cu(111) surface: confined electronic surface states in open and closed pores. *Chem. Commun.* **50**, 7628–7631 (2014).
37. Zhang, J. *et al.* Probing the spatial and momentum distribution of confined surface states in a metal coordination network. *Chem. Commun.* **50**, 12289–12292 (2014).
38. Kepčija, N., Huang, T.-J., Klappenberger, F. & Barth, J. V. Quantum confinement in self-assembled two-dimensional nanoporous honeycomb networks at close-packed metal surfaces. *J. Chem. Phys.* **142**, 101931 (2015).
39. Seufert, K. *et al.* Controlled Interaction of Surface Quantum-Well Electronic States. *Nano Lett.* **13**, 6130–6135 (2013).
40. Cheng, Z. *et al.* Adsorbates in a Box: Titration of Substrate Electronic States. *Phys. Rev. Lett.* **105**, 066104 (2010).

41. Theobald, J. A., Oxtoby, N. S., Phillips, M. A., Champness, N. R. & Beton, P. H. Controlling molecular deposition and layer structure with supramolecular surface assemblies. *Nature* **424**, 1029–1031 (2003).
42. Stepanow, S. *et al.* Steering molecular organization and host–guest interactions using two-dimensional nanoporous coordination systems. *Nat. Mater.* **3**, 229–233 (2004).
43. Barth, J. V., Costantini, G. & Kern, K. Engineering atomic and molecular nanostructures at surfaces. *Nature* **437**, 671–679 (2005).
44. Stöhr, M., Wahl, M., Spillmann, H., Gade, L. H. & Jung, T. A. Lateral Manipulation for the Positioning of Molecular Guests within the Confinements of a Highly Stable Self-Assembled Organic Surface Network. *Small* **3**, 1336–1340 (2007).
45. Wahl, M., Stöhr, M., Spillmann, H., Jung, T. A. & Gade, L. H. Rotation-libration in a hierarchic supramolecular rotor-stator system: Arrhenius activation and retardation by local interaction. *Chem. Commun.* 1349 (2007). doi:10.1039/b700909g
46. Cheng, Z. *et al.* Power of Confinement: Adsorbate Dynamics on Nanometer-Scale Exposed Facets. *Nano Lett.* **10**, 3700–3703 (2010).
47. Pivetta, M., Pacchioni, G. E., Schlickum, U., Barth, J. V. & Brune, H. Formation of Fe Cluster Superlattice in a Metal-Organic Quantum-Box Network. *Phys. Rev. Lett.* **110**, 086102 (2013).
48. Park, J.-Y. *et al.* Modification of surface-state dispersion upon Xe adsorption: A scanning tunneling microscope study. *Phys. Rev. B* **62**, R16341–R16344 (2000).
49. Hövel, H., Grimm, B. & Reihl, B. Modification of the Shockley-type surface state on Ag(1 1 1) by an adsorbed xenon layer. *Surf. Sci.* **477**, 43–49 (2001).
50. Andreev, T., Barke, I. & Hövel, H. Adsorbed rare-gas layers on Au(111): Shift of the Shockley surface state studied with ultraviolet photoelectron spectroscopy and scanning tunneling spectroscopy. *Phys. Rev. B* **70**, 205426 (2004).
51. Forster, F., Hüfner, S. & Reinert, F. Rare Gases on Noble-Metal Surfaces: An Angle-Resolved Photoemission Study with High Energy Resolution†. *J. Phys. Chem. B* **108**, 14692–14698 (2004).
52. Forster, F., Bendounan, A., Ziroff, J. & Reinert, F. Systematic studies on surface modifications by ARUPS on Shockley-type surface states. *Surf. Sci.* **600**, 3870–3874 (2006).
53. Dehmer, P. M. & Dehmer, J. L. Photoelectron spectrum of Xe₂ and potential energy curves for Xe+₂. *J. Chem. Phys.* **68**, 3462–3470 (1978).
54. Poliakoff, E. D., Dehmer, P. M., Dehmer, J. L. & Stockbauer, R. The photoelectron spectrum of Xe₃ by the photoelectron–photoion coincidence technique. *J. Chem. Phys.* **75**, 1568–1569 (1981).
55. Echt, O., Sattler, K. & Recknagel, E. Magic Numbers for Sphere Packings: Experimental Verification in Free Xenon Clusters. *Phys. Rev. Lett.* **47**, 1121–1124 (1981).
56. Tschaplyguine, M., Öhrwall, G. & Björneholm, O. in *Handbook of Nanophysics: Clusters and Fullerenes* **2**, (CRC Press, 2011).
57. Wiesendanger, R. *Scanning Probe Microscopy and Spectroscopy: Methods and Applications*. (Cambridge University Press, 1994). at <<http://ebooks.cambridge.org/ref/id/CBO9780511524356>>
58. Chen, C. J. *Introduction to Scanning Tunneling Microscopy*. (Oxford University Press, 2007).
59. Yazdani, A., Eigler, D. M. & Lang, N. D. Off-Resonance Conduction Through Atomic Wires. *Science* **272**, 1921–1924 (1996).

60. Jung, T. A., Schlittler, R. R., Gimzewski, Tang, H. & Joachim, C. Controlled Room-Temperature Positioning of Individual Molecules: Molecular Flexure and Motion. *Science* **271**, 181–184 (1996).
61. Hla, S.-W. Scanning tunneling microscopy single atom/molecule manipulation and its application to nanoscience and technology. *J. Vac. Sci. Technol. B* **23**, 1351–1360 (2005).
62. Moore, A. M. & Weiss, P. S. Functional and Spectroscopic Measurements with Scanning Tunneling Microscopy. *Annu. Rev. Anal. Chem.* **1**, 857–882 (2008).
63. Crommie, M. F., Lutz, C. P. & Eigler, D. M. Confinement of electrons to quantum corrals on a metal surface. *Science* **262**, 218–220 (1993).
64. Vitali, L. *et al.* Portrait of the potential barrier at metal-organic nanocontacts. *Nat. Mater.* **9**, 320–323 (2010).
65. Lobo-Checa, J. *et al.* Band Formation from Coupled Quantum Dots Formed by a Nanoporous Network on a Copper Surface. *Science* **325**, 300–303 (2009).
66. Mugarza, A. Electronic Structure of Low-Dimensional Systems Analyzed by Angle-Resolved Photoemission Spectroscopy. (PhD thesis, University of the Basque Country, 2002).
67. *Surface Analysis– The Principal Techniques.* (John Wiley & Sons, Ltd, 2009).
68. Park, J.-Y. *et al.* Adsorption and growth of Xe adlayers on the Cu(111) surface. *Phys. Rev. B* **60**, 16934–16940 (1999).

Acknowledgements

I am extremely happy that I received help and support in huge amounts during my PhD studies.

Especially I would like to express my gratefulness to my PhD supervisor **Thomas Jung** for giving me room for creativity and personal growth, for openness and flexibility, for many scientific discussions and help with writing of the manuscripts. Moreover I acknowledge his effort put into organizing many great group events, especially those including hiking and skiing.

I would like to thank all my former and present colleagues from the Nanolab: **Aneliia Wäckerlin, Marco Martina, Stefan Schnell, Shadi Fatayer, Thomas Nijs, Toni Ivas, Susanne Martens, Oliia Popova, Aisha Ahsan** and **Seyedeh Fatemeh Mousavi**, who not only helped me scientifically but with whom I had a great time filled with a lot of fun and laughter. Especially I am very grateful to Aneliia, who introduced me to the UHV system, with whom I had many great discussions and on whose help, support and creative approach for problem solving I could always count. Moreover special thanks go to Marco for his priceless support in the lab with all technical issues, for patience and for saving many of my samples with the use of ‘magical’ tricks.

I highly appreciate the collaboration with the Paul Scherrer Institute Team: **Jan Nowakowski, Christian Wäckerlin, Dorota Siwert, Milos Balijozovic, Harald Rossmann** and **Rolf Schelldorfer**. In particular I would like to acknowledge Janek for introducing me to the PSI UHV machine, assistance in the measurements, many scientific discussions and priceless support. I am also grateful to Christian for sharing his impressive scientific, IT and technical knowledge.

I sincerely thank **Lutz Gade** from University of Heidelberg for providing the molecules used in this thesis, for sharing his remarkable knowledge and for his enthusiastic engagement in the projects.

Many grateful acknowledgments to chemists from ETH Zürich: **Mariza Almperti**, **François Diederich** and **Carlo Thilgen** for synthesis of the molecules and for sharing their impressive chemical knowledge as well as giving me the opportunity to see the work in the chemical lab.

I sincerely thank **Jorge Lobo-Checa**, **Ignacio Piquero-Zulaica** and **J. Enrique Ortega** from Materials Physics Center in San Sebastián for creating a fantastic working atmosphere during joint ARPES measurement time, openness and readiness to help as well as for showing me the culture and the beauty of the Basque Country. I am deeply indebted to Jorge, **Manfred Matena** and **Jonas Björk** for sharing their impressive knowledge during our scientific discussions.

I would like to thank **Justin Wells**, **Federico Mazzola**, **Fei Song**, **Craig Polley** and **Mats Leandersson** for introducing me to synchrotron-based ARPES in MAX-lab and for a wonderful environment during the beamtimes.

I thank also **Shigeki Kawai** for introducing me to AFM/KPFM and for teaching me how to efficiently take high-quality data and manipulate single atoms.

Moreover I am grateful to **Meike Stöhr** and **Ernst Mayer** as well as the above mentioned collaborators for a careful proof-reading of the manuscripts and many helpful discussions.